AEROSPACE RECOMMENDED PRACTICE

ARP876™	REV. F

Issued 1978-03
Revised 2013-05
Reaffirmed 2021-01

Superseding ARP876E

Gas Turbine Jet Exhaust Noise Prediction

RATIONALE

Revision F corrects an error in Equation 9 for the single stream shock-associated noise prediction method, and corrects an error in Table 14 for the mixed component Z4 term of the subsonic coaxial jet mixing noise prediction method.

FOREWORD

AIR876, issued on 7 October 1965, presented a summary correlation of jet engine exhaust noise data available at that time. It dealt with both static and flight modes but, by virtue of the data largely being from full scale engines, no attempt was made to subdivide the information into the relevant component noise sources. Subsequently, work on high-quality noise facilities has established that most engine exhaust systems are influenced in their noise characteristics by far more than the noise due to the external mixing process alone, and this work has provided the opportunity to develop a clearer picture of the influence of other effects.

AIR876 was also limited to jet velocities above 1000 feet/second (300 m/s), i.e., the range of exhaust velocities associated with early jet engines. The introduction of more advanced engine designs demands a prediction technique for exhaust sources over a far wider range of velocity conditions.

Therefore, it is intended that ARP876 be developed on a long-term basis as a document definitive in most aspects of the prediction of exhaust noise, consistent with the state of the art. Specific recommended procedures will be issued as sections, both for completeness and to allow for future updating. Additionally, following a decision in 1979, explanatory background material detailing the rationale behind the selection of methods will be included in separate appendices to this document.

The document will offer a method of estimating the exhaust noise from single unsuppressed engines. To be useful in estimating the noise from aircraft installations, a number of additional effects must be considered, and it is intended that these also will be covered as substantive evidence becomes available.

Areas that will not be addressed in this ARP, due to source variability with detailed engine design parameters, are aerodynamic blade noise sources; that is, noise generated by interaction effects between rotating and stationary components of the fan, compressor and turbine systems.

Each section will be dated, and will represent an approach to a particular topic as agreed by members of the SAE A-21 Propulsion Noise Subcommittee who have experience or data on that subject. Lists of members and affiliated bodies contributing experimental data or other information used in compiling any one section will be included. Correspondence should be addressed to the SAE for the attention of the A-21 Committee and appropriate distribution.

TO PLACE A DOCUMENT ORDER: **Tel: 877-606-7323 (inside USA and Canada)**
Tel: +1 724-776-4970 (outside USA)
Fax: 724-776-0790
Email: CustomerService@sae.org
SAE WEB ADDRESS: **http://www.sae.org**

For more information on this standard, visit
https://www.sae.org/standards/content/ARP876F/

TABLE OF CONTENTS

1. SCOPE 5

2. SOURCES OF EXHAUST NOISE 5

3. NOTES ON USE OF PREDICTION PROCEDURES 5

4. SYMBOLS 6

5. PREDICTION OF SINGLE STREAM JET MIXING NOISE FROM SHOCK-FREE CIRCULAR NOZZLES 8
5.1 Static Conditions 9
5.2 Flight Condition 10
5.3 References 12
5.4 Parties Contributing to Formulation of Section 5 12

6. PREDICTION OF SINGLE STREAM SHOCK-ASSOCIATED NOISE FROM CONVERGENT NOZZLES AT SUPERCRITICAL CONDITIONS 48
6.1 Static Conditions 48
6.1.1 Overall Sound Pressure Level Prediction 50
6.1.2 Angular Range of Application 52
6.2 Flight Conditions 52
6.3 References 53
6.4 Parties Contributing to Compilation of Section 6 53

7. PREDICTION OF SUBSONIC COAXIAL JET MIXING NOISE 53
7.1 Scope 54
7.2 Development of the Coaxial Jet Noise Prediction Model 58
7.3 Component Sound Pressure Level Prediction 59
7.4 Sound Pressure Level Adjustments in Prediction 59
7.4.1 Normal Adjustments 59
7.4.2 Acoustic Excitation Adjustments 60
7.5 Mixed Jet Noise Component 60
7.6 Special Features 60
7.6.1 Near-Field Effects 61
7.6.2 Acoustic Excitation 62
7.6.3 Jet Noise Source Locations 62
7.7 Incorporation of Distributed Source Location 63
7.7.1 Wind Tunnel Coordinates 63
7.7.2 Ground-Fixed Coordinates for Flyover Jet Noise 64
7.8 Predictions of Jet Noise Levels for Full-Scale Tests 65
7.9 Prediction of Jet Noise Levels for Full-Scale Tests - Static or Flight (Section 7) 65
7.9.1 External Plug Effect 65
7.9.2 Ground Proximity Effect 65
7.9.3 Installation and Angle of Attack Effects 66
7.10 References 67
7.11 Parties Contributing to Formulation of Section 7 68

8. PREDICTION OF NOISE FROM CONVENTIONAL COMBUSTORS INSTALLED IN GAS TURBINE ENGINES 68
8.1 Static Conditions 68
8.2 Flight Conditions 75
8.3 References 75
8.4 Parties Contributing to the Formulation of Section 8 75

9. NOTES 76

APPENDIX A BACKGROUND TO PREDICTION OF SINGLE STREAM JET MIXING NOISE FROM SHOCK-FREE CIRCULAR NOZZLES (SECTION 5) 78
APPENDIX B BACKGROUND TO PREDICTION OF SINGLE STREAM SHOCK-ASSOCIATED NOISE FROM CONVERGENT NOZZLES AT SUPERCRITICAL CONDITIONS (SECTION 6) 90
APPENDIX C BACKGROUND TO PREDICTION OF SUBSONIC COAXIAL JET MIXING NOISE 97
APPENDIX D BACKGROUND TO PREDICTION OF NOISE FROM CONVENTIONAL COMBUSTORS INSTALLED IN GAS TURBINE ENGINES (SECTION 8) 99

FIGURE 1 11
FIGURE 2 VARIABLE DENSITY INDEX ω 13
FIGURE 3 CARPET PLOT FOR NORMALIZED OVERALL SOUND PRESSURE LEVELS OF PURE JET-MIXED NOISE 14
FIGURE 4 ADJUSTMENT FACTOR FOR NORMALIZED FREQUENCY 15
FIGURE 5 ONE-THIRD OCTAVE-BAND NORMALIZED SPECTRA $\theta_I \leq 90$ DEGREES 16
FIGURE 6 ONE-THIRD OCTAVE-BAND NORMALIZED SPECTRA $\theta_I = 100$ DEGREES 18
FIGURE 7 ONE-THIRD OCTAVE-BAND NORMALIZED SPECTRA $\theta_I = 110$ DEGREES 20
FIGURE 8 ONE-THIRD OCTAVE-BAND NORMALIZED SPECTRA $\theta_I = 120$ DEGREES 22
FIGURE 9 ONE-THIRD OCTAVE-BAND NORMALIZED SPECTRA $\theta_I = 130$ DEGREES 24
FIGURE 10 ONE-THIRD OCTAVE-BAND NORMALIZED SPECTRA $\theta_I = 140$ DEGREES 26
FIGURE 11 ONE-THIRD OCTAVE-BAND NORMALIZED SPECTRA $\theta_I = 150$ DEGREES 28
FIGURE 12 ONE-THIRD OCTAVE-BAND NORMALIZED SPECTRA $\theta_I = 160$ DEGREES 30
FIGURE 13 VARIATION OF VELOCITY EXPONENT $M(\theta_I)$ WITH ANGLE θ_I AND JET MACH NUMBER V_J/A_O 32
FIGURE 14 ESTIMATED RANGE OF UNCERTAINTY ASSOCIATED WITH CALCULATED VALUES OF Δ OASPL (θ_I) FOR VARIOUS JET VELOCITY RATIOS AND UNCERTAINTY IN $M(\theta_I)$ 33
FIGURE 15 MASTER SPECTRA FOR SHOCK-ASSOCIATED NOISE PREDICTION 51
FIGURE 16 SCHEMATIC COAXIAL JET NOISE MODEL IN WIND TUNNEL COORDINATES 58
FIGURE 17A IN-FLOW COORDINATES 64
FIGURE 17B FLYOVER COORDINATES 64
FIGURE 17 COORDINATE SYSTEMS FOR JET NOISE PREDICTION 64
FIGURE 18 SCHEMATIC OF INSTALLATION PARAMETERS 67
FIGURE 19 FLOW CHART FOR COMBUSTOR NOISE PREDICTION 70
FIGURE 20 SPECTRUM SHAPE FOR COMBUSTOR NOISE 71
FIGURE 21 FAIRFIELD DIRECTIVITY FOR COMBUSTOR NOISE 72

TABLE 1 VARIABLE DENSITY INDEX ω (REFERENCE FIGURE 2) 34
TABLE 2 PURE JET MIXING NOISE NORMALIZED POLAR OASPL (DB) VALUES (REFERENCE FIGURE 3) 35
TABLE 3 ADJUSTMENT FACTOR FOR NORMALIZED FREQUENCY 36
TABLE 4 GAS TURBINE JET EXHAUST NOISE PREDICTION θ_I ANGLE TO INTAKE ≤ 90 DEGREES 37
TABLE 5 GAS TURBINE JET EXHAUST NOISE PREDICTION θ_I ANGLE TO INTAKE = 100 DEGREES 38
TABLE 6 GAS TURBINE JET EXHAUST NOISE PREDICTION θ_I ANGLE TO INTAKE = 110 DEGREES 39
TABLE 7 GAS TURBINE JET EXHAUST NOISE PREDICTION θ_I ANGLE TO INTAKE = 120 DEGREES 40
TABLE 8 GAS TURBINE JET EXHAUST NOISE PREDICTION θ_I ANGLE TO INTAKE = 130 DEGREES 41
TABLE 9A GAS TURBINE JET EXHAUST NOISE PREDICTION θ_I ANGLE TO INTAKE = 140 DEGREES 42
TABLE 9B GAS TURBINE JET EXHAUST NOISE PREDICTION θ_I ANGLE TO INTAKE = 140 DEGREES 43
TABLE 10A GAS TURBINE JET EXHAUST NOISE PREDICTION θ_I ANGLE TO INTAKE = 150 DEGREES 44
TABLE 10B GAS TURBINE JET EXHAUST NOISE PREDICTION θ_I ANGLE TO INTAKE = 150 DEGREES 45
TABLE 11A GAS TURBINE JET EXHAUST NOISE PREDICTION θ_I ANGLE TO INTAKE = 160 DEGREES 46
TABLE 11B GAS TURBINE JET EXHAUST NOISE PREDICTION θ_I ANGLE TO INTAKE = 160 DEGREES 47
TABLE 12A RELATIVE VELOCITY EXPONENT $M(\theta_I)V$ 48
TABLE 12B RELATIVE VELOCITY EXPONENT $M(\theta_I)$ 48
TABLE 13 MASTER SPECTRA $H_O(\sigma)$ AND $C_1(\sigma)$ 52
TABLE 14 JET NOISE COMPONENT FORMULAS 54

TABLE 15 NORMAL ADJUSTMENT (DSPL)..... 56
TABLE 16 ACOUSTIC EXCITATION ADJUSTMENT (EX)..... 57
TABLE 17 SPECTRUM SHAPE FACTOR FOR COMBUSTOR NOISE..... 73
TABLE 18 FARFIELD DIRECTIVITY INDEX FOR COMBUSTOR NOISE..... 74

1. SCOPE

ARP876 is intended to provide specific recommended procedures for the prediction of gas turbine jet exhaust system noise sources. Procedures are issued as separate sections, to allow for future updating as additional methods, consistent with state-of-the-art, become available.

2. SOURCES OF EXHAUST NOISE

The exhaust system noise of gas turbine engines for aircraft applications can be considered to comprise the following main sources:

a. Pure jet mixing noise resulting from a hot core exhaust stream mixing with its surrounding environment (which may be influenced by a bypass flow)

b. Pure jet mixing noise resulting from a cold bypass stream mixing with both the surrounding environment and the core flow

c. Shock associated noise, where either or both hot and cold exhaust systems comprise a choked final nozzle

d. Noise from the core engine resulting from aerodynamic disturbances upstream of or at the final nozzle, including combustion noise.

e. Aerodynamic noise, tonal and broadband, resulting from blade interaction effects in fan, compressor or turbine systems

All the above sources combine in varying degrees to produce the overall exhaust noise characteristics. The relevance of each source is a function of both engine operating condition and aircraft speed. Because of the dependence of aerodynamic blading noise on the intimate design configuration of any given engine, this aspect is specifically excluded from subsequent consideration, and every attempt has been made to remove such phenomena from any engine data used.

3. NOTES ON USE OF PREDICTION PROCEDURES

3.1 Prediction methods included in this document are self-contained. To develop an estimate of the total exhaust noise signature from an engine it is necessary to integrate the individual source components.

This is effected by estimating each component spectrum and summing the energy in each one-third octave band. This is usually most conveniently carried out prior to any extrapolation to the relevant distance or corrections for atmospheric conditions and ground reflection effects. It is also necessary to incorporate any estimated turbo-machinery content (not covered herein) at the initial stage, in order to obtain a complete spectrum of engine noise. Furthermore, it is advisable that any assumed modification to the noise by virtue of suppression features or installation effects is made in the component calculation state.

3.2 Methods contained in this document are expressed in terms of noise levels that would be measured under free field conditions. Reflective augmentations and cancellations from real surfaces, primarily the ground surface over which measurements are made, produce peaks and troughs in the observed test spectra, and these have been corrected out of the experimental data used where they have not been obtained under anechoic conditions.

Spectra and directivity plots in this document must, therefore, be converted to non-free-field conditions to make them representative of typical measurements “in the field”. SAE AIR1327 provides guidance on such conversion for an acoustically hard surface (i.e., concrete, tarmac) and advice on how to deal with other typical surfaces (e.g., grassland).

3.3 The prediction methods provide spectral information derived from measurements taken in the acoustic far field, but corrected for loss due to atmospheric attenuation and normalized for distance.

Since practical distances involved in aircraft noise calculations are large, apart from the normal inverse square law correction, allowance must be made for atmospheric absorption. SAE ARP866A provides a standard method of allowing for atmospheric absorption under a range of ambient temperature and humidity conditions.

3.4 Prediction methods are directed at producing estimates of noise levels generated during the normal take-off and approach regimes of aircraft operation. Extrapolation of the methods to higher flight speeds, or use for estimation other than in the acoustic farfield, is not recommended since experimental evidence in support of such extrapolation was not available at the time of preparation of this document.

4. SYMBOLS

a_o	Ambient speed of sound	m/s
A	Cross-sectional area of jet exhaust nozzle (with subscripts to define nozzle referred to)	m^2
C_v	Velocity coefficient for relevant discharge nozzle	
DI	Farfield directivity index	dB
D	Exhaust nozzle diameter (with subscripts)	m
EXA	(distance from fan face to fan duct exit)/(fan diameter)	
f	Frequency	Hz
g	Gravitational constant; 9.80665	m/s^2
ISA	International Standard Atmosphere	
L	Sound pressure level	dB
$m(\theta_1)$	Relative Velocity exponent used in converting static mixing noise to flight conditions	
M	Jet Mach number (V_j/a_o)	
M_a	Aircraft flight Mach number (V_a/a_o)	
n	Jet velocity exponent	
N	Rotational speed (with subscripts)	rpm
NPR	Nozzle pressure ratio (P_j/P_o)	
OAPWL	Overall sound power level (re 1 pW)	dB
OASPL	Overall sound pressure level (re 20 μPa)	dB
p	Sound pressure	Pa

p_o	Ambient static pressure	Pa
p_{ISA}	Static pressure under ISA, sea level conditions	Pa
p_{ref}	Acoustic reference sound pressure, 20 μPa	Pa
P	Total pressure	Pa
P_o	Ambient-total pressure	Pa
P_{ISA}	Total pressure under ISA, sea level conditions	PA
PWL	One-third octave-band sound power level (re 1 pW)	dB
r	Radial distance from sound source (or nozzle exit) to observer	m
R	Gas constant with value 287.05 $J.kg^{-1}K^{-1}$ based on the universal gas constant of 8.31432 x 10^3 J/[K(kg-mol)] and mass per kilogram-mole in dry air of 28.9644 kg/(kg-mol)	$J.kg^{-1}K^{-1}$
Sr	Strouhal number	
S	Normalized free-field Overall Sound Pressure Level	dB
S(f)	Power level spectrum shape factor	dB
SPL	One-third octave-band sound pressure level (re 20 μPa)	dB
t	Static temperature	K
t_o	Ambient static temperature	K
T	Total temperature	K
T_o	Ambient total temperature	K
T_j	Jet total temperature	K
V_a	Forward speed of engine (i.e., airplane)	m/s
V	Fully expanded jet velocity (with subscripts)	m/s
W	Massflow rate	kg/s
x	Number of shocks in supercritical jet	
X	Noise source location downstream of primary nozzle exit	m
β	Jet pressure ratio parameter	
γ	Ratio of specific heats for propulsion medium	

θ	Angle to nozzle axis (with subscript i inlet, j jet)	degrees (except where stated)
λ	Wavelength	m
ξ	Strouhal frequency adjustment factor	
π_{ref}	Acoustic reference power, 1 pW	Watt
ρ	Density	kg/m^3
ρ_{ISA}	Atmospheric density under ISA conditions (1.225 kg/m^3 based on atmospheric pressure of 1.01325 x 10^5 Pa at an air temperature of 288.15 K)	kg/m^3
ρ_j	Fully expanded jet density	kg/m^3
ϕ	Angle between direction of aircraft motion and direction of sound propagation	degrees
ψ	Angle between airplane flight path and engine thrust axis	degrees
ω	Variable density index used in computing OASPL from jet mixing noise	

Subscripts:

i	intake
j	jet (general)
a or o	ambient
p	primary jet
s	secondary jet
m	mixed jet
std	standard (e.g., sea level, ISA)

NOTE: The units quoted for the physical quantities are the recommended Systeme Internationale units. Except for the logarithmic quantities, temperatures and angles, any other consistent system of units may be used since results are expressed as dimensionless ratios.

5. PREDICTION OF SINGLE STREAM JET MIXING NOISE FROM SHOCK-FREE CIRCULAR NOZZLES

DATE OF COMPILATION

Static Conditions - September 1976

Flight Conditions - November 1978

5.1 Static Conditions

Definitive model scale experimental work in the 1970s provided a firm data base for the study of mixing noise over a wide range of jet velocity and temperature conditions. That work showed that jet mixing noise level and spectral character is a function of the following principal parameters:

a. The velocity differential between that of the jet and its environment

b. The jet density relative to the density of the surrounding air

c. The jet dimensions

It has been concluded that one of the most convenient ways to express jet noise characteristics is to consider first the normalized overall sound pressure level (OASPL) as a function of jet velocity (V_j) and angle of measurement (θ_i or θ_j) and to then relate the spectrum (on a one-third octave-band basis) to the overall level at any point in the field. This procedure may be adopted by using Figures 2 through 12. The information in Figures 2 through 12 is also presented in Tables 1 through 11.

The method of calculation is as follows:

Step 1—Calculate the fully expanded mean jet velocity (V_j) from a knowledge of jet temperature and pressure, where:

$$V_j = C_v \left\{ \left[(2\gamma Rg)/(\gamma - 1) \right] \left[T_j \right] \left[1 - NPR^{-(\gamma-1)/\gamma} \right] \right\}^{1/2} \quad \text{(Eq. 1)}$$

or, where a knowledge of temperature and pressure is not readily available (for example, from engine test stand measurements) an alternative method of calculating V_j is from thrust and mass flow, where:

V_j = static gross thrust divided by mass flow

Step 2—Using V_j obtained from Step 1 and the ambient speed of sound (a_o) obtain the variable density index (ω) from Figure 2.

Step 3—For any desired angle and jet velocity use Figure 3 to obtain the normalized free-field overall sound pressure level (S) where:

$$S = OASPL - 10 \log_{10} \left\{ \left[\left(\rho_j / \rho_o \right)^{\omega} \right] \left(A_j / r^2 \right) \right\} - 20 \log_{10} \left(P_o / P_{ISA} \right) \quad \text{(Eq. 2)}$$

for the value of V_j at any desired angle.

Step 4—Calculate the overall sound pressure level (OASPL) from:

$$OASPL = S + 10 \log_{10} \left(\rho_j / \rho_o \right)^{\omega} + 10 \log_{10} \left(A_j / r^2 \right) + 20 \log_{10} \left(P_o / P_{ISA} \right)$$

Step 5—Calculate the one-third octave-band spectral levels from Figures 5 to 12, using jet velocity (V_j), temperature ratio (T_j/T_o), nozzle diameter (D_j) and the angle (θ_i) as follows:

Determine the Strouhal frequency adjustment factor ξ from Figure 4 and then calculate ($fD_j/\xi V_j$) for each one-third octave-band centre frequency. Enter Figures 5 to 12 with the values of ($fD_j/\xi V_j$), and values of (T_j/T_o) at the values of $\log_{10}$ (V_j/a_o) and θ_i to determine values of one-third octave-band relative sound pressure level (SPL - OASPL).

For values other than those specified in Figures 4 to 12, linear interpolation on angles (θ_i), and on the values for $\log_{10}$ ($fD_j/\xi V_j$), $\log_{10}$ (V_j/a_o) and (T_j/T_o) is recommended.

Step 6—From the values of OASPL and one-third octave-band relative sound pressure level (SPL - OASPL) as derived in steps 4 and 5, respectively, calculate values of one-third octave-band SPL.

These values represent the free-field jet noise spectrum at position (r, θ_i) in a loss free atmosphere.

NOTE 1: The spectra of Figures 4 to 12 satisfy the following condition:

$$\log_{10}\left[\sum_{i=1}^{33} 10^{0.1(SPL_i - OASPL)}\right] = 0 \qquad \text{(Eq. 3)}$$

over the range of one-third octave-band frequencies defined by:

$$-1.6 \le \log_{10}\left(fD_j / \xi V_j\right) \le 1.6 \qquad \text{(Eq. 4)}$$

NOTE 2: Accuracy of Prediction

The accuracy of prediction of OASPL at (r, θ_i) relative to the model data on which it is based varies between ±2 dB at low jet velocities to ±4 dB at very high jet velocities. The accuracy of prediction of one-third octave (SPL - OASPL) varies between ±1 dB at frequencies near the peak of the jet-noise spectrum. However, these limits apply to the extreme cases. For all normal purposes, the majority of predictions will be accurate within ±3 dB at all frequencies.

5.2 Flight Condition

Forward speed has the effect of reducing the shear between the jet and its environment. Work in the 1970s produced conflicting evidence on the change in jet mixing noise in going from static to flight conditions. Model scale wind tunnel testing has, in general, produced a greater reduction in level than tests carried out on ground based engine facilities and aircraft. The differences may be associated with contamination by other sources, both engine based and aircraft installation induced. The method herein is based upon data obtained on a ground based engine flight simulation facility. In general, the results of applying the prediction method fall between the extremes represented by some model tests and some aircraft flight tests.

The method relies upon a modification of the static sound pressure levels obtained in 5.1.

For a jet of given velocity V_j (corresponding to a given nozzle pressure ratio and temperature), moving at a flight speed V_a, the method of calculation is as follows:

Step 1—Calculate the free field static overall sound pressure levels (OASPL) as a function of angle to inlet axis, as outlined in steps 1 to 4 of 5.1, corresponding to the exhaust conditions.

Step 2—Calculate the OASPL in flight at any desired angle θ_i (20 degrees $\le \theta_i \le$ 160 degrees):

$$\left[OASPL\left(\theta_i\right)\right]_{flight} = \left[OASPL\left(\theta_i\right)\right]_{static} - \Delta OASPL\left(\theta_i\right) \qquad \text{(Eq. 5)}$$

where:

$$\Delta OASPL\left(\theta_i\right) = 10\log_{10}\left\{\left(\frac{V_j}{V_j - V_a}\right)^{m(\theta_i)}\left(1 - M_a\cos\phi\right)\right\},$$

with:

$m(\theta_i)$ = relative velocity exponent $m(\theta_i)$, a function of angle θ_i between the engine inlet axis and the line connecting an aircraft reference point and the observer location, shown in sketch, is given in Figure 13 and Table 12

$M_a = V_a/a_o$ = aircraft flight Mach number or ratio of airspeed V_a to speed of sound a_o at the ambient temperature of the surrounding medium

ϕ = angle between direction of aircraft motion and direction of sound propagation (see Figure 1)

V_j = fully expanded jet velocity, corresponding to a given pressure ratio and total temperature of the jet and being the same in static and in flight (see Equation 1)

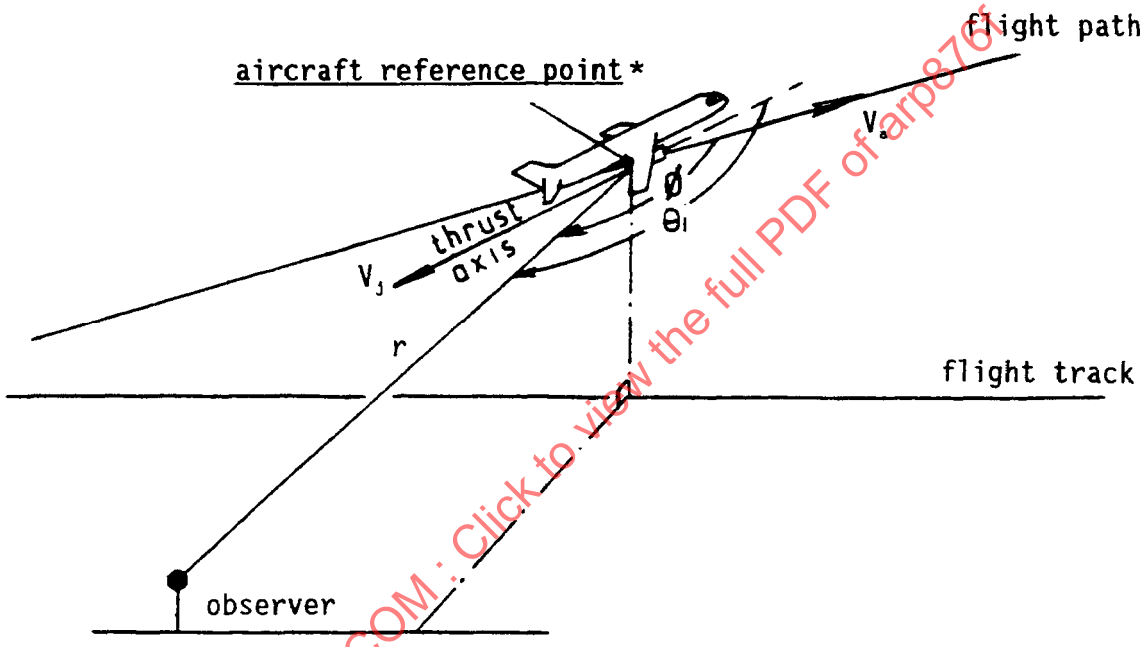

FIGURE 1

NOTE: For consistency with the prediction procedure under static conditions, the aircraft reference point * should be the center of the nozzle exit. For practical applications (aircraft noise predictions) alternative reference points may have to be selected (e.g., center of the engine nacelle, or centroid of the nozzle exits for airplanes powered by more than one engine, etc.)

Step 3—Calculate the one-third octave-band sound pressure levels in flight for any desired angle θ_i, following steps 5 and 6 of 5.1, with the exception that now the OASPL is the value in flight as derived in step 2 of this section and that the Strouhal number:

$$\left(fD_j / \xi V_j\right) \quad \text{(Eq. 6)}$$

has to be replaced by one based on relative jet velocity (V_j - V_a), that is:

$$\left[fD_j / \xi\left(V_j - V_a\right)\right] \quad \text{(Eq. 7)}$$

The value of ξ is still obtained from Figure 4 for the corresponding value of the jet velocity V_j.

NOTE: Accuracy of Prediction

The accuracy of ΔOASPL(θ_i) prediction, as calculated in step 2 for any angle θ_i, is a function of velocity ratio, and may be obtained from the following formula:

$$\pm\delta\left[\Delta OASPL\left(\theta_i\right)\right] = \pm\left[\delta m\left(\theta_i\right)\right] \times \left\{10 \log_{10}\left[V_j / \left(V_j - V_a\right)\right]\right\} \quad \text{(Eq. 8)}$$

$\delta m(\theta_i)$ being the uncertainty in $m(\theta_i)$.

In the present prediction procedure, the range of uncertainty of the exponent $m(\theta_i)$ with respect to aircraft flight test data is estimated not to exceed ±1 unit (see Figure 14). This comment does not apply to wind tunnel model data where the exponent $m(\theta_i)$ is always greater than ±1 unit over the angular range 60 degrees $\leq \theta_i \leq$ 130 degrees, and by as much as 0 to 5 units.

5.3 References

For the derivation and substantiation of the static prediction method, references may be made to the following documents:

5.3.1 Boeing Document No. D6 - 42929 - 1, Empirical Jet Noise Predictions for Single and Dual Flow Jets and without Suppressor Nozzles Volume 1. Single flow Subsonic and Supersonic Jets. C. L. Jaeck, S. J. Cowan, R. P. Gerend.

5.3.2 SNECMA Document YKA No. 5898/76, Comparaison des spectres 1/3 d'octave de bruit de jet mesurés en chambre sourde A 17 du CEPr aux diverses propositions de révision de l'ARP876 de la SAE.

5.3.3 SNECMA Document YKA No. 5317/75, Révision de la méthode de prévision du bruit des jets (SAE ARP876).

5.3.4 For a description of the facility on which much of the basic data used herein were acquired, reference may be made to the AIAA Paper No. 76-534, July 1976, entitled, "Use of the Bertin Aerotrain for the Investigation of Flight Effects on Aircraft Engine Exhaust Noise," by R. G. Hoch and M. Berthelot.

5.4 Parties Contributing to Formulation of Section 5

Department of Transportation, USA

Douglas Aircraft Company, USA

General Electric Company, USA

Hamilton Standard, USA

Lockheed California Company, USA

Lockheed Georgia Company, USA

National Aeronautics and Space Administration, USA

National Gas Turbine Establishment, United Kingdom

Pratt & Whitney Aircraft Company, USA

Rolls-Royce Limited, United Kingdom

SNECMA, France

The Boeing Company, USA

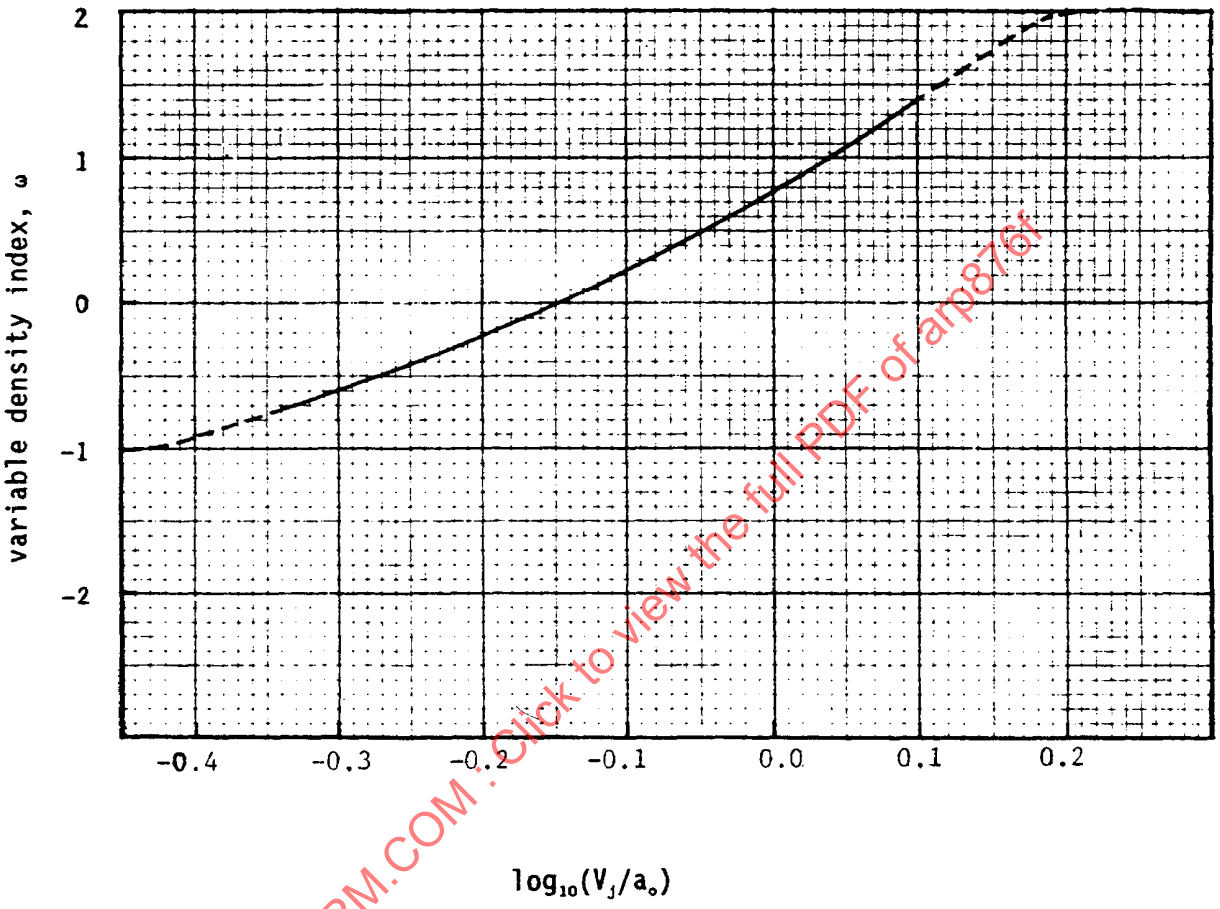

NOTE: Experimental evidence is represented by the solid line.

Above $\log_{10}(V_j/a_o) = 0.2$, the value of ω should be taken as 2.0

FIGURE 2 - VARIABLE DENSITY INDEX ω

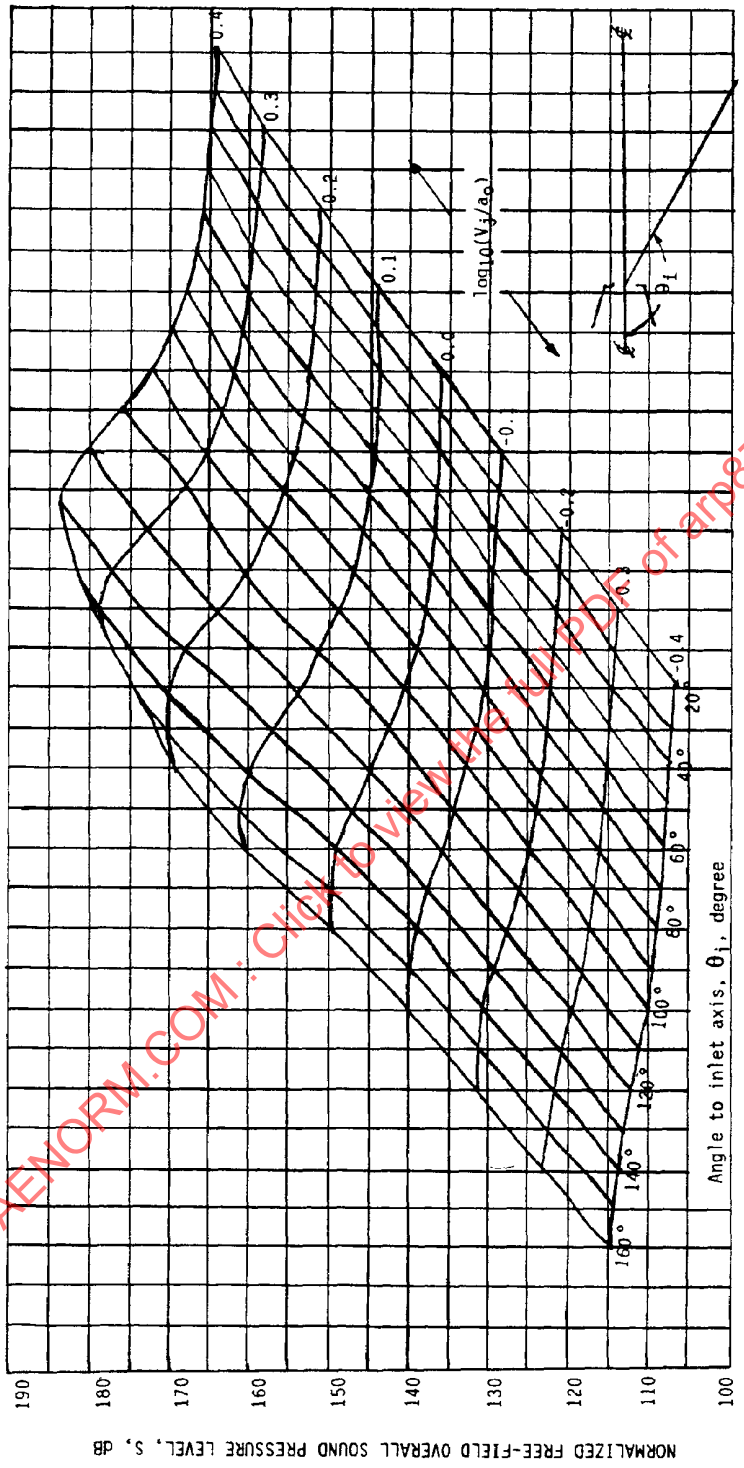

FIGURE 3 - CARPET PLOT FOR NORMALIZED OVERALL SOUND PRESSURE LEVELS OF PURE JET-MIXED NOISE

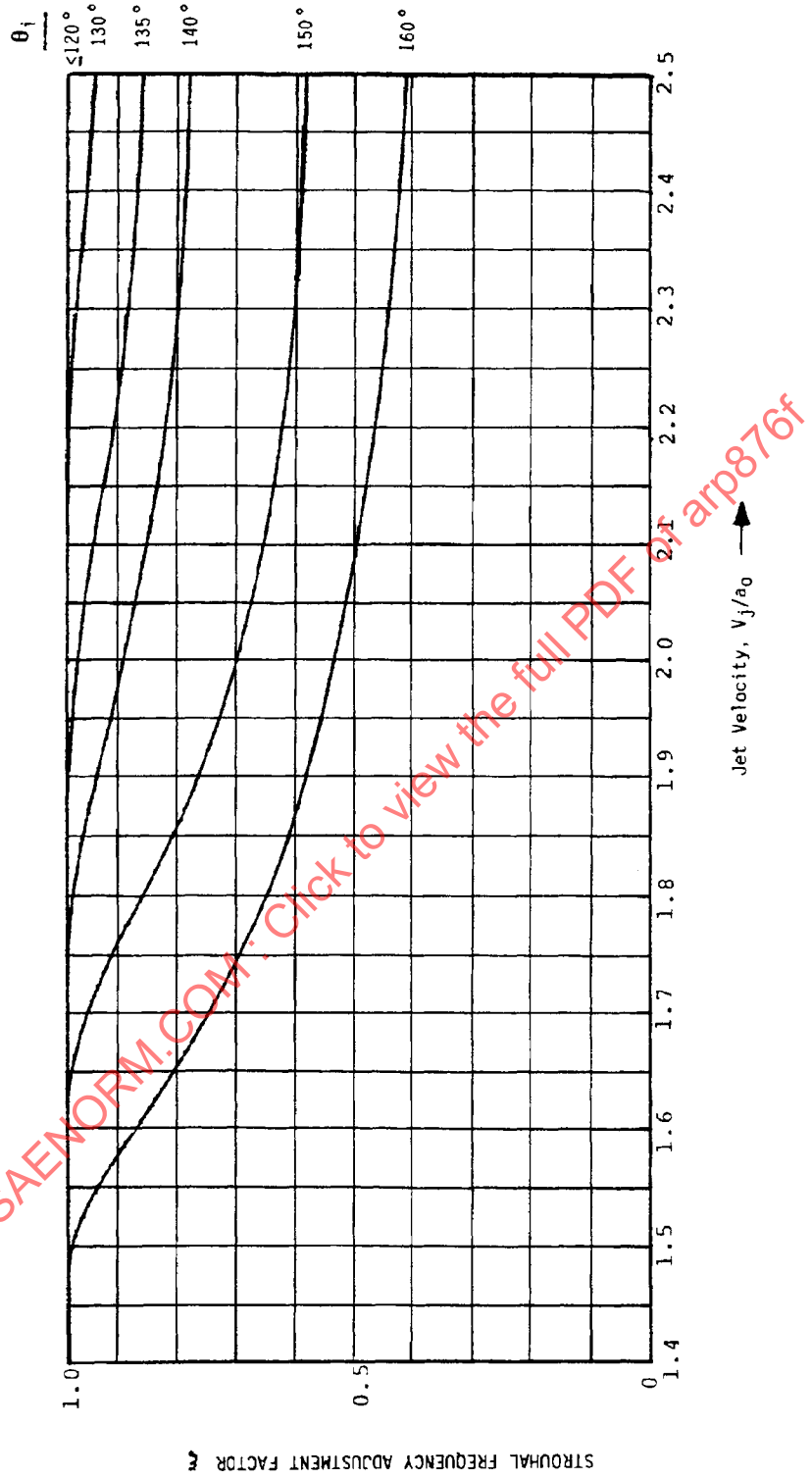

FIGURE 4 - ADJUSTMENT FACTOR FOR NORMALIZED FREQUENCY

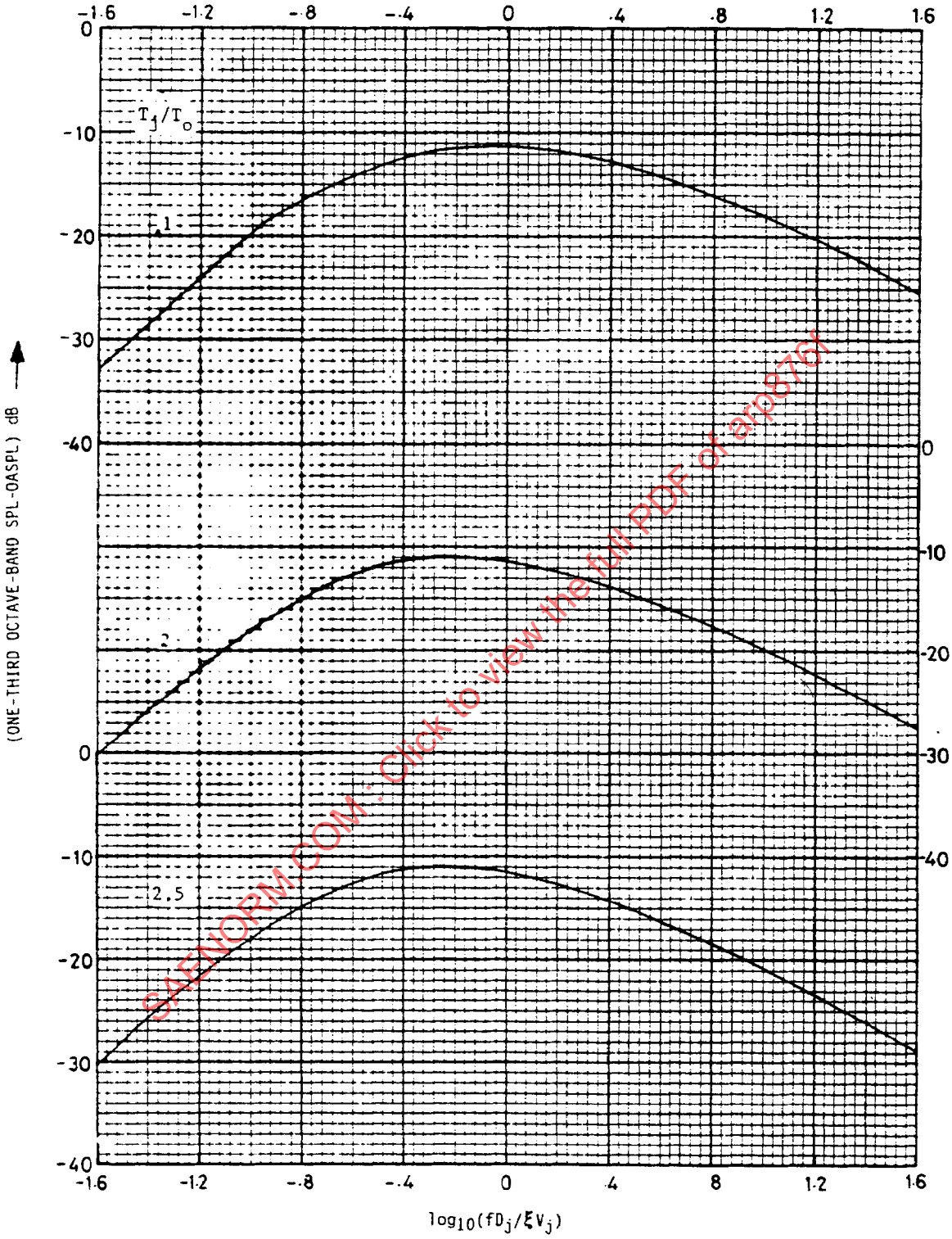

FIGURE 5 - ONE-THIRD OCTAVE-BAND NORMALIZED SPECTRA $\theta_l \leq 90$ DEGREES

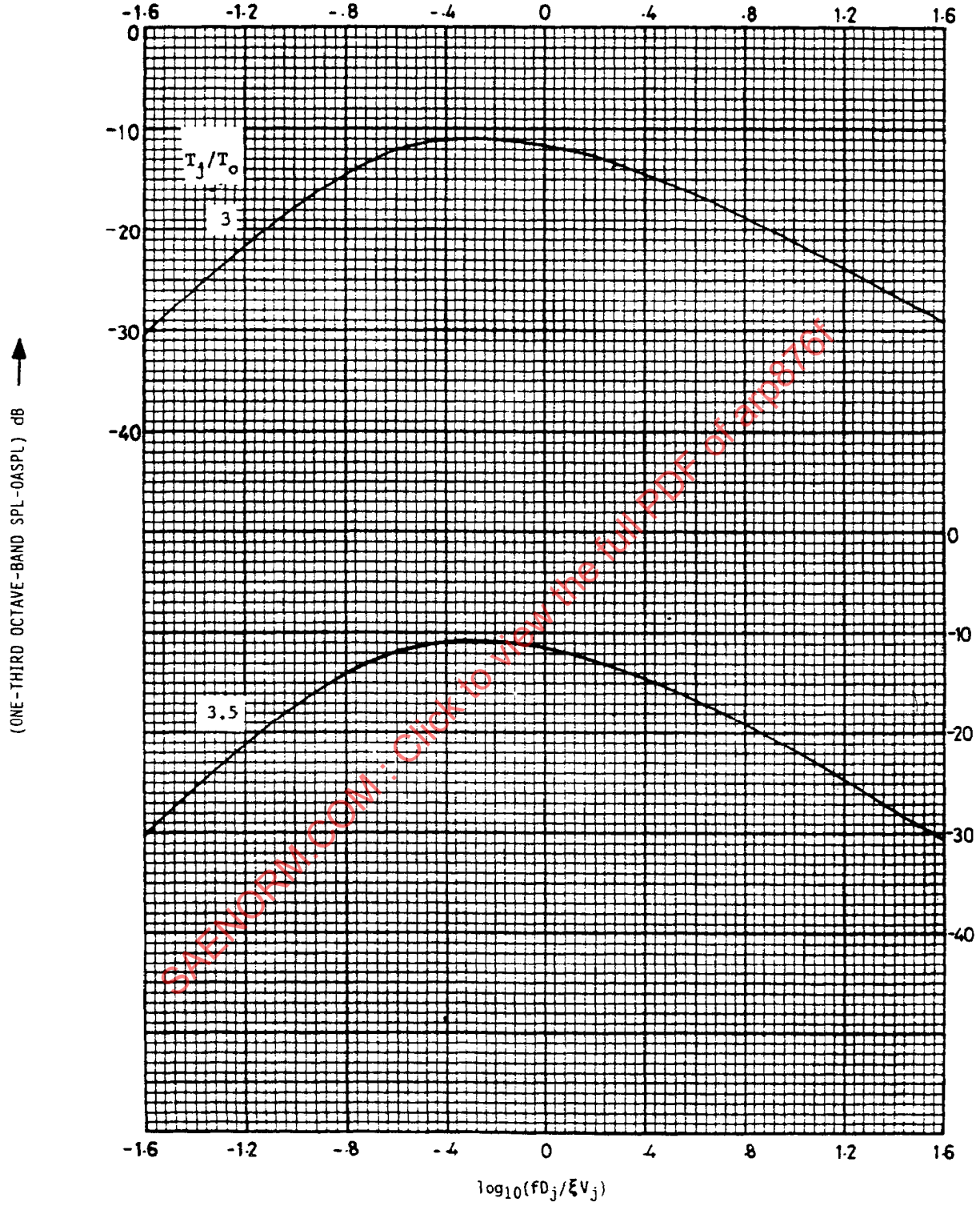

FIGURE 5 (CONTINUED)

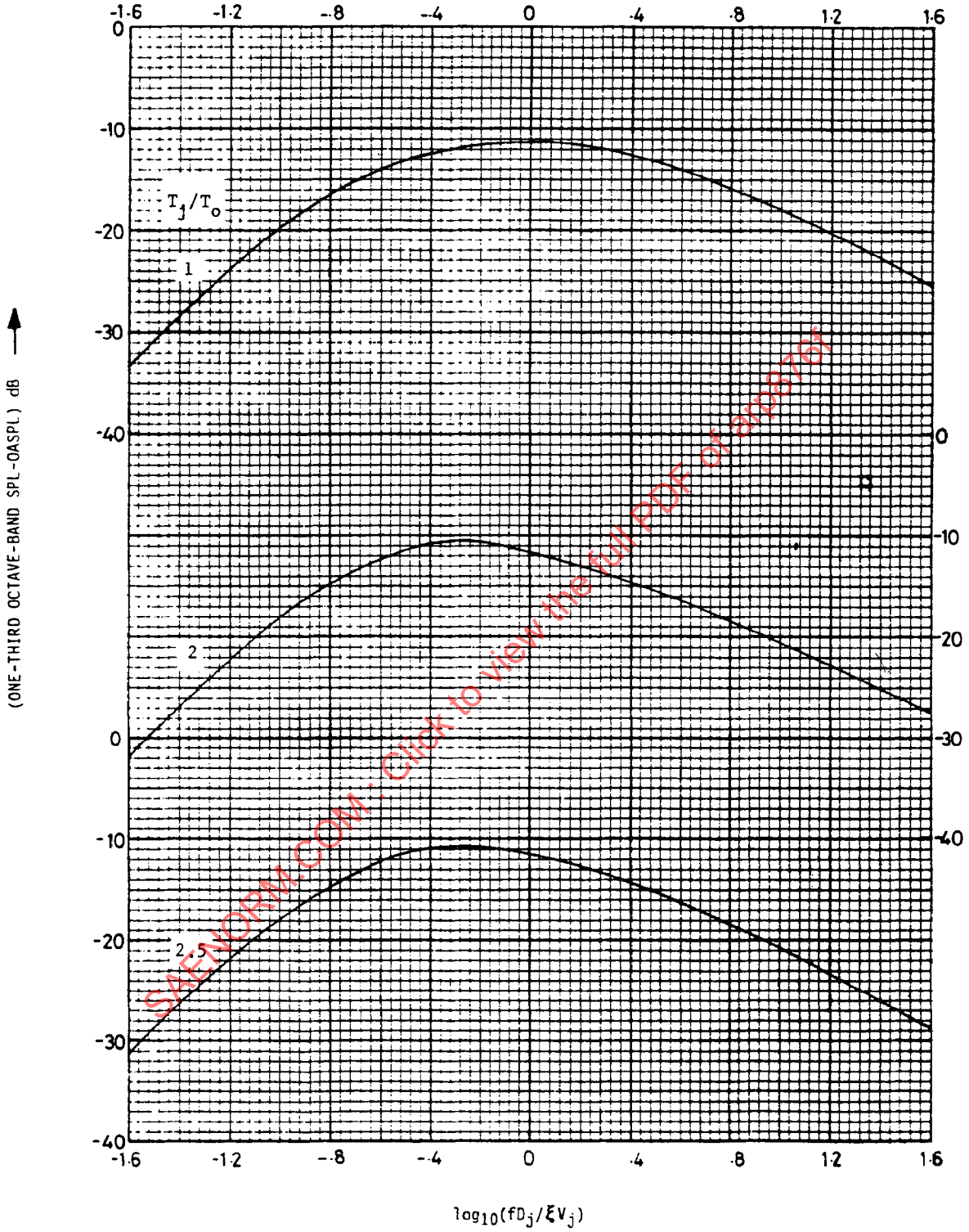

FIGURE 6 - ONE-THIRD OCTAVE-BAND NORMALIZED SPECTRA θ_l = 100 DEGREES

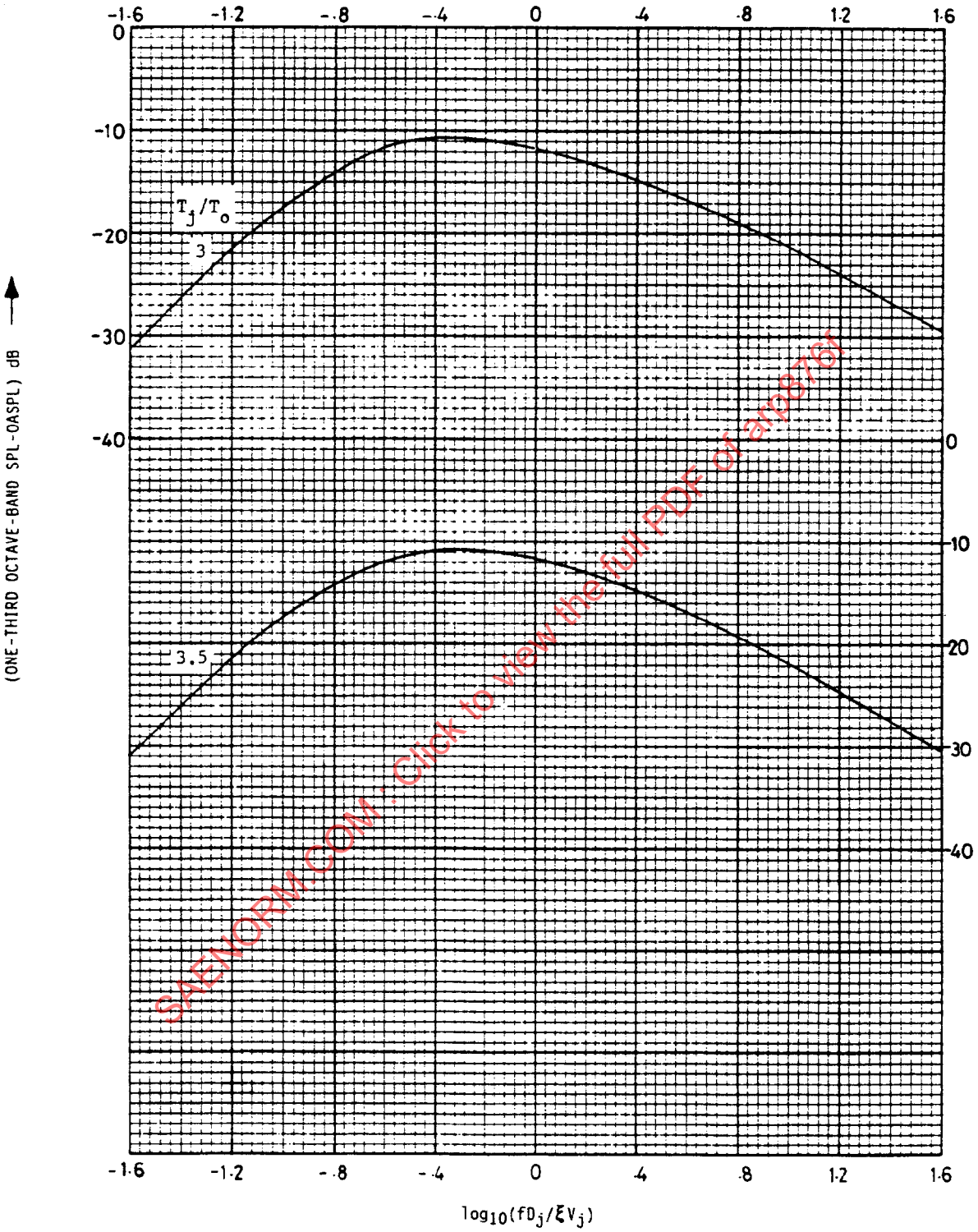

FIGURE 6 (CONTINUED)

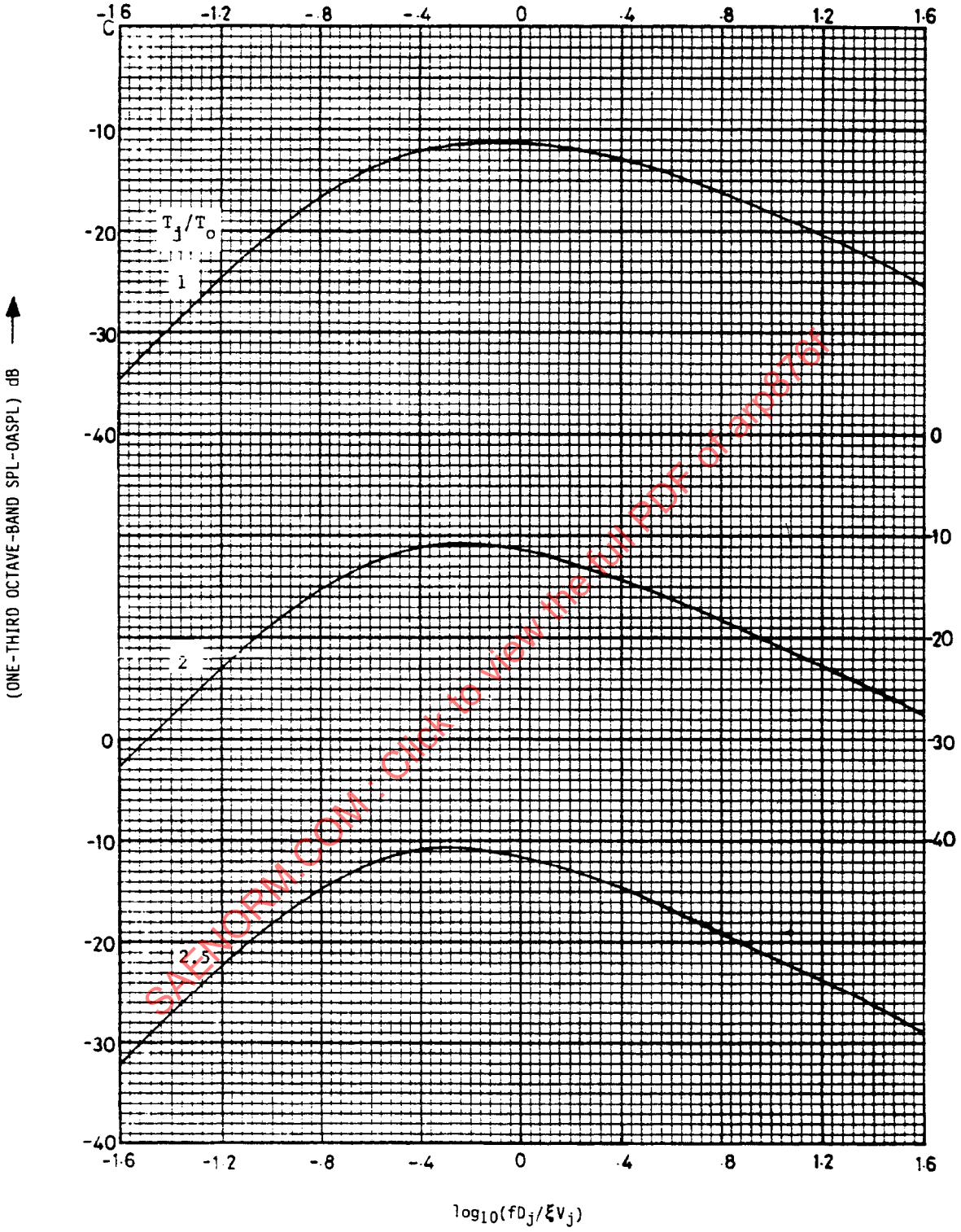

FIGURE 7 - ONE-THIRD OCTAVE-BAND NORMALIZED SPECTRA θ_l = 110 DEGREES

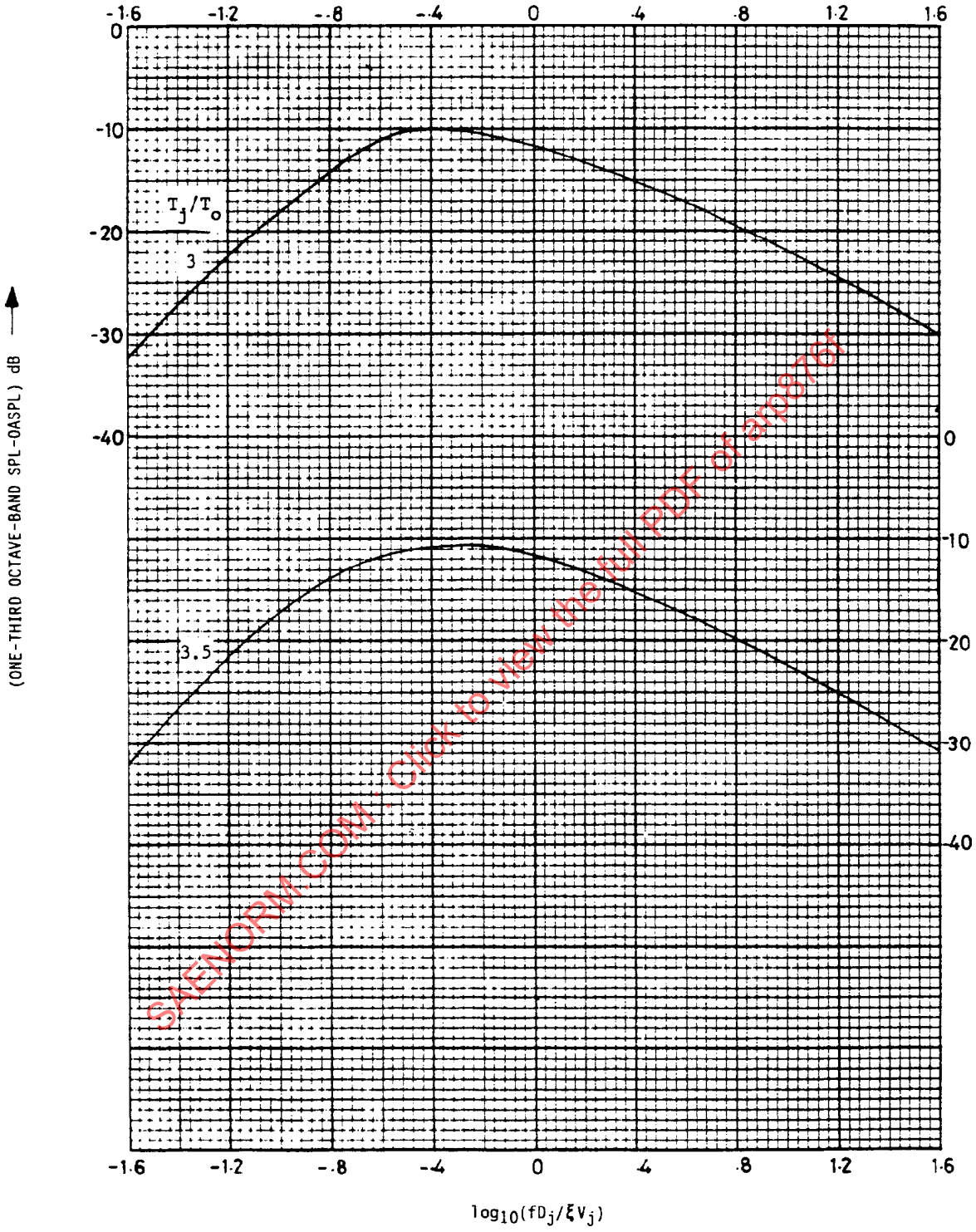

FIGURE 7 (CONTINUED)

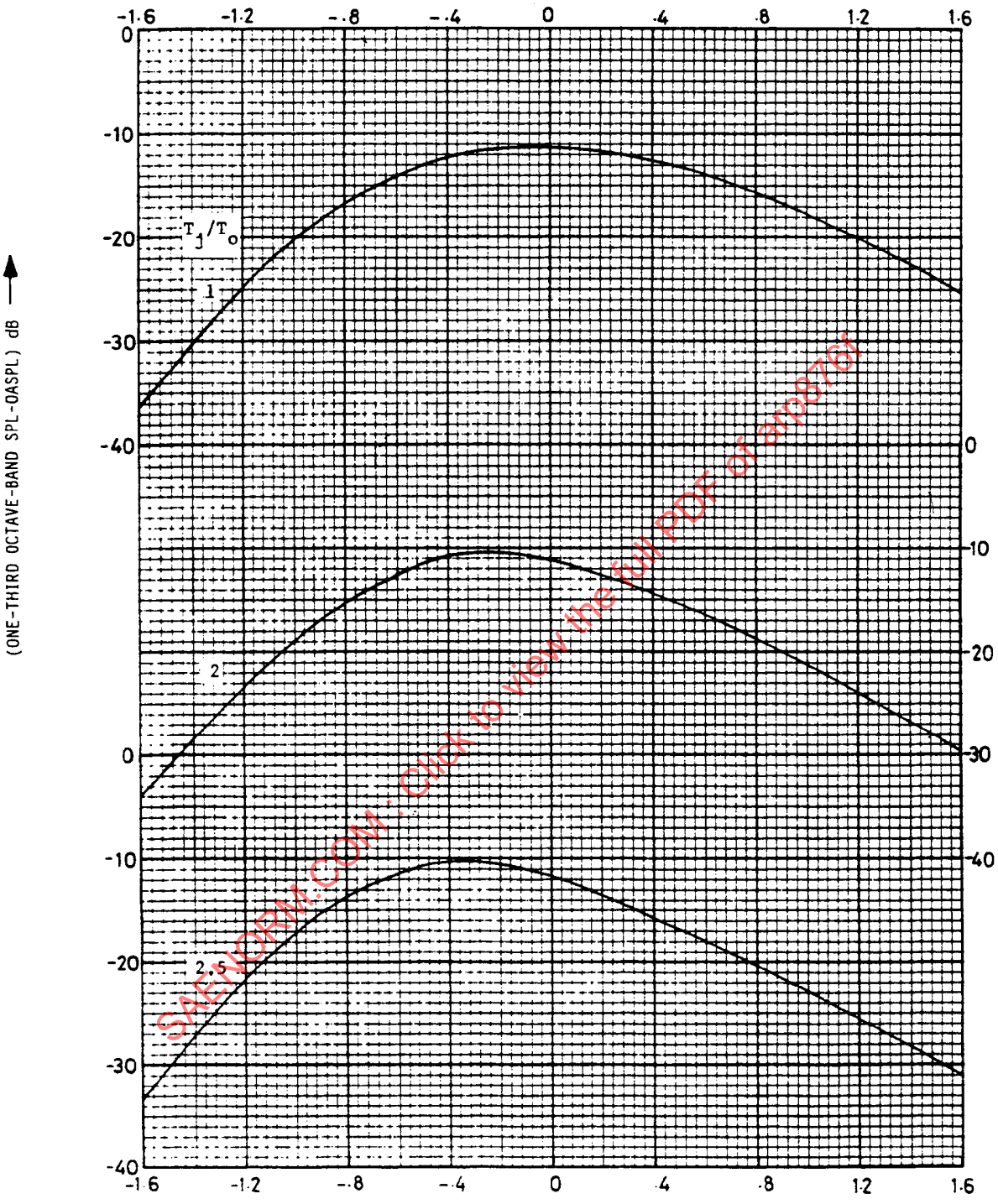

FIGURE 8 - ONE-THIRD OCTAVE-BAND NORMALIZED SPECTRA θ_l = 120 DEGREES

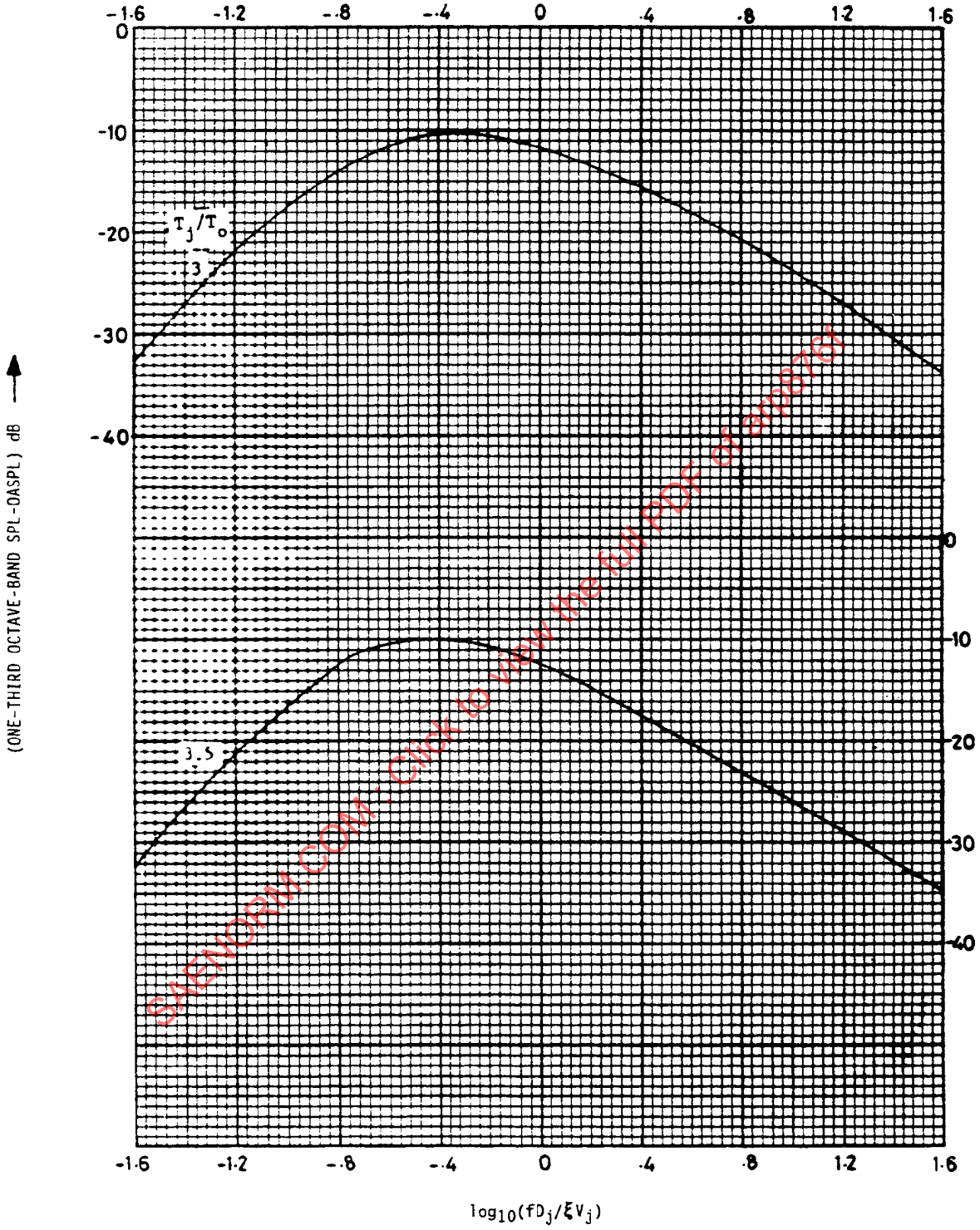

FIGURE 8 (CONTINUED)

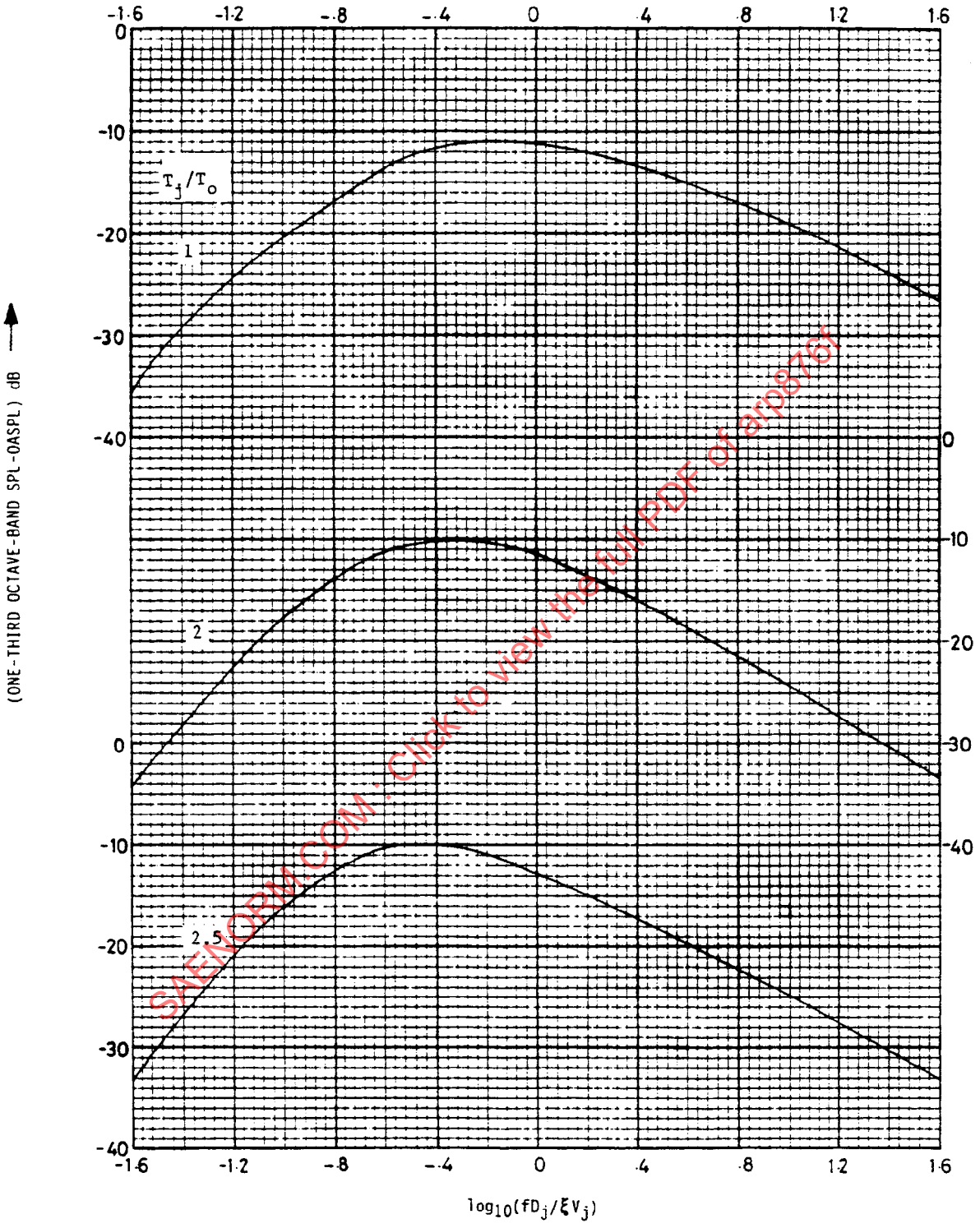

FIGURE 9 - ONE-THIRD OCTAVE-BAND NORMALIZED SPECTRA θ_l = 130 DEGREES

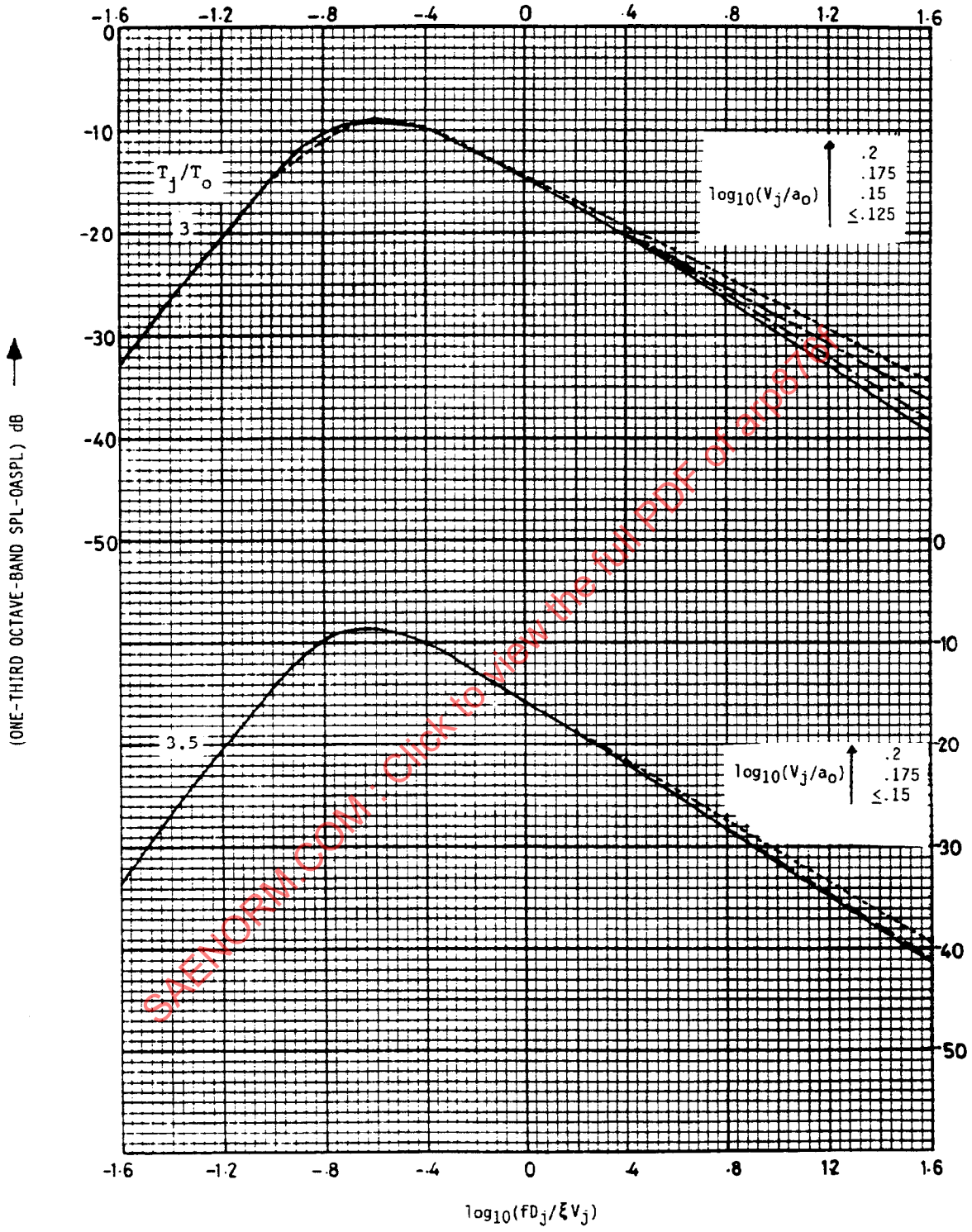

FIGURE 9 (CONTINUED)

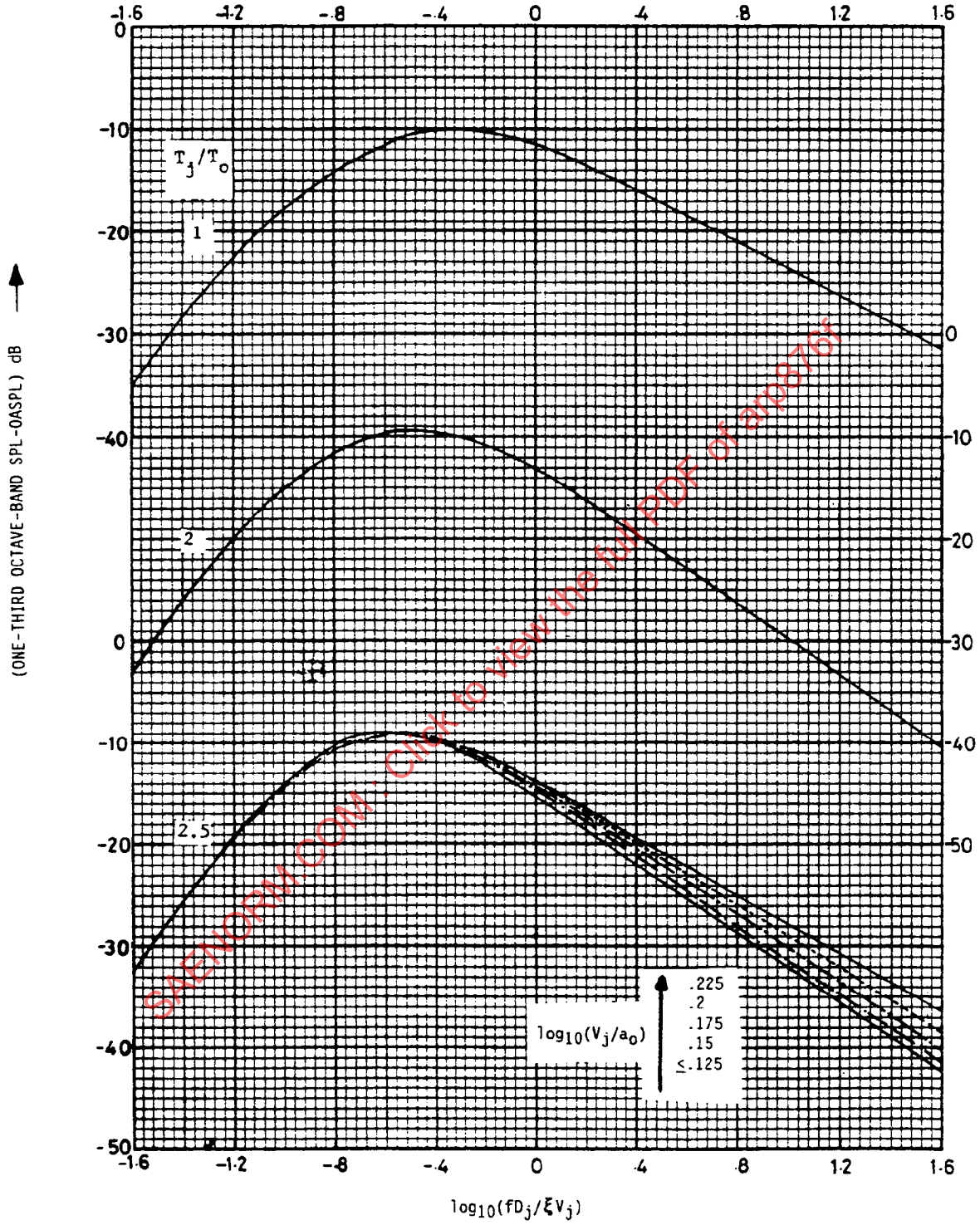

FIGURE 10 - ONE-THIRD OCTAVE-BAND NORMALIZED SPECTRA θ_l = 140 DEGREES

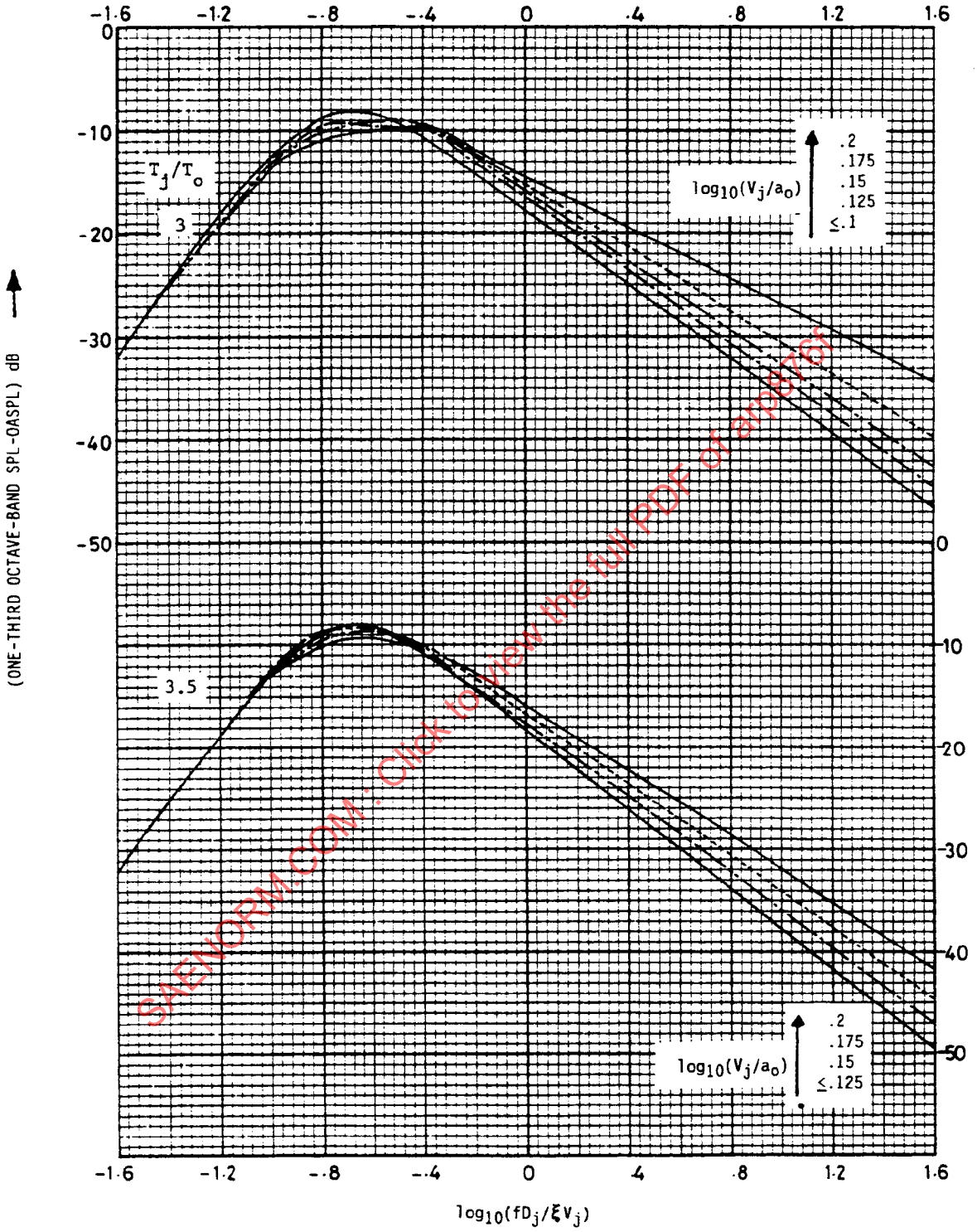

FIGURE 10 (CONTINUED)

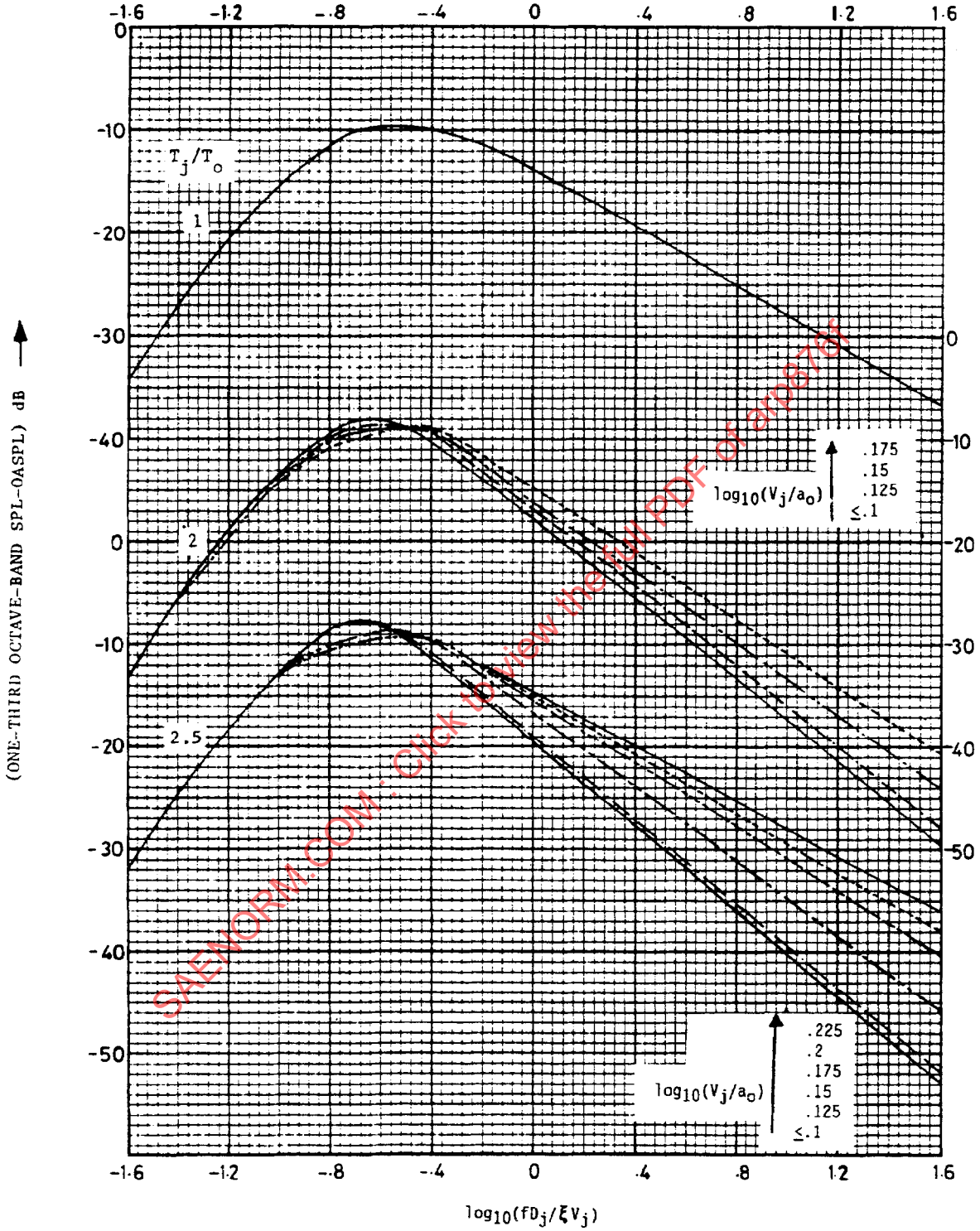

FIGURE 11 - ONE-THIRD OCTAVE-BAND NORMALIZED SPECTRA θ_l = 150 DEGREES

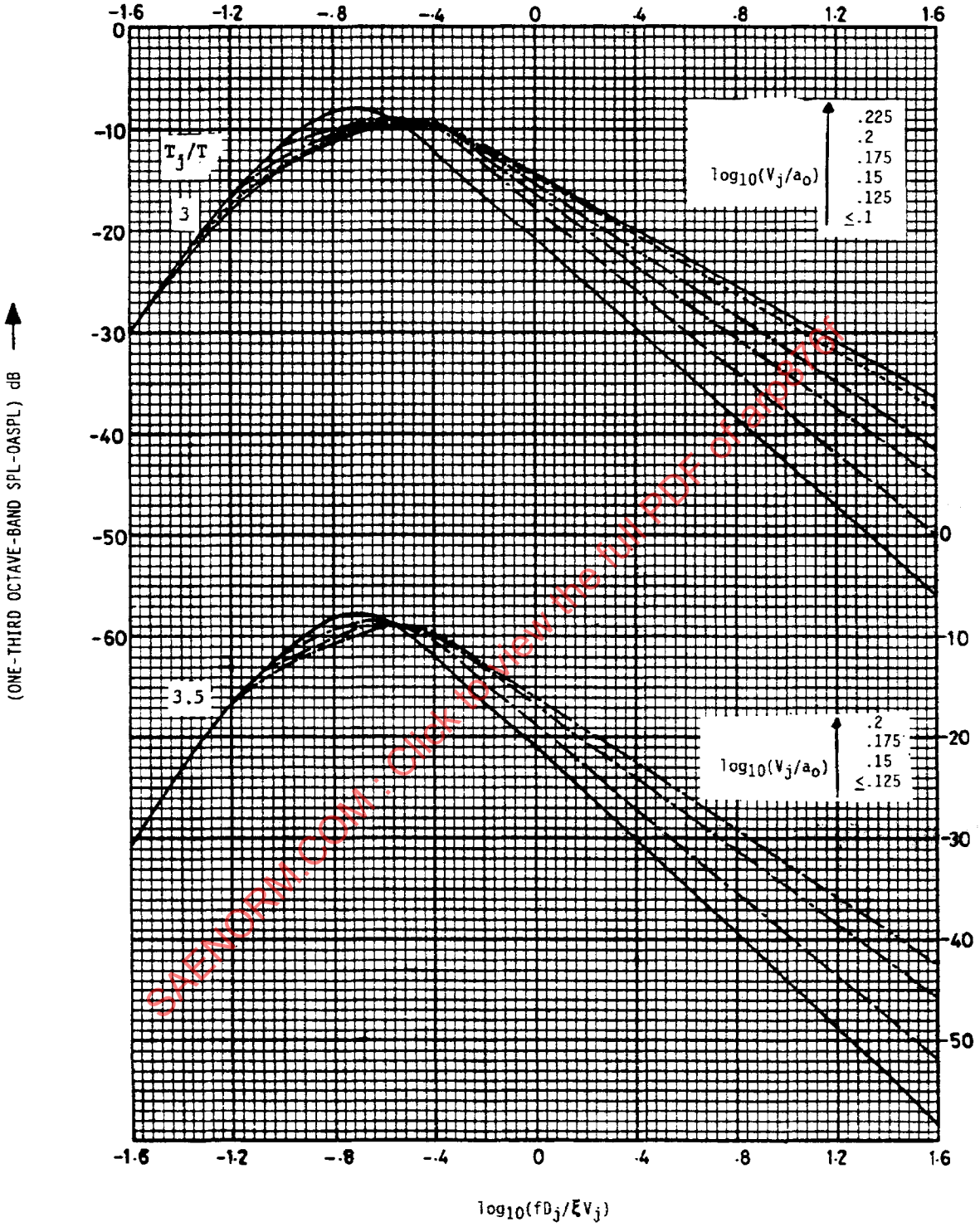

FIGURE 11 (CONTINUED)

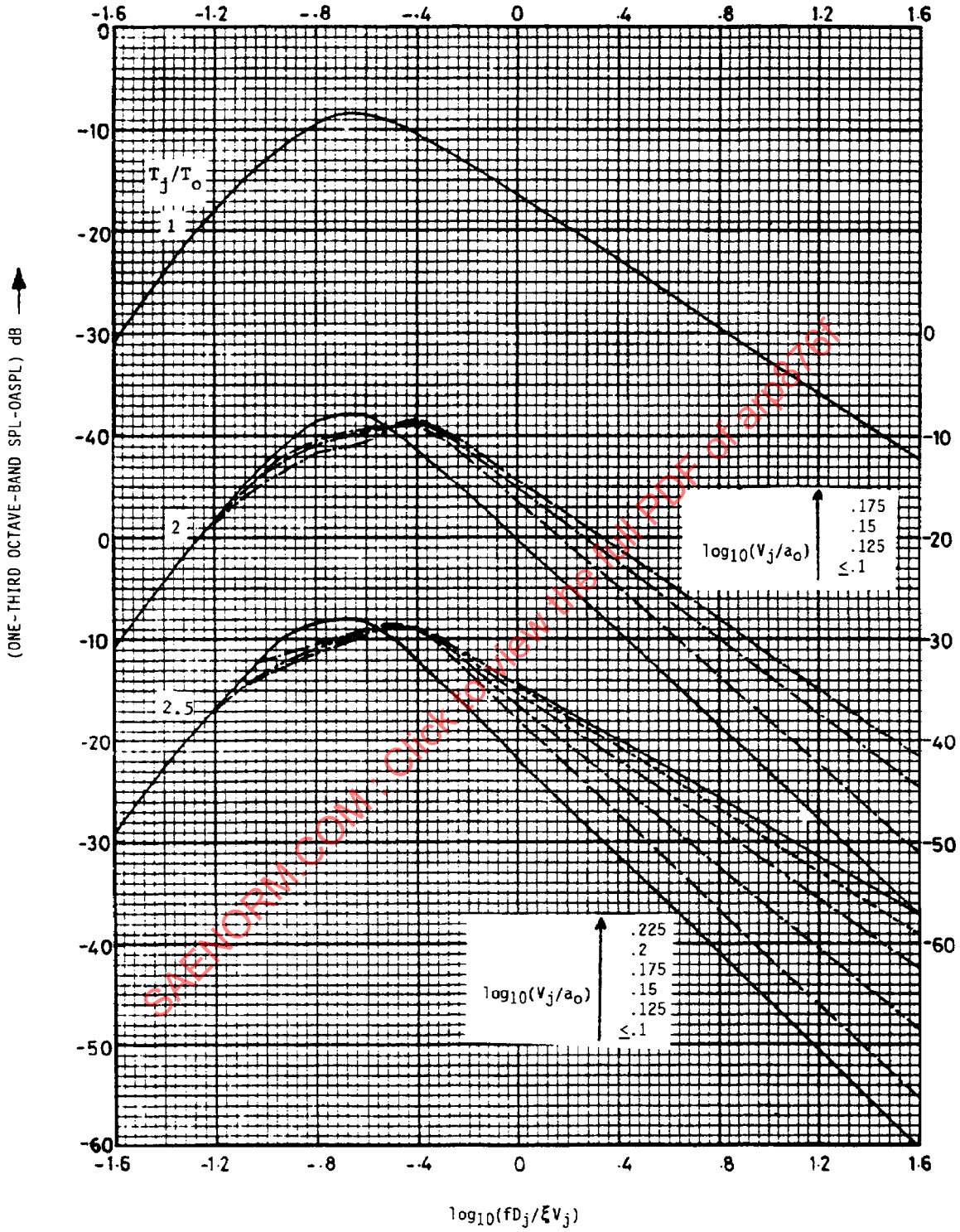

FIGURE 12 - ONE-THIRD OCTAVE-BAND NORMALIZED SPECTRA θ_l = 160 DEGREES

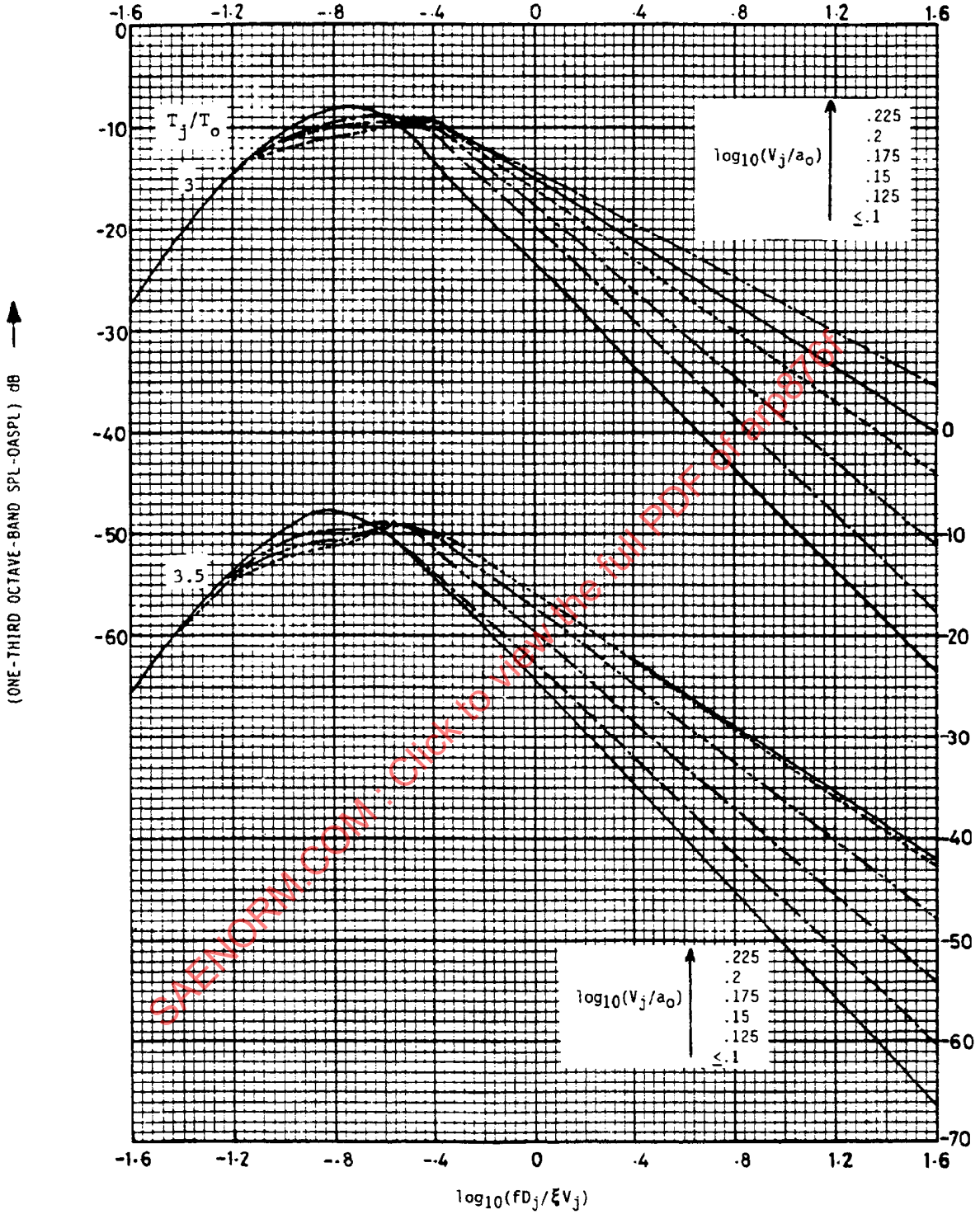

FIGURE 12 (CONTINUED)

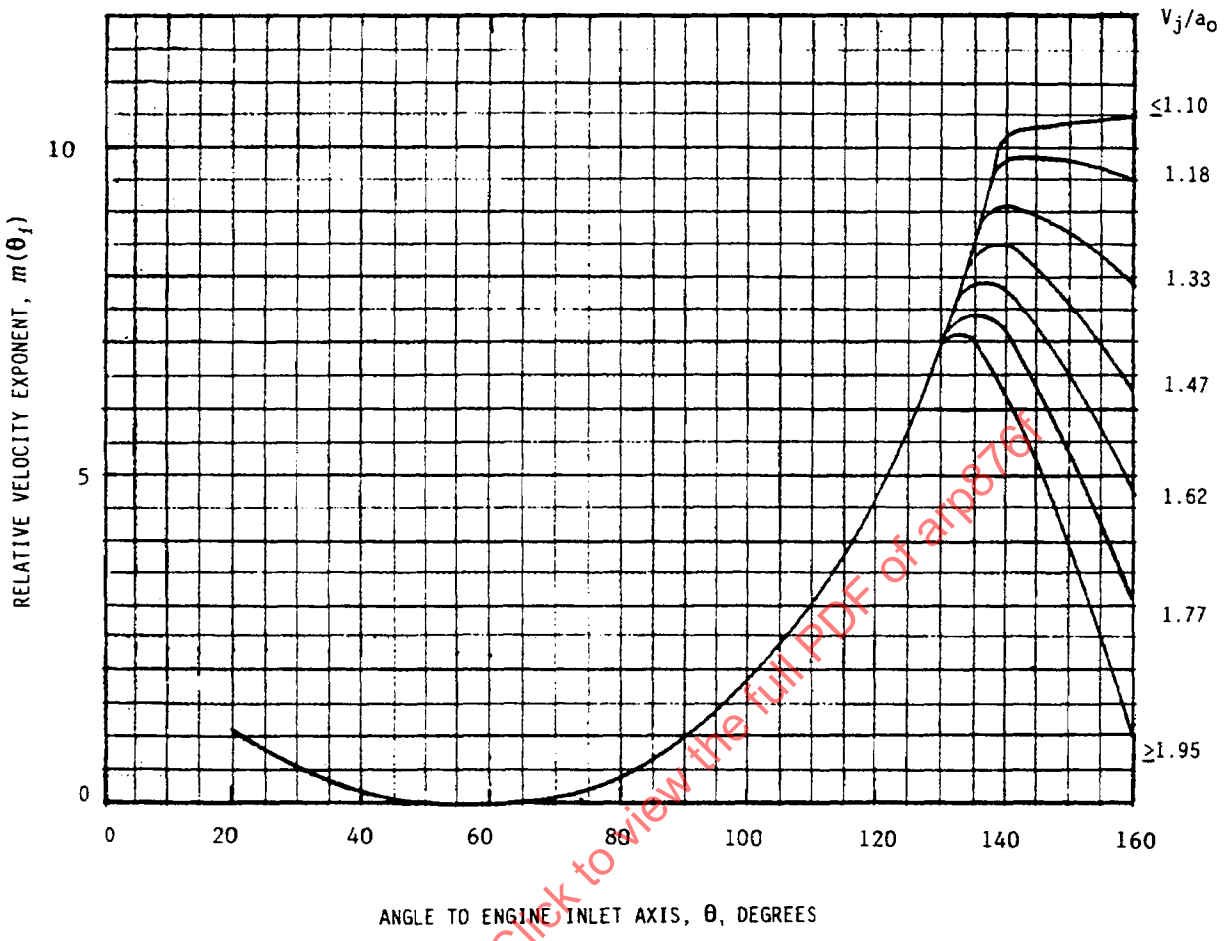

FIGURE 13 - VARIATION OF VELOCITY EXPONENT $M(\theta_I)$ WITH ANGLE θ_I AND JET MACH NUMBER V_J/A_O

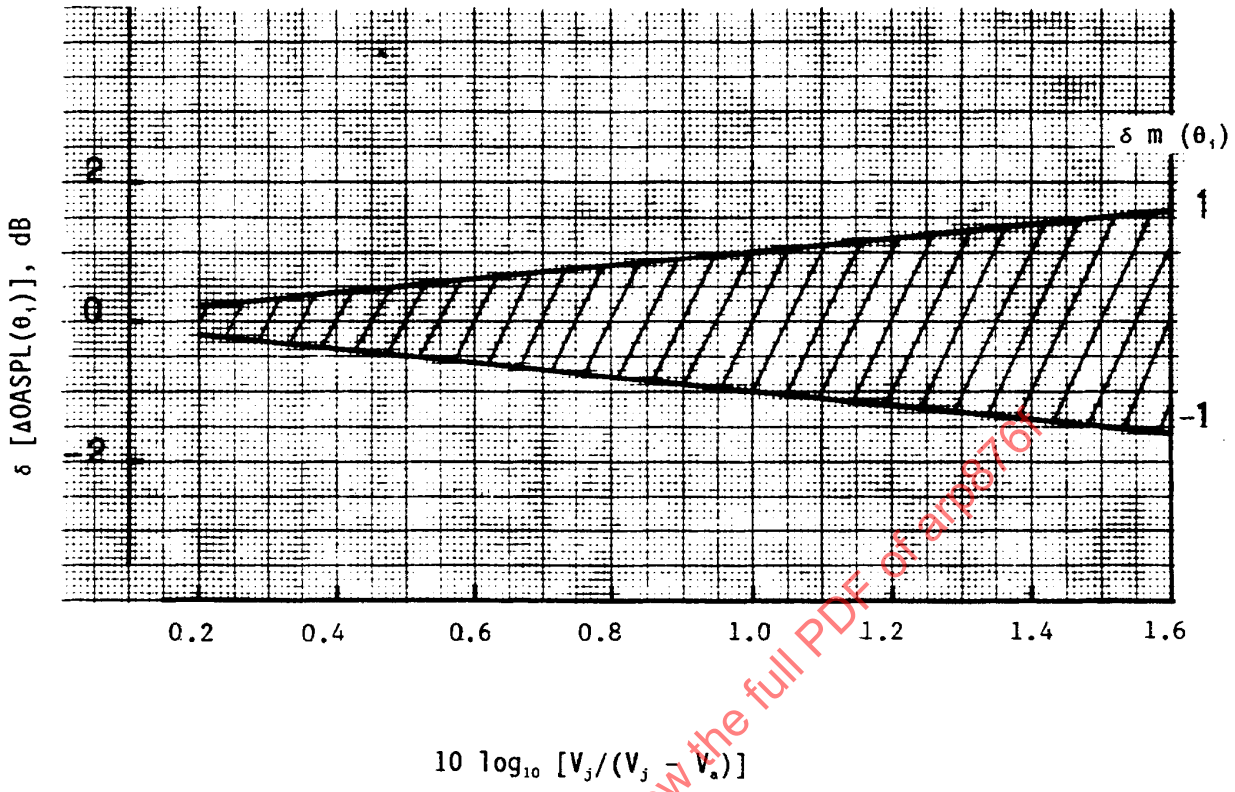

FIGURE 14 - ESTIMATED RANGE OF UNCERTAINTY ASSOCIATED WITH CALCULATED VALUES OF Δ OASPL (θ_l) FOR VARIOUS JET VELOCITY RATIOS AND UNCERTAINTY IN M(θ_l)

TABLE 1 - VARIABLE DENSITY INDEX ω
(REFERENCE FIGURE 2)

$\log_{10}(V_j/a_o)$	ω
-0.4	-0.90
-0.35	-0.76
-0.3	-0.58
-0.25	-0.41
-0.20	-0.22
-0.15	0.0
-0.10	+0.22
-0.05	+0.50
0.0	+0.77
+0.05	+1.07
+0.10	+1.39
+0.15	+1.74
+0.20	+1.95
+0.25	+2.0
+0.30	+2.0
+0.35	+2.0
+0.40	+2.0

NOTE: The values of ω in this table have been derived from rig data where jet temperature T_j varied from 288 to 1100 K.

TABLE 2 - PURE JET MIXING NOISE
NORMALIZED POLAR OASPL (DB) VALUES (REFERENCE FIGURE 3)

$\log_{10}(V_j/a_o)$	θ_1, Angle to Inlet														
	20	30	40	50	60	70	80	90	100	110	120	130	140	150	160
-.4	106.6	107.0	107.2	107.5	108.0	108.4	108.8	109.5	110.2	111.2	112.3	113.2	114.0	114.6	114.9
-.35	110.1	110.5	111.0	111.3	111.5	112.1	112.5	113.2	113.9	115.0	116.1	117.2	118.2	118.7	119.2
-.30	113.7	114.1	114.5	115.0	115.4	115.8	116.3	116.8	117.7	118.7	120.0	121.2	122.2	122.9	123.4
-.25	117.3	117.7	118.2	118.5	118.8	119.4	120.0	120.6	121.5	122.6	123.9	125.3	126.5	127.3	127.7
-.20	121.0	121.3	121.7	122.0	122.5	123.0	123.6	124.3	125.3	126.5	128.0	129.5	130.6	131.5	131.9
-.15	124.7	125.0	125.5	125.8	126.2	126.6	127.3	128.1	129.2	130.5	132.1	133.8	135.0	136.0	136.3
-.10	128.4	128.7	129.1	129.5	130.0	130.4	131.0	131.8	133.0	134.5	136.4	138.0	139.5	140.4	140.7
-.05	132.1	132.4	132.8	133.1	133.7	133.9	134.7	135.7	136.9	138.7	140.7	142.7	144.3	145.4	145.3
0	136.0	136.1	136.4	136.7	137.1	137.7	138.4	139.4	140.9	142.8	145.0	147.5	149.3	150.4	150.2
+.05	139.9	140.0	140.3	140.6	141.0	141.4	142.3	143.3	145.0	147.1	149.6	152.3	154.8	156.1	155.4
+.10	143.9	144.0	144.1	144.3	144.6	145.2	146.1	147.4	149.0	151.4	154.2	157.4	160.3	161.9	161.0
+.15	147.5	147.8	148.0	148.3	148.8	149.3	150.3	151.5	153.3	155.8	159.0	162.8	165.8	167.0	165.8
+.20	151.3	151.5	151.9	152.4	152.9	153.7	154.6	155.9	157.7	160.4	164.2	168.5	171.1	171.3	170.0
+.25	154.8	155.2	155.5	156.0	156.7	157.5	158.5	159.9	161.7	164.8	168.8	173.6	175.7	174.9	172.6
+.30	158.1	158.5	159.0	159.5	160.2	161.1	162.2	163.7	165.8	168.9	173.4	178.0	179.6	177.8	174.6
+.35	161.3	161.6	162.1	162.7	163.3	164.3	165.5	167.1	169.3	172.7	177.2	181.5	182.5	180.1	176.2
+.4	164.3	164.5	164.9	165.4	166.0	167.0	168.3	170.0	172.5	176.4	180.6	184.2	183.8	181.4	177.5

TABLE 3 - ADJUSTMENT FACTOR FOR NORMALIZED FREQUENCY

	Values of ξ (see Figure 4)					
(V_j/a_o)	$\theta_i \leq 120$ degrees	130 degrees	135 degrees	140 degrees	150 degrees	160 degrees
1.4	1.0	1.0	1.0	1.0	1.0	1.0
1.5	1.0	1.0	1.0	1.0	1.0	0.995
1.6	1.0	1.0	1.0	1.0	1.0	0.885
1.7	1.0	1.0	1.0	1.0	0.965	0.76
1.8	1.0	1.0	1.0	0.99	0.87	0.66
1.9	1.0	1.0	1.0	0.95	0.775	0.59
2.0	1.0	1.0	0.981	0.90	0.71	0.54
2.1	1.0	1.0	0.955	0.86	0.66	0.5
2.2	1.0	1.0	0.920	0.83	0.63	0.47
2.3	1.0	0.985	0.895	0.81	0.61	0.445
2.4	1.0	0.970	0.88	0.795	0.595	0.43
2.5	1.0	0.955	0.87	0.79	0.59	0.420

For $(V_j/a_o) < 1.4$, $\xi = 1.0$ for all angles

TABLE 4 - GAS TURBINE JET EXHAUST NOISE PREDICTION
θ_I ANGLE TO INTAKE ≤ 90 DEGREES

$\log_{10}(fD_i/\xi V_i)$	One-Third Octave-Band Sound Pressure Level (SPL-OASPL) dB				
-1.60	-32.95	-30.09	-30.12	-30.33	-30.23
-1.50	-30.75	-27.91	-27.88	-28.15	-28.04
-1.40	-28.53	-25.83	-25.71	-25.95	-25.81
-1.30	-26.35	-23.79	-23.62	-23.83	-23.63
-1.20	-24.31	-21.77	-21.66	-21.85	-21.57
-1.10	-22.04	-19.85	-19.80	-19.73	-19.41
-1.00	-19.65	-18.09	-18.02	-17.53	-17.23
-0.90	-17.95	-16.64	-16.39	-15.73	-15.47
-0.80	-16.50	-15.24	-14.86	-14.19	-14.00
-0.70	-15.16	-13.80	-13.43	-12.94	-12.84
-0.60	-14.13	-12.57	-12.40	-11.91	-11.81
-0.50	-13.05	-11.79	-11.52	-11.23	-11.23
-0.40	-12.26	-11.30	-11.03	-10.93	-10.83
-0.30	-11.84	-10.99	-10.62	-10.93	-10.83
-0.20	-11.42	-11.00	-10.88	-11.07	-10.84
-0.10	-11.35	-11.12	-11.10	-11.24	-11.13
0.0	-11.35	-11.40	-11.42	-11.53	-11.63
0.10	-11.46	-11.84	-11.94	-12.04	-12.20
0.20	-11.78	-12.44	-12.60	-12.71	-12.86
0.30	-12.24	-13.16	-13.37	-13.51	-13.62
0.40	-12.79	-13.96	-14.23	-14.40	-14.49
0.50	-13.39	-14.79	-15.14	-15.36	-15.46
0.60	-14.08	-15.68	-16.13	-16.40	-16.62
0.70	-14.90	-16.63	-17.20	-17.55	-17.93
0.80	-15.81	-17.64	-18.33	-18.75	-19.33
0.90	-16.80	-18.70	-19.51	-19.99	-20.75
1.00	-17.85	-19.80	-20.72	-21.23	-22.13
1.10	-18.94	-20.95	-21.96	-22.48	-23.45
1.20	-20.10	-22.13	-23.24	-23.74	-24.78
1.30	-21.32	-23.36	-24.55	-25.03	-26.12
1.40	-22.60	-24.63	-25.91	-26.34	-27.45
1.50	-23.94	-25.95	-27.29	-27.68	-28.79
1.60	-25.35	-27.31	-28.72	-29.03	-30.13
(T_j/T_o)	1.00	2.00	2.50	3.00	3.50
$\log_{10}(V_j/a_o)$	≤0.400	≤0.400	≤0.400	≤0.400	≤0.400

TABLE 5 - GAS TURBINE JET EXHAUST NOISE PREDICTION
θ_I ANGLE TO INTAKE = 100 DEGREES

$\log_{10}(fD_i/\xi V_i)$	One-Third Octave-Band Sound Pressure Level (SPL-OASPL) dB				
-1.60	-33.07	-31.77	-31.12	-31.11	-30.96
-1.50	-30.81	-29.34	-28.67	-28.79	-28.66
-1.40	-28.56	-26.95	-26.34	-26.50	-26.33
-1.30	-26.37	-24.67	-24.12	-24.31	-24.06
-1.20	-24.32	-22.66	-22.09	-22.31	-21.95
-1.10	-22.13	-20.17	-20.13	-20.25	-19.65
-1.00	-19.87	-17.47	-18.22	-18.10	-17.26
-0.90	-18.06	-16.26	-16.47	-16.04	-15.44
-0.80	-16.53	-15.13	-14.83	-14.21	-13.91
-0.70	-15.28	-13.58	-13.33	-12.82	-12.67
-0.60	-14.15	-12.45	-12.20	-11.69	-11.85
-0.50	-13.37	-11.47	-11.42	-10.91	-11.26
-0.40	-12.39	-10.78	-10.82	-10.61	-10.87
-0.30	-11.67	-10.57	-10.72	-10.61	-10.66
-0.20	-11.27	-10.58	-10.73	-10.76	-10.81
-0.10	-11.27	-10.92	-10.97	-11.16	-11.11
0.0	-11.27	-11.47	-11.42	-11.71	-11.56
0.10	-11.40	-12.09	-11.99	-12.33	-12.15
0.20	-11.74	-12.82	-12.70	-13.04	-12.86
0.30	-12.23	-13.63	-13.52	-13.82	-13.67
0.40	-12.80	-14.49	-14.41	-14.68	-14.59
0.50	-13.42	-15.38	-15.33	-15.63	-15.61
0.60	-14.12	-16.32	-16.32	-16.68	-16.78
0.70	-14.93	-17.30	-17.37	-17.83	-18.07
0.80	-15.84	-18.33	-18.48	-19.03	-19.43
0.90	-16.83	-19.39	-19.63	-20.27	-20.81
1.00	-17.87	-20.48	-20.82	-21.51	-22.16
1.10	-18.97	-21.59	-22.04	-22.75	-23.48
1.20	-20.13	-22.73	-23.30	-24.02	-24.81
1.30	-21.35	-23.90	-24.60	-25.31	-26.14
1.40	-22.63	-25.10	-25.93	-26.62	-27.48
1.50	-23.97	-26.33	-27.31	-27.95	-28.82
1.60	-25.37	-27.58	-28.72	-29.31	-30.16
(T_j/T_o)	1.00	2.00	2.50	3.00	3.50
$\log_{10}(V_j/a_o)$	≤0.400	≤0.400	≤0.400	≤0.400	≤0.400

TABLE 6 - GAS TURBINE JET EXHAUST NOISE PREDICTION
θ_I ANGLE TO INTAKE = 110 DEGREES

$\log_{10}(fD_i/\xi V_i)$	One-Third Octave-Band Sound Pressure Level (SPL-OASPL) dB				
-1.60	-34.57	-32.82	-32.12	-32.30	-32.03
-1.50	-32.12	-30.26	-29.55	-30.12	-29.36
-1.40	-29.69	-27.74	-27.08	-28.14	-26.64
-1.30	-27.27	-25.32	-24.72	-26.00	-24.03
-1.20	-24.87	-23.10	-22.58	-23.43	-21.69
-1.10	-22.40	-20.93	-20.41	-20.73	-19.26
-1.00	-19.97	-18.82	-18.22	-18.10	-16.83
-0.90	-18.18	-16.93	-16.26	-16.04	-15.17
-0.80	-16.57	-15.24	-14.54	-14.31	-13.82
-0.70	-14.98	-13.84	-13.14	-12.81	-12.64
-0.60	-13.75	-12.60	-12.10	-11.70	-11.52
-0.50	-12.67	-11.53	-11.22	-11.05	-11.03
-0.40	-12.08	-10.93	-10.63	-10.70	-10.64
-0.30	-11.57	-10.63	-10.52	-10.50	-10.53
-0.20	-11.45	-10.54	-10.67	-10.52	-10.69
-0.10	-11.39	-10.83	-10.92	-10.98	-11.02
0.0	-11.37	-11.33	-11.32	-11.70	-11.53
0.10	-11.50	-11.90	-11.96	-12.40	-12.24
0.20	-11.83	-12.56	-12.79	-13.16	-13.12
0.30	-12.32	-13.32	-13.73	-13.99	-14.11
0.40	-12.90	-14.15	-14.74	-14.91	-15.18
0.50	-13.51	-15.05	-15.76	-15.95	-16.29
0.60	-14.21	-16.04	-16.81	-17.14	-17.48
0.70	-15.03	-17.13	-17.93	-18.44	-18.76
0.80	-15.94	-18.26	-19.08	-19.81	-20.08
0.90	-16.93	-19.41	-20.25	-21.18	-21.42
1.00	-17.97	-20.54	-21.42	-22.50	-22.73
1.10	-19.06	-21.65	-22.59	-23.77	-24.02
1.20	-20.22	-22.78	-23.77	-25.03	-25.32
1.30	-21.44	-23.91	-24.97	-26.29	-26.62
1.40	-22.72	-25.04	-26.17	-27.53	-27.92
1.50	-24.06	-26.19	-27.39	-28.77	-29.22
1.60	-25.47	-27.34	-28.62	-30.00	-30.53
(T_j/T_o)	1.00	2.00	2.50	3.00	3.50
$\log_{10}(V_j/a_o)$	≤0.400	≤0.400	≤0.400	≤0.400	≤0.400

TABLE 7 - GAS TURBINE JET EXHAUST NOISE PREDICTION
θ_I ANGLE TO INTAKE = 120 DEGREES

$\log_{10}(fD_i/\xi V_i)$	One-Third Octave-Band Sound Pressure Level (SPL-OASPL) dB				
-1.60	-36.37	-33.75	-33.11	-32.50	-32.27
-1.50	-33.31	-31.00	-30.17	-29.66	-29.32
-1.40	-30.18	-28.25	-27.25	-26.97	-26.44
-1.30	-27.27	-25.65	-24.51	-24.50	-23.66
-1.20	-24.82	-23.35	-22.16	-22.52	-21.11
-1.10	-22.49	-21.13	-19.75	-20.30	-18.56
-1.00	-20.27	-18.95	-17.31	-17.80	-16.06
-0.90	-18.50	-16.88	-15.31	-15.63	-13.99
-0.80	-16.87	-15.06	-13.63	-13.82	-12.31
-0.70	-15.29	-13.66	-12.32	-12.51	-11.17
-0.60	-14.05	-12.43	-11.29	-11.28	-10.45
-0.50	-13.07	-11.35	-10.61	-10.60	-10.06
-0.40	-12.28	-10.76	-10.31	-10.30	-9.97
-0.30	-11.77	-10.46	-10.31	-10.30	-10.17
-0.20	-11.53	-10.37	-10.47	-10.46	-10.71
-0.10	-11.35	-10.65	-10.98	-10.88	-11.40
0.0	-11.27	-11.16	-11.71	-11.50	-12.27
0.10	-11.39	-11.79	-12.56	-12.29	-13.38
0.20	-11.71	-12.55	-13.54	-13.23	-14.67
0.30	-12.17	-13.42	-14.61	-14.30	-16.06
0.40	-12.72	-14.38	-15.74	-15.46	-17.49
0.50	-13.31	-15.41	-16.87	-16.69	-18.89
0.60	-14.01	-16.55	-18.03	-18.04	-20.29
0.70	-14.82	-17.79	-19.24	-19.50	-21.72
0.80	-15.74	-19.08	-20.48	-21.02	-23.17
0.90	-16.73	-20.39	-21.74	-22.56	-24.62
1.00	-17.77	-21.67	-23.00	-24.10	-26.07
1.10	-18.87	-22.94	-24.28	-25.63	-27.51
1.20	-20.02	-24.21	-25.58	-27.17	-28.96
1.30	-21.24	-25.49	-26.88	-28.73	-30.41
1.40	-22.52	-26.78	-28.21	-30.31	-31.86
1.50	-23.87	-28.08	-29.55	-31.90	-33.31
1.60	-25.27	-29.38	-30.90	-33.50	-34.77
(T_j/T_o)	1.00	2.00	2.50	3.00	3.50
$\log_{10}(V_j/a_o)$	≤0.400	≤0.400	≤0.400	≤0.400	≤0.400

TABLE 8 - GAS TURBINE JET EXHAUST NOISE PREDICTION
θ_I ANGLE TO INTAKE = 130 DEGREES

$\log_{10}(fD_j/\xi V_j)$	One-Third Octave-Band Sound Pressure Level (SPL-OASPL) dB									
-1.60	-35.40	-34.33	-33.16	-32.65	-32.67	-32.69	-32.70	-33.44	-33.44	-33.45
-1.50	-32.25	-31.23	-29.91	-29.53	-29.55	-29.57	-29.58	-30.18	-30.18	-30.19
-1.40	-29.26	-28.17	-26.69	-26.54	-26.55	-26.57	-26.59	-26.93	-26.93	-26.94
-1.30	-26.50	-25.23	-23.66	-23.65	-23.67	-23.69	-23.70	-23.74	-23.74	-23.75
-1.20	-24.17	-22.51	-21.01	-21.04	-21.05	-21.08	-21.09	-20.69	-20.69	-20.70
-1.10	-22.02	-19.97	-18.51	-18.01	-18.02	-18.04	-18.06	-17.45	-17.45	-17.46
-1.00	-20.00	-17.63	-16.16	-14.65	-14.66	-14.69	-14.70	-14.14	-14.14	-14.15
-0.90	-18.24	-15.60	-14.14	-11.87	-11.88	-11.90	-12.58	-11.37	-11.37	-11.50
-0.80	-16.60	-13.82	-12.35	-10.05	-10.06	-10.08	-11.15	-9.51	-9.51	-9.70
-0.70	-15.01	-12.34	-10.87	-9.36	-9.37	-9.39	-9.71	-8.74	-8.74	-8.75
-0.60	-13.77	-11.21	-10.15	-9.15	-9.16	-9.19	-8.70	-8.64	-8.64	-8.65
-0.50	-12.50	-10.43	-9.76	-9.25	-9.27	-9.29	-9.00	-9.04	-9.06	-8.95
-0.40	-11.61	-10.14	-9.85	-9.94	-9.95	-9.97	-9.78	-10.21	-10.21	-10.23
-0.30	-10.99	-10.14	-10.17	-10.87	-10.88	-10.90	-10.91	-11.45	-11.45	-11.46
-0.20	-10.80	-10.21	-10.84	-11.92	-11.93	-11.95	-11.97	-12.64	-12.64	-12.65
-0.10	-10.84	-10.70	-11.73	-13.25	-13.26	-13.23	-13.29	-14.15	-14.15	-14.16
0.0	-11.00	-11.44	-12.76	-14.66	-14.67	-14.69	-14.70	-15.74	-15.74	-15.75
0.10	-11.35	-12.40	-13.89	-16.08	-16.08	-16.08	-16.02	-17.30	-17.31	-17.25
0.20	-11.91	-13.54	-15.06	-17.54	-17.50	-17.45	-17.20	-18.87	-18.88	-18.68
0.30	-12.61	-14.80	-16.27	-19.01	-18.92	-18.80	-18.31	-20.44	-20.45	-20.06
0.40	-13.38	-16.13	-17.50	-20.50	-20.36	-20.15	-19.41	-22.02	-22.03	-21.45
0.50	-14.18	-17.46	-18.75	-22.00	-21.80	-21.50	-20.58	-23.61	-23.60	-22.89
0.60	-15.02	-18.83	-20.04	-23.51	-23.26	-22.85	-21.79	-25.19	-25.17	-24.37
0.70	-15.93	-20.27	-21.36	-25.03	-24.73	-24.19	-23.01	-26.77	-26.73	-25.86
0.80	-16.89	-21.73	-22.69	-26.56	-26.21	-25.53	-24.24	-28.35	-28.30	-27.36
0.90	-17.92	-23.21	-24.03	-28.11	-27.69	-26.86	-25.47	-29.94	-29.87	-28.86
1.00	-19.00	-24.66	-25.36	-29.66	-29.17	-28.19	-26.71	-31.54	-31.44	-30.35
1.10	-20.12	-26.09	-26.67	-31.22	-30.66	-29.53	-27.95	-33.15	-33.02	-31.83
1.20	-21.30	-27.53	-27.97	-32.79	-32.16	-30.87	-29.19	-34.76	-34.60	-33.31
1.30	-22.52	-28.96	-29.27	-34.37	-33.66	-32.20	-30.44	-36.38	-36.19	-34.78
1.40	-23.80	-30.39	-30.57	-35.96	-35.16	-33.53	-31.69	-37.99	-37.77	-36.24
1.50	-25.12	-31.83	-31.86	-37.55	-36.67	-34.87	-32.95	-39.61	-39.36	-37.70
1.60	-26.50	-33.26	-33.15	-39.16	-38.18	-36.20	-34.21	-41.24	-40.95	-39.16
(T_j/T_o)	1.00	2.00	2.50	3.00	3.00	3.00	3.00	3.50	3.50	3.50
$\log_{10}(V_j/a_o)$	≤0.400	≤0.400	≤0.400	≤0.125	0.150	0.175	0.200	≤0.150	0.175	0.200

TABLE 9A - GAS TURBINE JET EXHAUST NOISE PREDICTION
θ_I ANGLE TO INTAKE = 140 DEGREES

$\log_{10}(fD_j/\xi V_j)$	One-Third Octave-Band Sound Pressure Level (SPL-OASPL) dB												
-1.60	-35.00	-32.65	-32.39	-32.45	-32.63	-32.73	-32.80	-31.96	-31.60	-31.66	-31.67	-31.77	
-1.50	-31.51	-29.09	-28.90	-28.95	-29.14	-29.23	-29.30	-28.59	-28.23	-28.29	-28.30	-28.40	
-1.40	-28.16	-25.66	-25.43	-25.49	-25.67	-25.77	-25.84	-25.30	-24.94	-25.00	-25.01	-25.10	
-1.30	-25.10	-22.55	-22.19	-22.25	-22.43	-22.53	-22.60	-22.16	-21.80	-21.86	-21.87	-21.97	
-1.20	-22.65	-20.10	-19.42	-19.48	-19.66	-19.76	-19.83	-19.41	-19.06	-19.12	-19.13	-19.22	
-1.10	-20.28	-17.68	-16.69	-16.75	-16.93	-17.03	-17.09	-16.17	-15.84	-15.96	-16.01	-16.16	
-1.00	-17.90	-15.24	-13.99	-14.05	-14.23	-14.33	-14.40	-12.66	-12.50	-12.86	-13.07	-13.47	
-0.90	-15.85	-13.31	-11.73	-12.14	-12.33	-12.43	-12.49	-10.35	-10.60	-11.18	-11.45	-12.01	
-0.80	-14.15	-11.64	-10.08	-10.73	-10.92	-11.01	-11.08	-8.88	-9.60	-10.13	-10.47	-11.04	
-0.70	-12.92	-10.25	-9.20	-9.85	-10.04	-10.14	-10.20	-8.26	-9.20	-9.56	-9.97	-10.46	
-0.60	-11.58	-9.64	-8.99	-9.24	-9.43	-9.53	-9.59	-8.26	-9.70	-9.25	-9.56	-10.05	
-0.50	-10.60	-9.45	-9.09	-9.15	-9.33	-9.43	-9.50	-9.16	-8.30	-8.76	-9.17	-9.57	
-0.40	-10.21	-9.74	-9.88	-9.54	-9.62	-9.72	-9.79	-10.63	-9.70	-9.33	-9.36	-9.46	
-0.30	-9.90	-10.16	-10.90	-10.26	-10.24	-10.34	-10.41	-12.48	-11.33	-11.08	-10.49	-10.38	
-0.20	-10.19	-10.97	-12.20	-11.76	-11.42	-11.49	-11.35	-14.14	-13.17	-12.74	-12.25	-11.76	
-0.10	-10.64	-12.02	-13.65	-13.21	-12.78	-12.67	-12.63	-15.88	-14.70	-14.35	-13.80	-13.02	
0.0	-11.30	-13.26	-15.19	-14.75	-14.23	-13.93	-14.00	-17.66	-16.31	-15.97	-15.28	-14.27	
0.10	-12.23	-14.68	-16.82	-16.33	-15.76	-15.33	-15.33	-19.47	-18.15	-17.65	-16.78	-15.56	
0.20	-13.37	-16.22	-18.52	-17.89	-17.35	-16.81	-16.67	-21.30	-20.06	-19.35	-18.27	-16.87	
0.30	-14.63	-17.84	-20.24	-19.46	-18.96	-18.33	-18.00	-23.13	-21.99	-21.06	-19.75	-18.18	
0.40	-15.93	-19.49	-21.97	-21.07	-20.59	-19.36	-19.35	-24.97	-23.90	-22.77	-21.23	-19.48	
0.50	-17.19	-21.15	-23.68	-22.75	-22.21	-21.36	-20.71	-26.77	-25.72	-24.46	-22.73	-20.76	
0.60	-18.46	-22.83	-25.38	-24.45	-23.82	-22.89	-22.09	-28.56	-27.44	-26.14	-24.23	-22.02	
0.70	-19.76	-24.55	-27.08	-26.14	-25.45	-24.42	-23.47	-20.33	-29.07	-27.81	-25.74	-23.26	
0.80	-21.08	-26.28	-28.78	-27.85	-27.07	-25.95	-24.80	-32.10	-30.67	-29.47	-27.26	-24.49	
0.90	-22.40	-28.03	-30.48	-29.55	-28.71	-27.49	-26.28	-33.87	-32.27	-31.13	-28.77	-25.73	
1.00	-23.70	-29.77	-32.19	-31.26	-30.34	-29.03	-27.70	-35.66	-33.92	-32.78	-30.29	-26.97	
1.10	-24.99	-31.51	-33.90	-32.96	-31.97	-30.58	-29.14	-37.47	-35.61	-34.42	-31.80	-28.22	
1.20	-26.28	-33.25	-35.61	-34.66	-33.60	-32.14	-30.59	-39.29	-37.33	-36.05	-33.32	-29.47	
1.30	-27.57	-35.00	-37.33	-36.36	-35.23	-33.70	-32.05	-41.12	-39.05	-37.67	-34.83	-30.72	
1.40	-28.85	-36.76	-39.05	-38.06	-36.87	-35.27	-33.52	-42.96	-40.79	-39.28	-36.35	-31.97	
1.50	-30.13	-38.51	-40.77	-39.76	-38.50	-36.85	-35.00	-44.81	-42.55	-40.89	-37.87	-33.22	
1.60	-31.40	-40.28	-42.49	-41.46	-40.14	-38.43	-36.50	-46.66	-44.32	-42.48	-39.39	-34.47	
(T_j/T_∞)	1.00	2.00	2.50	2.50	2.50	2.50	2.50	3.00	3.00	3.00	3.00	3.00	
$\log_{10}(V_j/a_\infty)$	≤0.400	≤0.400	≤0.125	0.150	0.175	0.200	0.225	≤0.100	0.125	0.150	0.175	0.200	

TABLE 9B - GAS TURBINE JET EXHAUST NOISE PREDICTION
θ_I ANGLE TO INTAKE = 140 DEGREES

$\log_{10}(fD_i/\xi V_i)$	One-Third Octave-Band Sound Pressure Level (SPL-OASPL) dB				
-1.60	-32.16	-32.14	-31.97	-31.89	-31.75
-1.50	-28.71	-28.69	-28.52	-28.44	-28.30
-1.40	-25.31	-25.29	-25.12	-25.04	-24.90
-1.30	-22.06	-22.04	-21.87	-21.79	-21.65
-1.20	-19.13	-19.11	-18.94	-18.86	-18.72
-1.10	-16.03	-16.02	-15.85	-15.77	-15.63
-1.00	-12.86	-12.84	-12.77	-12.69	-12.65
-0.90	-10.32	-10.34	-10.68	-10.75	-11.08
-0.80	-8.67	-8.77	-9.28	-9.69	-10.27
-0.70	-8.06	-8.24	-8.57	-9.29	-9.85
-0.60	-8.16	-8.24	-8.37	-8.58	-9.13
-0.50	-8.76	-8.64	-8.57	-8.59	-8.45
-0.40	-10.82	-10.70	-10.03	-9.96	-9.82
-0.30	-12.88	-12.66	-12.39	-11.61	-11.17
-0.20	-14.67	-14.55	-14.18	-13.39	-12.81
-0.10	-16.61	-16.43	-15.99	-15.16	-14.39
0.0	-18.56	-18.35	-17.78	-16.89	-15.95
0.10	-20.47	-20.27	-19.56	-18.64	-17.54
0.20	-22.37	-22.19	-21.33	-20.39	-19.12
0.30	-24.27	-24.12	-23.10	-22.13	-20.72
0.40	-26.18	-26.05	-24.88	-23.86	-22.32
0.50	-28.11	-27.99	-26.70	-25.59	-23.92
0.60	-30.07	-29.94	-28.56	-27.30	-25.54
0.70	-32.04	-31.90	-30.44	-28.99	-27.17
0.80	-34.03	-33.86	-32.34	-30.67	-28.81
0.90	-36.00	-35.81	-34.22	-32.37	-30.44
1.00	-37.96	-37.75	-36.09	-34.10	-32.06
1.10	-39.90	-39.67	-37.93	-35.84	-33.67
1.20	-41.83	-41.58	-39.76	-37.60	-35.27
1.30	-43.75	-43.49	-41.58	-39.36	-36.88
1.40	-45.66	-45.39	-43.40	-41.13	-38.48
1.50	-47.57	-47.27	-45.20	-42.91	-40.07
1.60	-49.46	-49.15	-46.99	-44.70	-41.66
(T_j/T_o)	3.50	3.50	3.50	3.50	3.50
$\log_{10}(V_j/a_o)$	≤0.100	0.125	0.150	0.175	0.200

TABLE 10A - GAS TURBINE JET EXHAUST NOISE PREDICTION
θ_I ANGLE TO INTAKE = 150 DEGREES

$\log_{10}(fD_j/\xi V_j)$	One-Third Octave-Band Sound Pressure Level (SPL-OASPL) dB											
-1.60	-34.07	-33.04	-32.98	-33.20	-33.20	-31.93	-31.84	-31.40	-31.60	-31.74	-31.88	-29.85
-1.50	-30.40	-29.37	-29.30	-29.53	-29.52	-28.33	-28.24	-27.80	-28.00	-28.14	-28.27	-26.37
-1.40	-26.80	-25.71	-25.65	-25.88	-25.87	-24.72	-24.63	-24.19	-24.39	-24.53	-24.67	-23.07
-1.30	-23.47	-22.24	-22.18	-22.40	-22.40	-21.33	-21.24	-20.80	-21.00	-21.14	-21.28	-19.85
-1.20	-20.69	-19.09	-19.03	-19.26	-19.25	-18.42	-18.33	-17.89	-18.09	-18.23	-18.37	-16.65
-1.10	-17.96	-16.26	-16.20	-16.42	-16.45	-15.59	-15.50	-15.11	-15.31	-15.45	-15.58	-13.69
-1.00	-15.27	-13.74	-13.67	-13.90	-14.10	-12.83	-12.74	-12.70	-12.90	-13.04	-13.18	-11.15
-0.90	-13.13	-11.51	-11.55	-11.78	-12.20	-10.39	-10.33	-11.24	-11.56	-11.70	-11.84	-9.27
-0.80	-11.37	-9.62	-9.97	-10.20	-10.86	-8.57	-8.62	-10.26	-10.67	-10.81	-10.95	-8.17
-0.70	-10.07	-8.25	-9.18	-9.42	-10.22	-7.63	-7.94	-9.60	-10.00	-10.14	-10.28	-7.85
-0.60	-9.47	-7.75	-8.68	-8.91	-9.70	-7.74	-7.94	-8.68	-9.19	-9.33	-9.46	-8.37
-0.50	-9.47	-8.45	-8.48	-8.71	-9.41	-9.13	-9.14	-8.50	-8.90	-9.04	-9.18	-9.85
-0.40	-9.76	-10.22	-9.16	-8.98	-8.69	-11.29	-10.90	-9.37	-9.38	-9.52	-9.66	-12.10
-0.30	-10.27	-11.97	-10.91	-10.94	-10.13	-13.25	-12.86	-11.43	-11.02	-10.86	-10.89	-14.17
-0.20	-11.29	-13.88	-13.12	-12.50	-11.55	-15.28	-14.99	-18.20	-12.43	-12.25	-12.16	-16.54
-0.10	-12.32	-15.81	-14.96	-14.25	-13.17	-17.35	-17.02	-15.01	-14.02	-13.70	-13.47	-18.71
0.0	-13.47	-17.76	-16.81	-16.03	-14.81	-19.43	-19.05	-16.81	-15.60	-15.14	-14.78	-20.85
0.10	-14.82	-19.75	-18.71	-17.79	-16.41	-21.50	-21.09	-18.58	-17.11	-16.57	-16.08	-23.02
0.20	-16.29	-21.75	-20.63	-19.56	-18.00	-23.58	-23.15	-20.34	-18.59	-18.00	-17.38	-25.20
0.30	-17.81	-23.76	-22.57	-21.33	-19.59	-25.65	-25.21	-22.09	-20.06	-19.42	-18.67	-27.38
0.40	-19.33	-25.75	-24.51	-23.09	-21.18	-27.73	-27.27	-23.85	-21.54	-20.84	-19.97	-29.57
0.50	-20.79	-27.72	-26.46	-24.84	-22.78	-29.81	-29.32	-25.64	-23.06	-22.27	-21.23	-31.75
0.60	-22.20	-29.64	-28.41	-26.57	-24.40	-31.89	-31.36	-27.44	-24.61	-23.71	-22.60	-33.93
0.70	-23.59	-31.54	-30.36	-28.29	-26.04	-33.98	-33.40	-29.26	-26.18	-25.14	-23.91	-36.10
0.80	-24.97	-33.43	-32.31	-30.00	-27.67	-36.07	-35.44	-31.09	-27.77	-26.58	-25.24	-38.28
0.90	-26.36	-35.34	-34.26	-31.72	-29.30	-38.15	-37.49	-32.91	-29.35	-28.01	-26.56	-40.46
1.00	-27.77	-37.28	-36.23	-33.45	-30.91	-40.23	-39.55	-34.73	-30.91	-29.44	-27.88	-42.65
1.10	-29.19	-39.25	-38.18	-35.19	-32.51	-42.30	-41.62	-36.54	-32.46	-30.87	-29.20	-44.84
1.20	-30.63	-41.25	-40.13	-36.93	-34.11	-44.37	-43.69	-38.35	-34.00	-32.29	-30.51	-47.04
1.30	-32.07	-43.26	-42.06	-38.68	-35.69	-46.44	-45.75	-40.15	-35.54	-33.71	-31.83	-49.23
1.40	-33.53	-45.28	-43.99	-40.44	-37.27	-48.51	-47.81	-41.95	-37.07	-35.12	-33.15	-51.44
1.50	-34.99	-47.33	-45.91	-42.20	-38.85	-50.57	-49.88	-43.75	-38.59	-36.53	-34.46	-53.64
1.60	-36.47	-49.39	-47.84	-43.96	-40.41	-52.63	-51.95	-45.54	-40.11	-37.94	-35.78	-55.85
(T_j/T_o)	1.00	2.00	2.00	2.00	2.00	2.50	2.50	2.50	2.50	2.50	2.50	3.00
$\log_{10}(V_j/a_o)$	≤0.400	≤0.100	0.125	0.150	0.175	≤0.100	0.125	0.150	0.175	0.200	0.225	≤0.100

TABLE 10B - GAS TURBINE JET EXHAUST NOISE PREDICTION
θ_I ANGLE TO INTAKE = 150 DEGREES

$\log_{10}(fD_j/\xi V_j)$	One-Third Octave-Band Sound Pressure Level (SPL-OASPL) dB												
-1.60	-29.97	-29.98	-30.03	-30.02	-30.07	-30.64	-30.39	-30.40	-30.39	-30.40			
-1.50	-26.49	-26.50	-26.56	-26.58	-26.65	-26.86	-26.51	-26.62	-26.62	-26.62			
-1.40	-23.20	-23.21	-23.26	-23.38	-23.53	-23.14	-22.89	-22.90	-22.89	-22.92			
-1.30	-19.97	-19.98	-20.03	-20.32	-20.56	-19.64	-19.39	-19.39	-19.39	-19.50			
-1.20	-16.89	-17.06	-17.23	-17.53	-17.87	-16.61	-16.46	-16.74	-16.69	-16.82			
-1.10	-14.06	-14.54	-14.90	-15.25	-15.51	-13.91	-13.97	-14.40	-14.57	-14.65			
-1.00	-11.66	-12.47	-13.03	-13.52	-13.56	-11.53	-11.88	-12.29	-12.89	-12.90			
-0.90	-10.69	-11.24	-11.74	-12.24	-12.27	-9.41	-10.31	-10.98	-11.63	-11.63			
-0.80	-10.07	-10.38	-10.84	-11.33	-11.37	-8.15	-9.28	-10.09	-10.69	-10.70			
-0.70	-9.27	-9.58	-10.14	-10.53	-10.57	-7.83	-8.68	-9.40	-9.90	-9.91			
-0.60	-8.86	-9.07	-9.32	-9.51	-9.75	-8.25	-8.48	-8.78	-8.88	-8.88			
-0.50	-8.87	-8.98	-9.13	-9.22	-9.37	-9.64	-8.79	-8.79	-8.79	-8.80			
-0.40	-9.63	-9.45	-9.52	-9.51	-9.55	-11.90	-10.55	-9.97	-9.67	-9.67			
-0.30	-11.70	-11.10	-10.55	-10.43	-10.38	-14.07	-12.72	-11.62	-11.11	-11.12			
-0.20	-13.63	-12.88	-12.09	-11.83	-11.66	-16.57	-14.65	-13.30	-12.75	-12.75			
-0.10	-15.65	-14.69	-13.77	-13.22	-13.00	-18.82	-16.72	-15.15	-14.37	-14.32			
0.0	-17.68	-16.49	-15.44	-14.62	-14.37	-21.05	-18.80	-17.00	-16.00	-15.90			
0.10	-19.74	-18.28	-17.05	-16.05	-15.76	-23.36	-20.86	-18.77	-17.62	-17.52			
0.20	-21.81	-20.08	-18.64	-17.50	-17.17	-25.69	-22.92	-20.51	-19.25	-19.15			
0.30	-23.87	-21.86	-20.22	-18.96	-18.59	-28.04	-24.98	-22.23	-20.88	-20.79			
0.40	-25.93	-23.64	-21.81	-20.41	-20.00	-30.37	-27.03	-23.95	-22.52	-22.43			
0.50	-27.96	-25.40	-23.41	-21.85	-21.38	-32.68	-29.09	-25.71	-24.18	-24.08			
0.60	-29.95	-27.13	-25.03	-23.29	-22.73	-34.94	-31.14	-27.50	-25.86	-25.74			
0.70	-31.92	-28.85	-26.65	-24.73	-24.07	-37.17	-33.19	-29.29	-27.55	-27.41			
0.80	-33.87	-30.56	-28.28	-26.16	-25.39	-39.40	-35.23	-31.10	-29.24	-29.08			
0.90	-35.83	-32.28	-29.91	-27.60	-26.72	-41.65	-37.28	-32.91	-30.93	-39.75			
1.00	-37.80	-34.00	-31.54	-29.02	-28.07	-43.96	-39.32	-34.71	-32.60	-32.41			
1.10	-39.79	-35.74	-33.18	-30.45	-29.43	-46.30	-41.36	-36.51	-34.25	-34.05			
1.20	-41.79	-37.49	-34.81	-31.87	-30.81	-48.63	-43.40	-38.31	-35.90	-35.69			
1.30	-43.79	-39.24	-36.44	-33.29	-32.19	-50.97	-45.44	-40.11	-37.54	-37.33			
1.40	-45.79	-40.99	-38.08	-34.70	-33.57	-53.32	-47.47	-41.91	-39.17	-38.96			
1.50	-47.80	-42.75	-39.71	-36.11	-34.97	-55.68	-49.51	-43.71	-40.79	-49.59			
1.60	-49.81	-44.51	-41.35	-37.52	-36.37	-58.07	-51.54	-45.51	-42.40	-42.21			
(T_j/T_o)	3.00	3.00	3.00	3.00	3.00	3.50	3.50	3.50	3.50	3.50			
$\log_{10}(V_j/a_o)$	0.125	0.150	0.175	0.200	0.225	≤0.125	0.150	0.175	0.200	0.225			

TABLE 11A - GAS TURBINE JET EXHAUST NOISE PREDICTION
θ_I ANGLE TO INTAKE = 160 DEGREES

$\log_{10}(fD_j/\xi V_j)$	One-Third Octave-Band Sound Pressure Level (SPL-OASPL) dB													
-1.60	-30.74	-30.49	-30.08	-30.50	-30.50	-29.05	-28.90	-29.05	-29.20	-29.38	-29.48	-27.13		
-1.50	-27.37	-27.40	-26.99	-27.41	-27.41	-25.76	-25.60	-25.75	-25.90	-26.09	-26.18	-23.66		
-1.40	-24.18	-24.31	-23.90	-24.33	-24.33	-22.51	-22.35	-22.50	-22.65	-22.84	-22.93	-20.28		
-1.30	-21.14	-21.29	-20.88	-21.31	-21.31	-19.45	-19.30	-19.45	-19.60	-19.78	-19.88	-17.13		
-1.20	-18.37	-18.44	-18.23	-18.66	-18.77	-16.84	-17.00	-17.09	-17.30	-17.49	-17.58	-14.35		
-1.10	-15.68	-15.39	-15.70	-16.13	-16.41	-14.11	-14.94	-14.99	-15.24	-15.42	-15.52	-12.00		
-1.00	-13.14	-12.29	-13.38	-13.81	-14.10	-11.95	-11.90	-11.95	-13.39	-13.58	-13.68	-10.13		
-0.90	-11.17	-10.00	-11.55	-11.98	-12.81	-9.97	-11.10	-11.90	-12.34	-12.53	-12.62	-8.82		
-0.80	-9.58	-8.52	-10.17	-10.80	-11.80	-8.13	-10.77	-10.92	-11.46	-11.65	-11.74	-8.15		
-0.70	-8.54	-7.89	-9.88	-10.31	-11.31	-7.65	-10.00	-10.15	-10.60	-10.79	-10.88	-8.03		
-0.60	-8.54	-7.89	-9.37	-9.79	-10.58	-8.07	-9.08	-9.23	-9.67	-9.86	-9.95	-8.66		
-0.50	-9.24	-8.59	-8.88	-9.31	-9.31	-9.65	-8.40	-8.55	-8.69	-8.88	-8.97	-10.63		
-0.40	-10.42	-11.34	-8.87	-8.80	-8.40	-12.30	-8.87	-8.82	-8.88	-9.07	-9.16	-13.38		
-0.30	-11.76	-13.72	-9.92	-9.83	-9.32	-14.67	-10.73	-10.47	-10.21	-10.19	-10.29	-16.06		
-0.20	-13.28	-15.88	-12.18	-11.40	-10.78	-16.86	-13.01	-12.38	-11.87	-11.61	-11.68	-18.37		
-0.10	-14.85	-18.07	-14.30	-13.25	-12.53	-19.28	-15.35	-14.36	-13.58	-13.20	-13.08	-20.89		
0.0	-16.44	-20.30	-16.41	-15.13	-14.31	-21.75	-17.71	-16.36	-15.30	-14.78	-14.47	-23.43		
0.10	-18.04	-22.59	-18.56	-16.95	-16.01	-24.18	-20.08	-18.35	-16.98	-16.29	-15.86	-25.90		
0.20	-19.66	-24.90	-20.73	-18.77	-17.68	-26.62	-22.45	-20.34	-18.66	-17.78	-17.23	-28.35		
0.30	-21.27	-27.23	-22.90	-20.58	-19.34	-29.06	-24.83	-22.34	-20.33	-19.25	-18.60	-30.79		
0.40	-22.89	-29.55	-25.07	-22.42	-21.01	-31.49	-27.20	-24.33	-22.01	-20.73	-19.99	-33.23		
0.50	-24.52	-31.84	-27.23	-24.28	-22.70	-33.90	-29.56	-26.32	-23.69	-22.23	-21.40	-35.70		
0.60	-26.14	-34.08	-29.37	-26.18	-24.42	-36.30	-31.90	-28.31	-25.37	-23.75	-22.84	-38.20		
0.70	-27.77	-36.31	-31.51	-28.11	-26.14	-38.68	-34.24	-30.30	-27.05	-25.28	-24.30	-40.70		
0.80	-29.41	-38.53	-33.65	-30.05	-27.87	-41.06	-36.56	-32.29	-28.73	-26.82	-25.77	-43.21		
0.90	-31.03	-40.76	-35.80	-31.97	-29.59	-43.45	-38.89	-34.28	-30.41	-28.35	-27.23	-45.73		
1.00	-32.64	-43.02	-37.95	-33.85	-31.31	-45.85	-41.23	-36.28	-32.10	-29.88	-28.68	-48.23		
1.10	-34.24	-45.31	-40.11	-35.69	-33.02	-48.26	-43.56	-38.27	-33.80	-31.40	-30.10	-50.74		
1.20	-35.84	-47.61	-42.28	-37.50	-34.73	-50.69	-45.90	-40.27	-35.49	-32.92	-31.51	-53.24		
1.30	-37.42	-49.92	-44.44	-39.28	-36.43	-53.12	-48.23	-42.27	-37.19	-34.44	-32.92	-55.74		
1.40	-39.00	-52.24	-46.61	-41.04	-38.13	-55.55	-50.57	-44.28	-38.89	-35.96	-34.31	-58.24		
1.50	-40.58	-54.58	-48.79	-42.77	-39.82	-58.00	-52.90	-46.28	-40.60	-37.47	-35.70	-60.74		
1.60	-42.14	-56.93	-50.97	-44.48	-41.51	-60.45	-55.24	-48.29	-42.31	-38.98	-37.08	-63.24		
(T_j/T_o)	1.00	2.00	2.00	2.00	2.00	2.50	2.50	2.50	2.50	2.50	2.50	3.00		
$\log_{10}(V_j/a_o)$	≤0.400	≤0.100	0.125	0.150	0.175	≤0.100	0.125	0.150	0.175	0.200	0.225	≤0.100		

TABLE 11B - GAS TURBINE JET EXHAUST NOISE PREDICTION
θ_I ANGLE TO INTAKE = 160 DEGREES

$\log_{10}(fD_j/\xi V_j)$	One-Third Octave-Band Sound Pressure Level (SPL-OASPL) dB												
-1.60	-27.01	-26.93	-26.88	-26.90	-27.07	-25.49	-25.41	-25.88	-25.97	-25.76	-25.77		
-1.50	-23.54	-23.46	-23.41	-23.43	-23.60	-22.09	-22.01	-22.48	-22.57	-22.36	-22.37		
-1.40	-20.17	-20.08	-20.03	-20.06	-20.23	-18.82	-18.74	-19.21	-19.30	-19.09	-19.11		
-1.30	-17.01	-16.93	-16.88	-16.90	-17.07	-15.89	-15.81	-16.28	-16.37	-16.16	-16.17		
-1.20	-14.32	-14.42	-14.69	-14.83	-15.00	-13.60	-13.59	-14.17	-14.30	-14.31	-14.32		
-1.10	-12.30	-12.59	-13.12	-13.42	-13.59	-11.54	-11.60	-12.35	-12.64	-13.02	-13.04		
-1.00	-11.01	-11.43	-11.98	-12.41	-12.58	-9.69	-9.81	-10.78	-11.37	-12.06	-12.07		
-0.90	-10.13	-10.76	-11.46	-11.83	-12.00	-8.21	-8.40	-9.84	-10.85	-11.31	-11.33		
-0.80	-9.62	-10.33	-11.08	-11.40	-11.57	-7.72	-7.93	-9.56	-10.74	-11.06	-11.07		
-0.70	-9.31	-9.93	-10.59	-11.01	-11.18	-8.28	-8.40	-9.28	-10.27	-10.96	-10.97		
-0.60	-8.91	-9.42	-9.87	-11.31	-11.48	-9.72	-9.74	-8.78	-9.35	-10.24	-10.25		
-0.50	-9.22	-9.33	-9.39	-9.41	-9.58	-11.69	-11.42	-9.18	-9.27	-9.46	-9.47		
-0.40	-10.49	-9.91	-9.37	-9.40	-9.57	-14.24	-13.68	-11.35	-10.04	-9.84	-9.86		
-0.30	-12.66	-11.56	-10.90	-10.42	-10.59	-16.51	-15.95	-13.32	-11.59	-10.87	-10.88		
-0.20	-15.06	-13.48	-12.57	-11.94	-12.08	-19.05	-18.22	-15.70	-13.48	-12.31	-12.32		
-0.10	-17.46	-15.49	-14.38	-13.48	-13.30	-21.62	-20.47	-17.78	-15.26	-14.07	-14.04		
0.0	-19.84	-17.55	-16.19	-15.01	-14.48	-24.19	-22.73	-19.80	-17.07	-15.86	-15.77		
0.10	-22.20	-19.61	-17.94	-16.52	-15.75	-26.74	-25.02	-21.92	-18.98	-17.53	-17.42		
0.20	-24.56	-21.68	-19.66	-18.02	-17.05	-29.28	-27.32	-24.06	-20.94	-19.15	-19.02		
0.30	-26.90	-23.76	-21.37	-19.52	-18.35	-31.83	-29.63	-26.21	-22.92	-20.77	-20.62		
0.40	-29.24	-25.85	-23.07	-21.03	-19.67	-34.39	-31.95	-28.36	-24.88	-22.39	-22.22		
0.50	-31.58	-27.94	-24.79	-22.56	-20.98	-36.99	-34.27	-30.50	-26.82	-24.04	-23.85		
0.60	-33.90	-30.04	-26.51	-24.11	-22.30	-39.62	-36.62	-32.62	-28.73	-25.73	-25.51		
0.70	-36.20	-32.16	-28.23	-25.68	-23.63	-42.26	-38.97	-34.74	-30.63	-27.44	-27.19		
0.80	-38.50	-34.28	-29.95	-27.25	-24.96	-44.95	-41.33	-36.86	-32.51	-29.15	-28.86		
0.90	-40.81	-36.38	-31.67	-28.83	-26.28	-47.63	-43.69	-38.99	-34.40	-30.86	-30.53		
1.00	-43.15	-38.47	-33.40	-30.41	-27.58	-50.29	-46.05	-41.12	-36.28	-32.56	-32.18		
1.10	-45.52	-40.53	-35.13	-31.98	-28.86	-52.94	-48.40	-43.26	-38.17	-34.24	-33.81		
1.20	-47.91	-42.59	-36.86	-33.56	-30.13	-55.59	-50.75	-45.40	-40.06	-35.92	-35.42		
1.30	-50.30	-44.63	-38.59	-35.14	-31.38	-58.25	-58.10	-47.55	-41.94	-37.59	-37.03		
1.40	-52.71	-46.66	-40.33	-36.73	-32.63	-60.89	-55.46	-49.71	-43.83	-39.25	-38.62		
1.50	-55.13	-48.68	-42.06	-38.32	-33.86	-63.54	-57.81	-51.86	-45.71	-40.91	-40.21		
1.60	-57.56	-50.68	-43.80	-39.90	-35.08	-66.19	-60.16	-54.03	-47.59	-42.56	-41.78		
(T_j/T_o)	3.00	3.00	3.00	3.00	3.00	3.50	3.50	3.50	3.50	3.50	3.50	3.50	3.50
$\log_{10}(V_j/a_o)$	0.125	0.150	0.175	0.200	0.225	≤0.100	0.125	0.150	0.175	0.200	0.225		

TABLE 12A - RELATIVE VELOCITY EXPONENT $M(\theta_i)V$

θ_i degrees	$m(\theta_i)$
20	1.1
30	0.5
40	0.2
50	0
60	0
70	0.1
80	0.4
90	1.0
100	1.9
110	3.0
120	4.7
130	7.0

TABLE 12B - RELATIVE VELOCITY EXPONENT $M(\theta_I)$

		$m(\theta_i)$						
θ_i degrees	V_j/a_o	1.10	1.18	1.33	1.47	1.62	1.77	1.95
140		10.2	9.8	9.1	8.5	7.8	7.2	6.3
150		10.4	9.8	8.7	7.6	6.5	5.4	4.0
160		10.5	9.5	7.9	6.3	4.7	3.1	1.0

6. PREDICTION OF SINGLE STREAM SHOCK-ASSOCIATED NOISE FROM CONVERGENT NOZZLES AT SUPERCRITICAL CONDITIONS

DATE OF COMPILATION: March 1980

6.1 Static Conditions

An incorrectly expanded supersonic jet contains shock waves which interact with jet turbulence to produce a source of noise in addition to that due to the turbulent mixing process. While shock-associated noise may be reduced by attention to nozzle design, this source of noise is always present with a circular convergent nozzle. Allied to the theoretical approach of 6.3.1, definitive model and full scale experimental work (6.3.2 and 6.3.3) have provided the following procedure for estimating the broadband shock-associated noise content. Taken together with the mixing noise prediction procedure of Section 5, this enables the prediction of total noise from the shock-containing under-expanded jet to be executed. The method provides for the estimation of the one-third octave band sound pressure levels, which may be combined with the sound pressure levels obtained from Section 5 by adding the squared sound pressures.

NOTE: A comparison of broadband shock-associated noise prediction methods, including the method presented here, is provided in 6.3.4. Users are encouraged to consult this reference for additional guidance material.

Shock waves in a choked jet are responsible for a source of broadband noise which is a function of nozzle pressure ratio and nozzle diameter. The method of estimation relies upon the derivation of the one-third octave band sound pressure level at any angle from the inlet axis θ_i and frequency f from the formula:

$$SPL(r,\theta_i,f) = 10\log_{10}\left(1+\left[4/(xb)\right]\sum_{i=1}^{x-1}\left\{\left[C_1(\sigma)\right]^{i^2}\sum_{s=0}^{x-(i+1)}\left[1/(\sigma q_{is})\right]\right.\right.$$
$$\left.\left.\times\left[\cos(\sigma q_{is})\right]\left[\sin(b\sigma q_{is}/2)\right]\right\}\right) \qquad \text{(Eq. 9)}$$
$$+10\log_{10}\left[(D_j/r)^2\,\beta^y\right]+10\log_{10}(b\sigma)+H_o(\sigma)+148.8$$

where:

$$q_{is} = \left[1.7\,i/\left(V_j/a_o\right)\right]\left(1-0.06\left\{s+\left[(i+1)/2\right]\right\}\right)\left(1+\left[0.7\left(V_j/a_o\right)\cos\theta_i\right]\right)$$

NOTE 1: Symbols in Section 4 apply and:

$H_o(\sigma)$ = group source strength spectrum, dB master spectra given in Figure 15 and Table 13

$C_1(\sigma)$ = correlation coefficient spectrum, master spectra given in Figure 15 and Table 13

x = number of shocks (assumed to be 8)

b = 0.2316 (for one-third octave-band proportional bandwidth)

s = shock index

σ = dimensionless frequency parameter = $2\pi fl/a_o$

β = nozzle pressure ratio parameter = $(M_j^2 - 1)^{1/2}$

y = exponent of nozzle pressure ratio parameter β

l = 1.1 β D_j, meters

M_j = fully-expanded jet Mach number

NOTE 2: Equation 9 requires two master spectra as input for the prediction. These two master spectra, $H_o(\sigma)$ and $C_1(\sigma)$, are presented in Figure 15 and the values are also tabulated for convenience in Table 13. The $C_1(\sigma)$ spectrum can be used for heated as well as unheated jet conditions. The $H_o(\sigma)$ spectrum shown here should be used for heated jets only. A heated jet is defined here as a jet having total temperature ratio greater than 1.1. For prediction at unheated conditions, the $H_o(\sigma)$ spectrum presented here should be reduced in level by 2 dB at all values of σ.

NOTE 3: Moreover, for the heated and unheated cases, the exponent y of the nozzle pressure ratio parameter β takes the following values:

$\beta \leq 1.0$, heated and unheated jets: y = 4

$\beta > 1.0$, heated jet: y = 2

$\beta > 1.0$, unheated jet: y = 1

6.1.1 Overall Sound Pressure Level Prediction

It is recommended that the wideband or overall sound pressure levels for shock-associated noise should be predicted strictly by adding the squared pressures from individual one-third octave SPLs. However, an approximate prediction of OASPL can also be obtained by using the following empirical relationships (which are independent of angle θ_i):

a. Heated jet, $\beta \leq 1.0$:

$$OASPL\ (dB) = 157.5 - 20 \log_{10} (r/D_j) + 40 \log_{10} \beta \quad \text{(Eq. 10)}$$

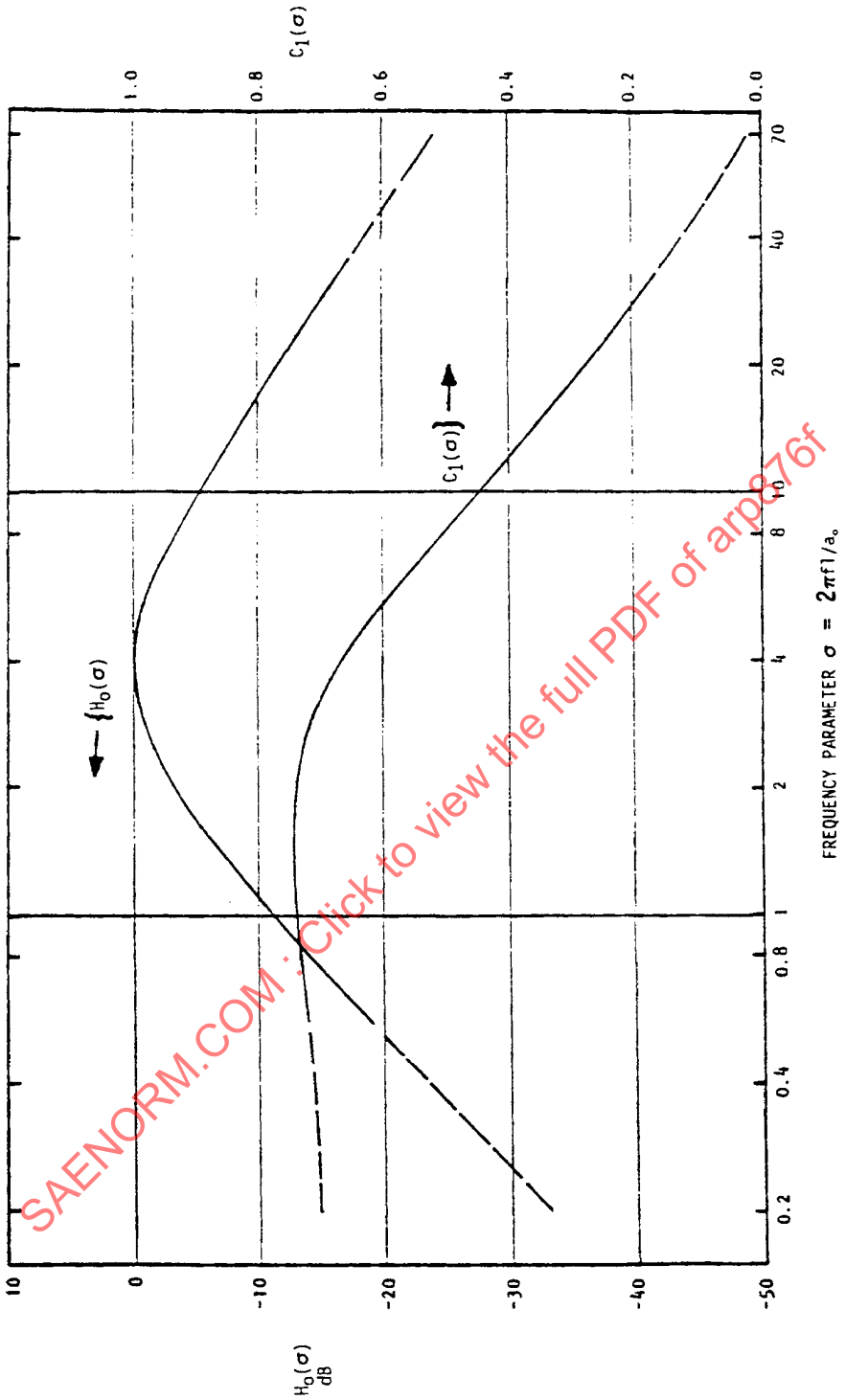

FIGURE 15 - MASTER SPECTRA FOR SHOCK-ASSOCIATED NOISE PREDICTION

TABLE 13 - MASTER SPECTRA $H_O(\sigma)$ AND $C_1(\sigma)$

$\sigma = 2\pi fl/a_o$	$H_o(\sigma)$, dB	$C_1(\sigma)$
0.2	-33.2	0.70
0.3	-27.6	0.71
0.4	-23.7	0.71
0.7	-16.1	0.72
1.0	-11.5	0.73
1.5	-6.5	0.74
2.0	-3.5	0.74
3.0	-0.7	0.71
3.5	-0.1	0.69
4.0	0.0	0.67
4.5	-0.1	0.64
5.0	-0.4	0.62
6.0	-1.3	0.58
7.0	-2.5	0.54
8.0	-3.5	0.50
10.0	-5.5	0.45
20.0	-11.8	0.28
40.0	-18.7	0.12
68.0	-23.8	0.02
70.0	-24.0	0.02

b. Heated jet, $\beta > 1.0$:

$$OASPL\ (dB) = 157.5 - 20\log_{10}(r/D_j) + 20\log_{10}\beta \qquad \text{(Eq. 11)}$$

c. Unheated jet, $\beta \leq 1.0$:

$$OASPL\ (dB) = 155.5 - 20\log_{10}(r/D_j) + 40\log_{10}\beta \qquad \text{(Eq. 12)}$$

d. Unheated jet, $\beta > 1.0$:

$$OASPL\ (dB) = 155.5 - 20\log_{10}(r/D_j) + 10\log_{10}\beta \qquad \text{(Eq. 13)}$$

6.1.2 Angular Range of Application

For unheated jets the method is accurate for $\theta_i \leq 130$ degrees. For larger angles detailed analysis indicates that some over-prediction may occur. However, at those angles the shock-cell noise contribution is small and prediction may be based on the mixing noise contribution alone.

For heated jets (total temperature ratios greater than approximately 1.1) the present prediction method can be applied for all $\theta_i \leq 150$ degrees. The over prediction mentioned above is unimportant (and uncheckable) for the majority of rear arc angles due to the complete dominance of the contribution of jet-mixing noise.

6.2 Flight Conditions

It is widely accepted that the effect of forward speed on a source (such as the shock-cell component), which is effectively moving at the same speed as the aircraft, is affected by a 4th-power Doppler amplification factor.

To translate the spectrum levels or overall sound pressure level obtained in 6.1 to flight conditions, a 4th-power amplification factor should be applied as follows:

$$SPL_{(flight)} = SPL_{(static)} - 40 \log_{10} (1 - M_a \cos \phi) \quad \text{(Eq. 14)}$$

where:

M_a = aircraft Mach number

ϕ = θ_i - ψ

θ_i = angle to engine intake axis, or (180 - ϕ_j) where intake and jet axes are dissimilar

ψ = angle between airplane flight path and engine thrust axis

6.3 References

6.3.1 Harper-Bourne, M. and Fisher, M. J., The Noise from Shock Waves in Supersonic Jets. AGARD Proceedings CP-131, September 1973.

6.3.2 Tanna, H. K., An Experimental Study of Jet Noise, Part II: Shock Associated Noise. Journal of Sound and Vibration, Vol. 50, No. 3, 1977.

6.3.3 Chapter 4 (Shock-Associated Noise) of Technical Report AFAPL-TR-78-85. (The Generation, Radiation and Prediction of Supersonic Jet Noise - Vol. I.) Prepared by Lockheed-Georgia Company, October 1978.

6.3.4 Dahl, M. D., Predictions of Supersonic Jet Mixing and Shock-Associated Noise Compared with Measured Far-Field Data, NASA TM 2010-216328, 2010.

6.4 Parties Contributing to Compilation of Section 6

General Electric Company, USA

Lockheed-Georgia Company, USA

Rolls-Royce Limited, United Kingdom

SNECMA, France

The University of Southampton, United Kingdom

7. PREDICTION OF SUBSONIC COAXIAL JET MIXING NOISE

DATE OF COMPILATION: June 1989

The procedure of this section predicts the free-field one-third octave-band sound pressure levels of coaxial subsonic jets for turbofan engines or models under the following conditions:

a. Flyover (observer on ground)

b. Static (observer on ground)

c. In-flight or in-flow (observer on airplane or in a wind tunnel)

7.1 Scope

This jet noise prediction procedure was developed for nozzle area ratio, gas conditions, and aircraft Mach numbers in the following ranges of primary and secondary jet ratios:

$1.5 < A_s/A_p < 3.5$

$2.0 < W_s/W_p < 6.5$

$0.6 < V_s/V_p < 0.95$

$0.4 < V_s/a_o < 1.0$

$0.35 < T_s/T_p < 0.5$

$M_a < 0.3$

The method assumes that the jet mixing process can be subdivided into three noise producing regions, each having its own frequency range. However, all three components have to be added to obtain a prediction of total jet noise level in a specified frequency range. For best accuracy, the frequency range should correspond to a mixed-jet Strouhal number range of:

$$0.1 < S_r < 40 \qquad \text{(Eq. 15)}$$

where:

$$S_r = fD_m/(V_m - V_a)$$

The formulae in Tables 14, 15, and 16 cover an angular range[1] from 60 to 160 degrees ($\pi/3$ to $8\pi/9$ radians). For locations outside the specified angular range, the limiting angles of $\pi/3$ of $8\pi/9$ radians are used in the formulae. The source location procedure in 7.6.3 gives the correct sound propagation distance for any location of the receiver.

The coaxial jet noise prediction method was formulated for the general case of a coaxial jet in parallel ambient flow, and, therefore, does not require correction for additional “static-to-flight” effects.

TABLE 14 - JET NOISE COMPONENT FORMULAS

Parameter Definition	Primary Component	Secondary Component	Mixed Component
Component 1/3 O.B. SPL	$\left[(Z1)\log(FV)+(Z2)\right]\left[\log S-(Z3)\log(FV)-(Z4)\right]^2+(Z5)\log(FV)+(Z6)$		
Source Strength Function (FV)	$M_p\left(\frac{DVPS}{a_o}\right)^{0.6}\left(\frac{V_p+V_s}{a_o}\right)^{0.4}\left(\frac{V_p-V_a}{V_p}\right)^{n_p}$	$\left(\frac{V_s-V_a}{a_o}\right)^{n_s}\left(\frac{V_s+V_a}{a_o}\right)^{1-n_s}$	$\left(\frac{V_m-V_a}{a_o}\right)^{n_m}\left(\frac{V_m+V_a}{a_o}\right)^{1-n_m}$
Velocity Exponent (n)	$1.5, \theta_p \le 2.2$ $1.5\exp\left[-10(\theta_p-2.2)^2\right], \theta_p > 2.2$	$0.5+0.1\theta_s$	$\left(\frac{V_m}{a_o}\right)^{1/2}\left\{0.6+\frac{0.2}{0.2+S_m}\exp\left[-0.3\left(\theta_m+\frac{S_m}{1+S_m}-2.7\right)^2\right]\right\}$
Strouhal Number (S)	$fD_p/(DVPS)$	$fD_m/(V_s-V_a)$	$fD_m/(V_m-V_a)$

[1] NOTE: Throughout Section 7 angles referred to are in radians, not degrees.

TABLE 14 - JET NOISE COMPONENT FORMULAS (CONTINUED)

Parameter Definition	Primary Component	Secondary Component	Mixed Component
Coefficients (Z1)	$-18\left[\left(1.8\theta_p/\pi\right)-0.6\right]^2$	$-18\left[\left(1.8\theta_s/\pi\right)-0.6\right]^2$	$-30\left[\left(1.8\theta_m/\pi\right)-0.6\right]^2$
(Z2)	$-18-18\left[\left(1.8\theta_p/\pi\right)-0.6\right]^2$	$-14-8\left[\left(1.8\theta_s/\pi\right)-0.6\right]^3$	$-9-4\left(\frac{V_p-V_s}{a_o}\right)-38\left[\left(1.8\theta_m/\pi\right)-0.6\right]^3$ $+30\left[0.6-\log\left(1+\frac{A_s}{A_p}\right)\right]\left(\frac{1.8\theta_m}{\pi}-0.6\right)$
(Z3)	0	–0.7	$1-0.4\left[\left(1.8\theta_m/\pi\right)-0.6\right]^2$
(Z4)	$-0.1-0.75\left(\frac{V_p-V_s-V_a}{a_o}\right)$ $\times\left[\left(1.8\theta_p/\pi\right)-0.6\right]^3$ $+0.8\left[0.6-\log\left(1+\frac{A_s}{A_p}\right)\right]$	$0.6-0.5\left[\left(1.8\theta_s/\pi\right)-0.6\right]^2$ $+0.5\left[0.6-\log\left(1+\frac{A_s}{A_p}\right)\right]$	$0.44-0.5/\exp\left[\left(4.5\theta_m/\pi\right)-4\right]^2$ $+0.2\frac{V_p}{a_o}-0.7\frac{V_m}{a_o}-0.2\log\left(1+\frac{A_s}{A_p}\right)$ $+0.05\,(XBPR)\exp\left[-5\left(\theta_m-2.4\right)^2\right]$
(Z5)	$50+20\exp\left[-\left(\theta_p-2.6\right)^2\right]$	$51+54\theta_s/\pi$ $-9\left[\left(1.8\theta_s/\pi\right)-0.6\right]^3$	$34+81\theta_m/\pi$ $-20\left[\left(1.8\theta_m/\pi\right)-0.6\right]^3$
(Z6)	$94+46\exp\left[-\left(\theta_p-2.5\right)^2\right]$ $-\frac{26\left[0.6-\log\left(1+\frac{A_s}{A_p}\right)\right]}{\exp\left[5\left(\theta_p-2.3\right)^2\right]}$ $+(DSPL)+(EX)$	$99+36\theta_s/\pi$ $-15\left[\left(1.8\theta_s/\pi\right)-0.6\right]^4$ $+5V_s\left(V_p-V_s\right)/a_o^2$ $+(DSPL)+(EX)$	$108+37.8\theta_m/\pi+5V_m\left(V_p-V_s\right)/a_o^2$ $-\exp\left[-5\left(\theta_m-1.8\right)^2\right]$ $+\frac{7V_m}{a_o}\left[1-0.4\frac{V_p}{a_o}\exp\left(-0.7\left\lvert S_m-0.8\right\rvert\right)\right]$ $/\exp\left[8\left(\theta_m-2.4\right)^2\right]$ $+0.8\,(XBPR)\exp\left(\theta_m-2.3-V_m/a_o\right)$ $+(DSPL)+(EX)$

NOTE: $DVPS=\left\lvert V_p-\left(V_sA_s+V_aA_p\right)/\left(A_s+A_p\right)\right\rvert$ Let DVPS = 0.3 m/s if DVPS < 0.3 m/s

$XBPR=\left(W_s/W_p\right)-5.5$ Let XBPR = 0 if XBPR < 0 and let XBPR = 4 if XBPR > 4.

TABLE 15 - NORMAL ADJUSTMENT (DSPL)

Effects	Primary Component	Secondary Component	Mixed Component
Ambient Pressure	$+20 \log \left(P_o / P_{ISA}\right)$	$+20 \log \left(P_o / P_{ISA}\right)$	$+20 \log \left(P_o / P_{ISA}\right)$
Density	$+20 \log \left(\frac{\rho_p + \rho_s}{2\rho_a}\right)$	$+20 \log \left(\frac{\rho_s + \rho_a}{2\rho_a}\right)$	$+20 \log \left(\frac{\rho_m + \rho_a}{2\rho_a}\right)$
Spherical Divergence	$+20 \log \left(D_p / r_p\right)$	$+20 \log \left(D_m / r_s\right)$	$+20 \log \left(D_m / r_m\right)$
Geometric Near-Field	$-10 \log \left(1+\frac{b}{r_p}\right)$ $b = 2D_p + \left(D_p a_o / f\right)^{1/2}$	$-10 \log \left(1+\frac{b}{r_s}\right)$ $b = 2D_m + \left(D_m a_o / f\right)^{1/2}$	$-10 \log \left(1+\frac{b}{r_m}\right)$ $b = 2D_m + \left(D_m a_o / f\right)^{1/2}$
Acoustic Near-Field	$+10 \log \left[1+0.13\left(\frac{a_o}{r_p f}\right)^2\right]$	$+10 \log \left[1+0.13\left(\frac{a_o}{r_s f}\right)^2\right]$	$+10 \log \left[1+0.13\left(\frac{a_o}{r_m f}\right)^2\right]$
Atmospheric Attenuation Coefficient [AC(f)]	$-\left[AC\left(f_p\right)\right] r_p$ $f_p = f / \left(1 - M_a \cos \theta_p\right)$	$-\left[AC\left(f_s\right)\right] r_s$ $f_s = f / \left(1 - M_a \cos \theta_s\right)$	$-\left[AC\left(f_m\right)\right] r_m$ $f_m = f / \left(1 - M_a \cos \theta_m\right)$

NOTE: AC(f) is obtained from ARP866A.

TABLE 16 - ACOUSTIC EXCITATION ADJUSTMENT (EX)

Parameter Definition	Primary Component	Secondary Component	Mixed Component
Excitation Adjustment (EX)	$+5\,(EXD)\,(EXPS)$	$+2\,a_o/[V_s(ZK)]$	$+(EXD)\,(EXS)\,(EXC)$
Excitation Strouhal Number (S1)	$(N1/60)\,(D_m/V_m)$		
Effectiveness (EXPS)	$\exp(-SX)$, $SX = 50\,(S1-0.25)\,(S1-0.5)$ $SX = 0$ *if* $0.25 < S1 < 0.5$		
Spectral Shape Factor (EXS)	$5\,(EXPS)\exp\left[-\left(\log\frac{S_m}{2\,(S1)+0.00001}\right)^2\right]$		
Fan Duct Length Factor (EXD)	$\exp\left[0.6-(EXA)^{1/2}\right]$		
Directivity Factor (EXC)	a_o/V_m, *if* $\theta_m \le 1.4$ $(a_o/V_m)\left[1-(1.8/\pi)(\theta_m-1.4)\right]$ *if* $\theta_m > 1.4$		
Source Location Factor (ZK)	$1-0.4\,(EXD)\,(EXPS)$		

NOTE: $EXA = \dfrac{\text{Distance from fan face to fan exit}}{\text{Fan Diameter}}$

7.2 Development of the Coaxial Jet Noise Prediction Model

The model predicts the noise produced by a subsonic coaxial jet. The jet is conceptually divided into three regions: the primary jet, the secondary jet, and the mixed (merged) jet. Each region generates a component of jet noise and has its own noise source distribution. Figure 16 illustrates sound propagation from a source on the centerline in the mixed jet region at X_m for a frequency f radiating at emission angle θ_m indicated by the wave-normal vector perpendicular to the wave front. Motion of the ambient air convects the sound wave to the receiver (microphone) location shown.

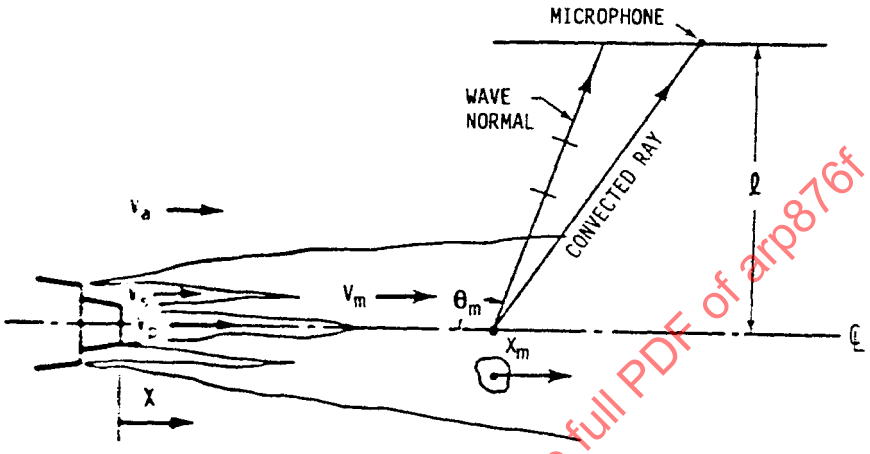

FIGURE 16 - SCHEMATIC COAXIAL JET NOISE MODEL IN WIND TUNNEL COORDINATES

The calculation procedure predicts the one-third octave-band sound pressure level (L) for each component of jet noise at any location. The total jet sound pressure level is 10 log of the sum of the time-mean-square sound pressures from the three components, i.e.,

$$L = 10 \log \left(10^{0.1 L_p} + 10^{0.1 L_s} + 10^{0.1 L_m} \right) \quad \text{(Eq. 16)}$$

where:

L_p, L_s, and L_m are the one-third octave-band sound pressure levels of the primary, secondary, and mixed jet components, respectively

Although, the noise prediction method was derived from an extensive collection of experimental data, consideration was given to the physics of jet noise generation and propagation in selecting the parameters to correlate the data. Static tests provided near- and far-field jet noise for unexcited and acoustically excited model jets that simulate the jet-exhaust flow from a turbofan engine excited by upstream sources such as core or fan noise. An elliptic mirror system was used to measure the relative sound pressure levels for the different mixing regions to determine the distributed source locations. Wind tunnel tests of coaxial model jets provided simulated in-flight jet noise data. Full-scale, static-engine noise measurements and flight test data were used to evaluate the method and to modify the empirical formulations. The empirical formulae were written for predictions of coaxial jet noise levels in wind tunnel-fixed coordinates or airplane-fixed coordinates. Prediction of flyover jet noise is obtained by a coordinate transformation as described in 7.7.2.

Expressions for calculation of jet noise contain three principal groups:

a. The basic normalized one-third octave-band sound pressure level associated with the shear-layer velocity difference, turbulent eddy convection velocities, and ambient-flow effects (Table 14).

b. Normal adjustments to account for effects of ambient air pressure, air density (or temperature), spherical divergence, geometric and acoustic near-field effects, and atmospheric absorption (Table 15).

c. Adjustments to account for the effects of internal acoustic excitation (Table 16).

7.3 Component Sound Pressure Level Prediction

Table 14 gives the basic formulae for calculation of the free-field one-third octave-band sound pressure levels for the three jet noise components. These levels are calculated at a distance of one component-jet diameter from the corresponding source locations of each component. Description of the calculation of the sound pressure level of the mixed-jet component and the corresponding calculation of mixed-jet parameters are provided in 7.5. Angle θ with subscript is the sound emission angle from each component source. For a given observer location, the procedure for calculation of sound emission angles from the distributed source locations is explained in 7.7.

The shear layer source strength function FV in Table 14 is a function of nondimensional shear layer velocity difference, eddy convection velocity, and the airplane forward speed (or equivalent airspeed in a wind tunnel). For the primary jet, the Mach number is included.

The exponents in the shear layer source strength function FV provide the scaling of sound pressure level with the jet and ambient-flow dimensionless velocities. The velocity exponents in Table 14 have a strong directivity dependence and a weak Strouhal number dependence.

Strouhal number S with subscript is specified separately for each jet component using the shear layer velocity difference, the component-jet diameter, and frequency.

Coefficients Z1 to Z6 in Table 14 are more directivity dependent than Strouhal number dependent. The expression for Z6 includes an adjustment term, DSPL, and an acoustic excitation adjustment, EX, listed in Tables 15 and 16, respectively.

7.4 Sound Pressure Level Adjustments in Prediction

7.4.1 Normal Adjustments

For each component-source, the total normal adjustment DSPL is the sum of all the adjustments listed in Table 15. The ambient pressure adjustment is the same for all three components. The density effect and spherical divergence are expressed for each component separately.

7.4.1.1 Near-Field Adjustments

Empirical adjustments for the separate effects encountered in the acoustic near-field and the geometric near-field were derived from general acoustic and geometric near-field properties. For either acoustic or geometric near-field, the form of adjustment is the same for all three source components and is described in more detail in 7.6.1.

7.4.1.2 Atmospheric Attenuation

The atmospheric attenuation formulas in Table 15 include Doppler frequency shift. For flyover noise predictions, the received frequencies used in this procedure have already been Doppler shifted (see 7.7.2). In a wind tunnel, the locations of the sound sources are stationary and the measured frequencies are the source frequencies. To calculate atmospheric absorption, the measured frequency has to be Doppler shifted and the sound propagation distance through air at rest has to be used.

7.4.2 Acoustic Excitation Adjustments

Adjustment of the sound pressure level as a result of acoustic excitation in the fan flow is given by the expressions for EX in Table 16.

As a consequence of the increased mixing rate of an acoustically excited jet, the axial distribution of jet noise sources is more compact than in an unexcited jet (Reference 7.10.1). Empirical formulas for the three jet noise source locations are given in 7.6.3.

7.5 Mixed Jet Noise Component

The mixed jet region of a coaxial jet usually starts at approximately three mixed-jet diameters downstream of the exit of the primary or the common-flow nozzle. There is no clear boundary for the transition from the primary and secondary jets into the mixed jet. For turbofan engines having moderate-to-high bypass ratios, the mixed-jet component usually dominates the wideband jet noise level in the low-to-mid-frequency region from takeoff to cutback power settings. The mixed jet is, in most practical cases, the predominant component in coaxial subsonic jet noise.

For a set of given primary and secondary jet exit gas conditions, the “fully” mixed jet condition is defined by the following formulae:

$$V_m = \left(W_p V_p + W_s V_s\right) \Big/ \left(W_p + W_s\right) \quad \text{(Eq. 17)}$$

The mixed jet total temperature:

$$T_m = \left(W_p T_p + W_s T_s\right) \Big/ \left(W_p + W_s\right) \quad \text{(Eq. 18)}$$

The mixed jet density:

$$\rho_m = P_a \Big/ \left[RT_m - \left(0.5\, RV_m^2 / C_p\right)\right] \quad \text{(Eq. 19)}$$

where:

R = gas constant

C_p = constant pressure specific heat of the mixed jet at the mixed jet temperature

The mixed jet area:

$$A_m = A_p \rho_p V_p \left[1 + \left(W_s / W_p\right)\right] \Big/ \left(\rho_m V_m\right) \quad \text{(Eq. 20)}$$

The mixed jet diameter:

$$D_m = \left(4A_m / \pi\right)^{1/2} \quad \text{(Eq. 21)}$$

The mixed jet diameter is used to calculate the Strouhal number and spherical-divergence for the secondary and mixed jet components of jet noise.

7.6 Special Features

The coaxial jet noise prediction method incorporates several special features that are discussed in this section.

7.6.1 Near-Field Effects

This procedure includes adjustments for a geometric near-field effect and an acoustic near-field effect. Modeling of those effects is necessary for prediction of the level of jet noise that impinges on the fuselage of an aircraft in flight or for comparison with in-flow (usually near-field) wind tunnel data.

Relative to the basic far-field sound pressure levels calculated from the expressions in Table 14, the acoustic near-field adjustment increases the sound pressure level while the geometric near-field adjustment decreases the sound pressure level. For practical cases, at the frequency corresponding to the maximum one-third octave-band sound pressure level and for higher frequencies, the geometric near-field term is more influential than the acoustic near-field. The acoustic near-field adjustment predominates at low frequencies, i.e., at low Strouhal numbers.

7.6.1.1 Geometric Near-Field

Jet noise sources are distributed throughout the jet flow field. The prediction method uses the effective center of a source distribution for each jet noise component at a given frequency and far-field radiation angle. When the observer (microphone) is close to the jet, the acoustic field is simulated better than a line source than a point source. Transition from the near-field to the far-field is made by an empirical formula for mean-square sound pressure p^2 given by:

$$p^2 \alpha (D/r)^2 / [1 + (b/r)] \quad \text{(Eq. 22)}$$

Equation 22 includes spherical divergence and geometric near-field effects. Atmospheric absorption is calculated separately.

In Equation 22, D is the effective diameter for each component of the jet, r is the distance from the apparent source to the observer, and b is an empirically defined source length provided in Table 15 for each component. Application of Equation 22 to calculate sound pressure level yields 10 log $(D/r)^2$ for spherical divergence and -10 log [1 + (b/r)] for a geometric near-field adjustment term that, for a given source length b, approaches zero as distance r increases to infinity in the far-field limit.

For each frequency of interest, the empirical geometric near-field effect is calculated for each jet component (primary, secondary, mixed) in the prediction method.

7.6.1.2 Acoustic Near-Field

The mean-square sound pressure p^2 in the near-field and far-field is given by the following relation:

$$p^2 \propto (\lambda/r)^2 \left[1 + 0.13 (\lambda/r)^2\right] \quad \text{(Eq. 23)}$$

where:

$\lambda = a_o/f$ is the wavelength of sound in ambient air at rest and the constant (0.13) was determined empirically.

Application of Equation 23 to calculate sound pressure level yields 10 log $(\lambda/r)^2$ for the spherical divergence and 10 log $[1+0.13(\lambda/r)^2]$ for the acoustic near-field adjustment.

7.6.2 Acoustic Excitation

Acoustic excitation from nonjet noise sources, e.g., fan or core noise, can amplify jet noise. Experimental findings (7.10.1) were incorporated into the prediction method by means of the various sound pressure level adjustments listed in Table 16.

For prediction of engine jet noise, the prediction model uses readily available engine geometric and cycle parameters. For moderate-to-high bypass-ratio turbofan engines, the second harmonic of the fan rotational speed at takeoff power corresponds to a frequency of sound that may be effective in exciting the jet. Parameter EXPS, defined by the equations in Table 16, provide a measure of how effective an internal sound source is in exciting a jet exhaust stream. EXPS is unity when the Strouhal number based on fan rotational speed is between 0.25 and 0.5 and decreases exponentially for Strouhal numbers less than 0.25 and greater than 0.5.

The dimensionless fan duct length, EXA (see 7.1), is related to the boundary layer thickness at the fan exit and the sound pressure level of the fan tones at the fan nozzle. A longer fan duct usually implies a thicker boundary layer, a lower level of the fan tones at the nozzle exit, and a reduction in the effectiveness of jet noise excitation.

For the primary and the secondary jets, the increase in noise levels due to excitation are assumed to be omnidirectional. The directivity factor, EXC, applied to the mixed jet excitation adjustment, results in smaller jet excitation effects being added in the aft quadrant compared with those in the forward arc. The adjustment is inversely proportional to the normalized mixed jet velocity based on the speed of sound in ambient air.

The more compact axial distribution of sources of excited jet noise is adjusted from that of an unexcited jet by the empirical factor ZK in Table 16.

Parameter EXS is used to adjust the shape of the spectrum. The expression in Table 16 assigns a maximum amplification at approximately twice the fan rotational frequency. The small number 0.0001 in the denominator is used to avoid a singularity at zero fan rotational speed (S1 = 0). The sound pressure level adjustment for an excited jet is broadband in nature and generally is less than 5 dB.

7.6.3 Jet Noise Source Locations

Important sources of jet noise are distributed over a wide range of the jet mixing region from the nozzle exit up to 15 mixed-jet diameters downstream. For static tests of engines, noise is typically measured at positions on a 150-foot (45-m) polar arc. Identification of noise source locations as well as the direction and distance of each microphone from the source is necessary for accurate prediction of jet noise.

The primary jet noise source location X_p normalized by the primary jet diameter D_p is given by:

$$X_p/D_p = \left\{4 + 4\tan^{-1}\left[\left(18\,\theta_p/\pi\right) - 9\right] + \left(A_s/A_p\right)\right\}\ (ZK) \qquad \text{(Eq. 24)}$$

where:

ZK = excitation source location factor from Table 16

Equation 24 shows that the source for jet noise radiated to the forward arc is located close to the nozzle exit while the source for jet noise radiated to the aft arc is relatively far downstream. The noise source location formula in Equation 24 is independent of frequency.

The secondary-jet noise source location normalized by the mixed-jet diameter from Equation 21 is given by:

$$X_s/D_m = \left\{2 + 1.6\tan^{-1}\left[\left(4.5\,\theta_s/\pi\right) - 2.25\right]\right\}\left(1 + 0.5\,S^{-0.5}\right) \times \left[1 + \left(0.7\,V_s/a_o\right)\right]^{0.5}\left[V_s/\left(V_s - V_a\right)\right]\ (ZK) \qquad \text{(Eq. 25)}$$

High-frequency sources (large values of Strouhal number S_s) are located close to the nozzle exit while low-frequency sources are farther downstream.

The mixed jet noise source location normalized by mixed-jet diameter is given by:

$$\frac{X_m}{D_m} = \left\{3 + \exp\left(-S_m\right) + \left[2 + 1.1\tan^{-1}\left(18\frac{\theta_m}{\pi} - 13\right)\right] + \left(1 + 0.5\,S_m^{-1/2}\right)\right\}\left(0.5 + \frac{0.5\,V_m}{a_o}\right)^{1/2}\left(\frac{V_m}{V_m - V_a}\right)(ZK) \quad \text{(Eq. 26)}$$

Although the mixed jet does not have a potential core, the characteristics of the mixed-jet noise source locations are similar to those of the primary and secondary jets.

7.7 Incorporation of Distributed Source Location

As described earlier, the prediction formulae were derived for airplane-fixed or wind-tunnel coordinates. Sound pressure level is a function of source frequency (or Strouhal number) and sound radiation angle. However, because of the distributed nature of the sources of jet noise, the geometric angle used to identify the observer location is different from the sound radiation angle. Furthermore, in the case of a flyover, the received frequency is, in general, different from the source frequency. In order to predict the jet noise for a given observer location, it is necessary to find the corresponding source location, radiation angle, and in case of flyover noise predictions, the source frequency. The recommended methods are described in 7.7.1 and 7.7.2.

7.7.1 Wind Tunnel Coordinates

For the situation where there is no relative motion between the observer and the nozzle (see Figure 17A) the source for a given component of jet noise is located at a distance X_j downstream of the origin of coordinates and radiates the sound at an angle θ_j where the subscript j = p, s, or m for each jet-noise component. The observer (microphone) is at sideline distance ℓ and angle θ from the center of coordinates as shown in Figure 17A. The center of the nozzle exit is located at X_o on the coordinate system. The distance X_o is introduced to enable prediction of as-measured sound pressure levels, since most full scale tests are conducted with the center of coordinates set at a convenient location not at the nozzle exit.

For a free-stream Mach number $M_a < 1$:

$$\theta_j = \sin^{-1}\left\{\left[-M_a B + \left(B^2 - M_a^2 + 1\right)^{1/2}\right] \Big/ \left(B^2 + 1\right)\right\} \quad \text{(Eq. 27)}$$

where:

$$B = \left[\left(X_o + X_j\right)/\ell\right] + \cot\theta \quad \text{(Eq. 28)}$$

The following iteration procedure is recommended for determining the source location X_j which corresponds to a given component source radiation angle θ_j.

a. For a given one-third octave band center frequency (Strouhal number S_j), assume $\theta_j = \pi/2$ and find X_j from Equations 24, 25, and 26.

b. Use Parameter B from Equation 28 to find a new angle θ_j from Equation 27. Use the new angle θ_j to find a new distance X_j from Equations 24, 25, and 26.

c. Let $\theta_{j1} = \theta_j$ and use the new distance X_j to find a new angle θ_j from Equations 27 and 28 and let $\theta_{j2} = \theta_j$.

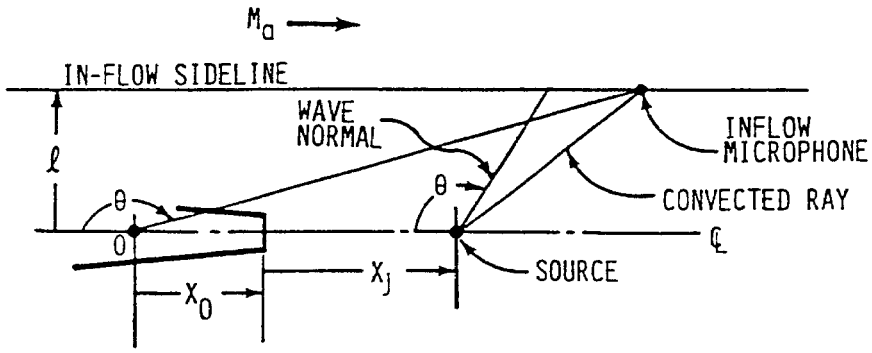

FIGURE 17A - IN-FLOW COORDINATES

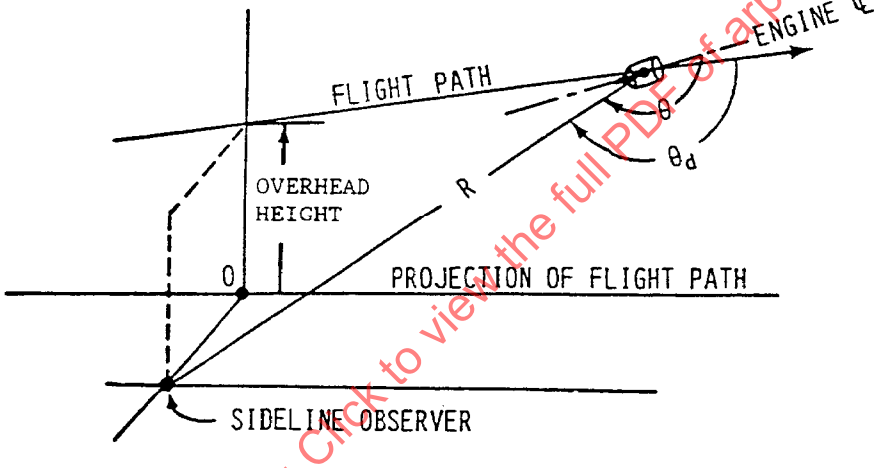

FIGURE 17B - FLYOVER COORDINATES

FIGURE 17 - COORDINATE SYSTEMS FOR JET NOISE PREDICTION

d. Let $\theta_j = (\theta_{j1} + \theta_{j2})/2$ and find a new distance X_j.

e. Repeat steps c and d until the absolute value of the difference between two successive calculations of the effective source location is equal to, or less than, $D_p/20$ for the primary-jet component or $D_m/20$ for the secondary or mixed-jet components.

7.7.2 Ground-Fixed Coordinates for Flyover Jet Noise

The coordinate system for a straight flight path with the jet axis aligned with the free stream, or at a small angle of attack relative to the free stream, is shown in Figure 17B. The radiation angle or the retarded angle is given by:

$$\theta_j = \sin^{-1}\left[\left(B^2 + 1\right)^{-1/2}\right] \qquad \text{(Eq. 29)}$$

where:

B = given by Equation 28

The source frequency f_{source} is given by:

$$f_{source} = \left(1 - M_a \cos \theta_d\right) f \quad \text{(Eq. 30)}$$

where:

f = received frequency

θ_d sound-propagation angle relative to the flight path

The Strouhal number is defined by using the source frequency. The iteration procedure is the same as the wind tunnel case except using Equation 29 instead of Equation 27. In the flyover case, atmospheric attenuation is calculated at the received frequency.

7.8 Predictions of Jet Noise Levels for Full-Scale Tests

This procedure predicts the noise of an “isolated” coaxial jet, i.e., without the presence of solid surfaces in the vicinity of the jet other than those of the nozzles. The presence of the solid surfaces can change the jet noise source and propagation mechanisms from those of an isolated jet. In practical applications, the solid surfaces are not always far from the jet exhaust flow field. Depending upon the specific configuration and condition, measured noise levels may not represent the sound pressure levels of an isolated jet and, therefore, cannot be predicted without further adjustment.

Effects due to the presence of solid surfaces are not included in this procedure. For the convenience of predicting the measured jet noise levels from full scale tests, empirical formulae that may be considered for adjusting the predicted levels are provided in the Appendix D.

7.9 Prediction of Jet Noise Levels for Full-Scale Tests - Static or Flight (Section 7)

7.9.1 External Plug Effect

Tests of coaxial jet noise with different external plugs indicated that an external plug decreases the level of jet noise, particularly, in the aft arc. Let PLUGD be the diameter of the external plug at the primary nozzle exit for a coplanar or extended primary configuration, or at the secondary nozzle exit for a common-flow nozzle. The adjustment, in decibels, to be added to the predicted jet noise level is given by:

$$PG_p = 0.1\left(V_p/a_o\right)\left[10 - \left(18\,\theta_p/\pi\right)\right](PLUGD)/D_p \quad \text{(Eq. 31)}$$

$$PG_s = 0.1\left(V_s/a_o\right)\left[6 - \left(18\,\theta_s/\pi\right)\right](PLUGD)/D_m \quad \text{(Eq. 32)}$$

$$PG_m = 0.1\left(V_p V_m/{a_o}^2\right)\left[9 - \left(18\,\theta_m/\pi\right)\right](PLUGD)/D_m \quad \text{(Eq. 33)}$$

for the primary, secondary and the mixed jet noise component, respectively.

7.9.2 Ground Proximity Effect

For test stand installations, where the test stand height is less than three times the diameter of the mixed jet, it may be necessary to include an adjustment for a ground proximity effect in the prediction of static engine jet noise. Analysis of sound pressure levels measured by ground-plane microphones in engine static tests indicated that the ground proximity effect is greatest in the frequency region where the wavelength is approximately equal to engine centerline height. The data also indicated that when the centerline height is greater than four times the diameter of the mixed jet the ground proximity effect is negligible. Based on these observations, an empirical ground proximity effect (GPROX) was derived. The value of GPROX is subtracted from the calculated mixed jet noise levels to predict the sound pressure levels at ground-plane microphone locations around a full-scale engine test stand.

The ground proximity effect in decibels is given empirically by:

$$GPROX = (5V_m/a_o)\exp\left\{-\left[9(\theta_m/\pi)-6.75\right]^2-\left[(H/D_m)-2.5\right]^2\right\} \times\left\{1+\sin^2\left[(\pi Hf/a_o)-(\pi/2)\right]\right\}\Big/\left[2+\left|(Hf/a_o)-1\right|\right] \quad \text{(Eq. 34)}$$

where:

H = engine centerline height above the ground plane

7.9.3 Installation and Angle of Attack Effects

To accurately predict the jet noise of a jet-powered airplane in flight, it is necessary to include the effects of engine installation and angle of attack. These effects depend strongly upon the installation configuration (7.10.2) of the specific airplane and its operation (e.g., flap setting and angle of attack). For general applications regarding wing-mounted engine configurations, simplified models are described in the following paragraphs.

It is assumed that the primary jet component does not have installation or angle-of-attack effects, and no adjustment in sound pressure level is made for the primary component.

For the secondary jet component, no angle-of-attack effect is assigned. The installation effect, INST in decibels, to be added to the predicted secondary jet noise level is given by (see Figure 18):

$$INST = 0.5\left[(C_e - X_e)^2/(C_eD_m)\right]\left[\exp(-Y_e/D_m)\right] \times\left[(1.8\theta_s/\pi)-0.6\right]^2 \quad \text{(Eq. 35)}$$

where:

C_e = wing chord length at the engine location

X_e = fan exit location downstream of the leading edge (X_e<C_e)

Y_e = separation distance from the wind chord line to nozzle lip as shown in Figure 18

D_m = mixed jet diameter calculated from the jet prediction procedure

The magnitude of the installation effect is between 0 and 2.5 dB. If the calculated installation effect exceeds 2.5 dB, the limiting value is used.

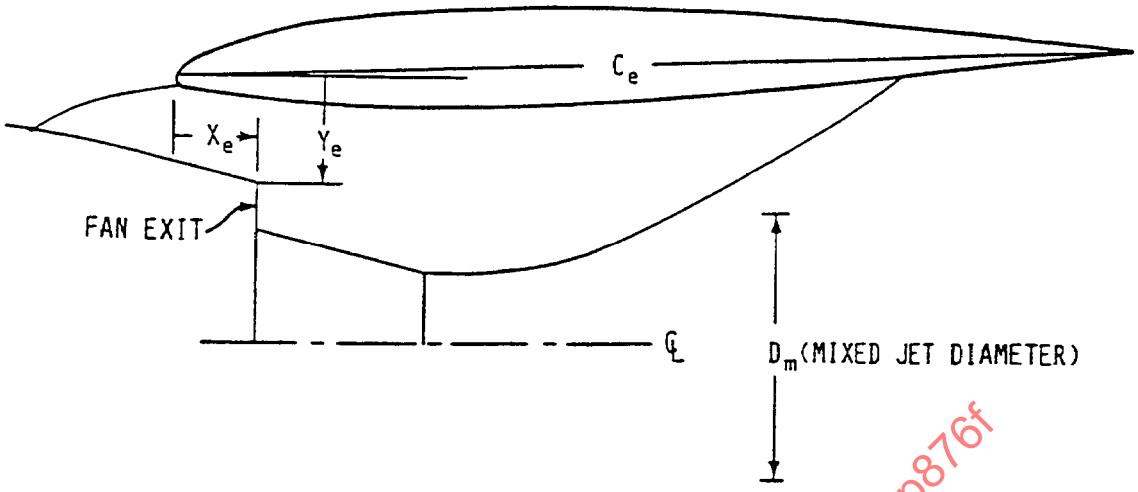

FIGURE 18 - SCHEMATIC OF INSTALLATION PARAMETERS

The angle-of-attack effect, ATK in decibels, is added to the predicted mixed jet component and is given by:

$$ATK = 0.5 \propto M_a \left[(1.8\, \theta_m / \pi) - 0.6 \right]^2 \qquad \text{(Eq. 36)}$$

where:

$\propto$ = angle of attack in degrees

M_a = flight Mach number

No installation effect is applied to the mixed jet component.

7.10 References

7.10.1 Lu, H. Y., “Effects of Excitation on Coaxial Jet Noise as Observed by an Elliptic Mirror”, J. AIAA, Vol. 21, No. 2, pp. 214-220, February 1983.

7.10.2 Glover, Jr., B. M. and Shivashankara, B. N., “Aeroacoustic Testing in Wind Tunnel”, AIAA Paper No. 86-1886, AIAA 10th Aeroacoustics Conference, Seattle, WA, July 9-11, 1986.

7.10.3 Lu, H. Y., “An Empirical Model for Prediction of Coaxial Jet Noise in Ambient Flow”, AIAA Paper No. 86-1912, July 1986.

7.11 Parties Contributing to Formulation of Section 7

General Electric, USA

Lockheed Georgia Company, USA

National Aeronautics and Space Administration, USA

Pratt & Whitney Aircraft Company, USA

Rolls-Royce plc, United Kingdom

The Boeing Company, USA

Royal Aerospace Establishment, United Kingdom

8. PREDICTION OF NOISE FROM CONVENTIONAL COMBUSTORS INSTALLED IN GAS TURBINE ENGINES

DATE OF COMPILATION: February 1980

8.1 Static Conditions

The advent of the modern high-bypass-ratio turbofan engine incorporating quiet fan technology has focused attention on internally generated core engine noise. The inherent low jet noise floor due to reduced mass efflux velocity and shielding by the fan stream has revealed low frequency noise emanating from within the core nozzle. This has variously been termed as core noise, tailpipe noise, internal noise, excess noise, and so on. Core noise has been attributed to several different sources, but the combustor in particular has received the most attention in the form of both direct combustion noise and indirect “entropy” noise. This noise source is common also to turbojet and turboshaft engines. This section is concerned with prediction of combustor noise from gas turbine engines.

The best definition of combustor noise is probably provided by turboshaft engines because of negligible jet noise and absence of a fan. The initial formulation of the proposed prediction method was therefore based on turboshaft engine data. However, the final correlation utilized data from all three classes of engines and the recommended spectrum and directivity have been validated using component and model data. The combustors were of various conventional types, i.e., annular, can-type, and “coannular” or hybrid type.

The prediction procedure is outlined in Figure 19. The overall sound power level (OAPWL) is found as a function of the combustor operating parameters and turbine temperature extraction. A power level spectrum is derived by imposing a spectrum and a directivity assigned to obtain the sound pressure level (SPL) distribution at any angle. This procedure may be implemented by using Figures 20 and 21. For consistent application, the basic information in Figures 20 and 21 is repeated in Tables 17 and 18.

The method of calculation is as follows:

Step 1—Calculate the OAPWL using the normalized sound power correlation.

$$OAPWL = 10\log_{10}\left[\frac{W_p {a_o}^2}{W_{ref}}\right] + 10\log_{10}\left\{\left(\frac{T_4 - T_3}{T_3}\right)^2\left(\frac{P_3}{P_o}\right)^2\left[\frac{(T_4 - T_5)_{ref}}{T_o}\right]^{-4}\right\} - 60.5 \quad \text{(Eq. 37)}$$

where:

W = primary (core) mass flow rate, kg/s

P_3 = combustor inlet total pressure, Pa

$(T_4 - T_3)$ = combustor total temperature rise, K

$(T_4 - T_5)_{ref}$ = reference total temperature extraction by the turbines, at maximum takeoff conditions, K

W_{ref} = reference power, 10^{-12} watt (1pW)

Temperature T_o = 288.15 K

Pressure P_o = 101.325 kPa

Speed of Sound a_o = 340.294 m/s for T_o = 288.15 k (15 °C)

Step 2—Use Figure 20 or Table 17 to define the power level spectrum. For basic prediction purposes, the peak one-third octave band in the power spectrum is assumed to be 400 Hz. However, when the method is being used with data where the peak is known to be slightly above or below 400 Hz, it is recommended that the power spectrum herein be adjusted such that its symmetrical shape is retained, but based upon the observed peak freefield value. Such an adjustment would not be expected to be more than one-third octave on either side of 400 Hz. The PWL spectrum is given by:

$$PWL(f) = OAPWL + S(f) \quad \text{(Eq. 38)}$$

where:

S (f) = the spectrum shape factor of Figure 20 and Table 17

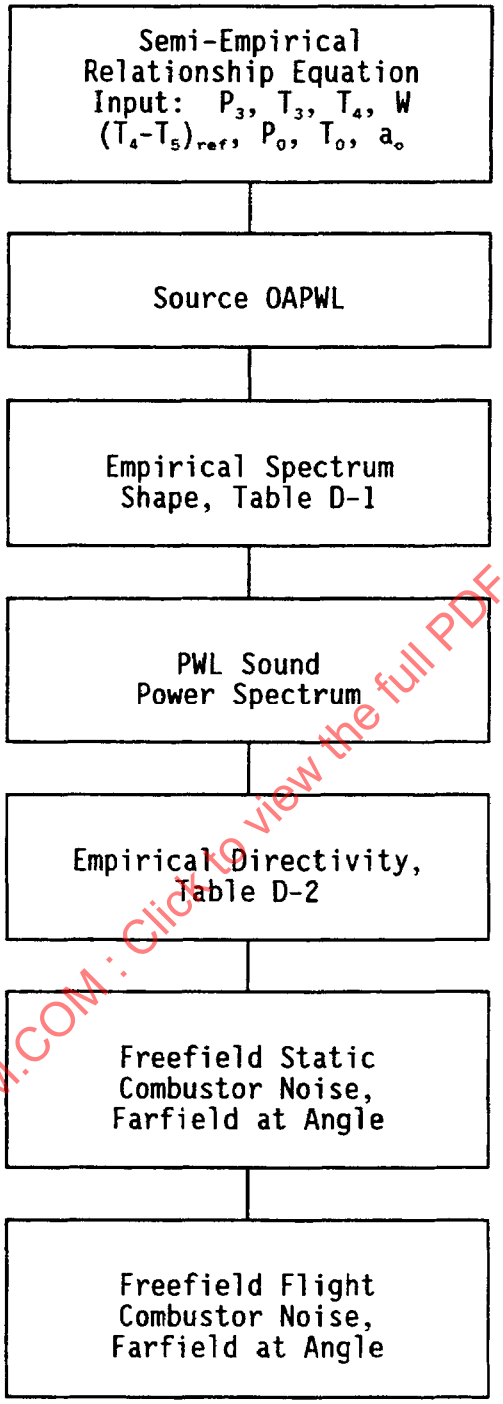

FIGURE 19 - FLOW CHART FOR COMBUSTOR NOISE PREDICTION

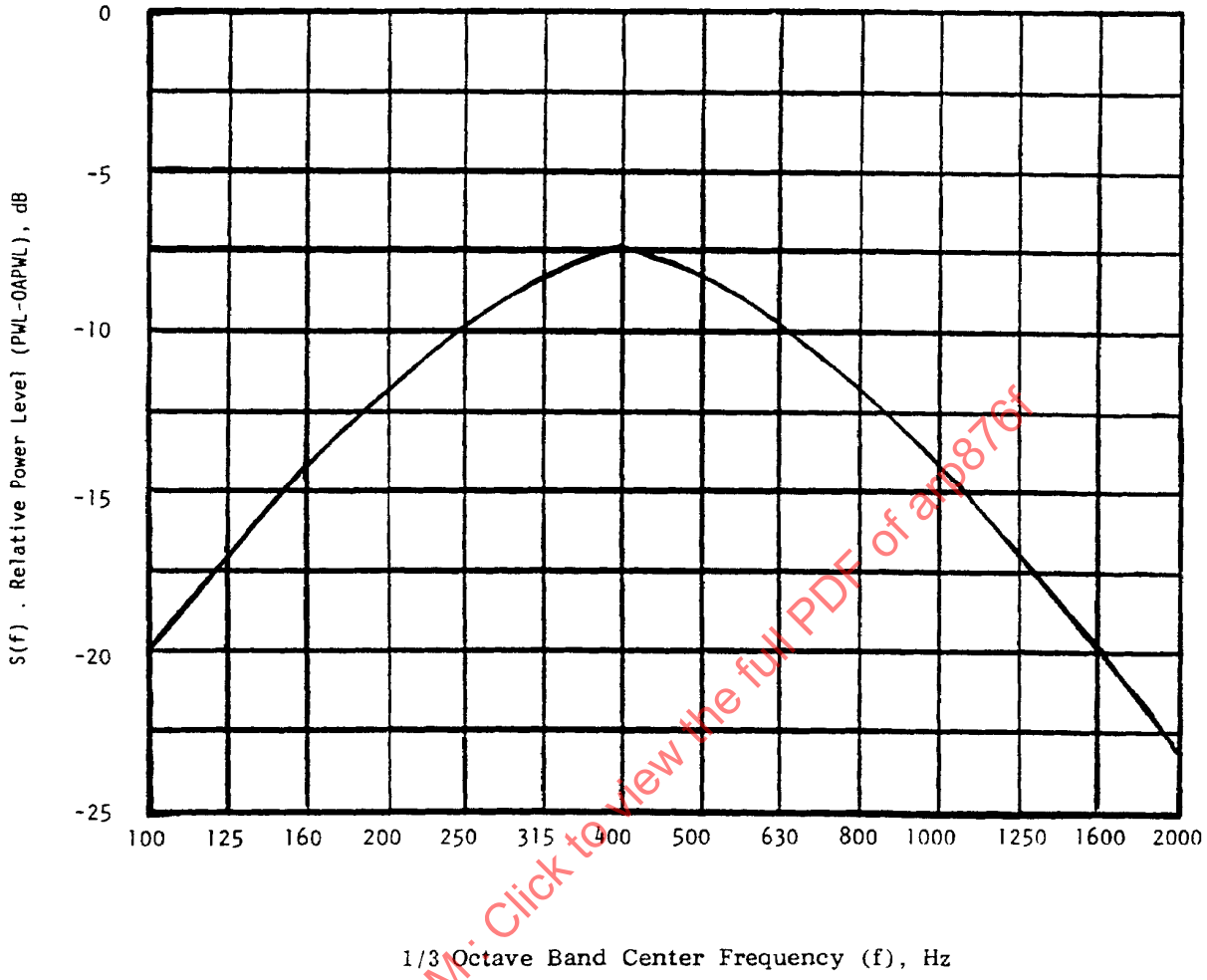

FIGURE 20 - SPECTRUM SHAPE FOR COMBUSTOR NOISE

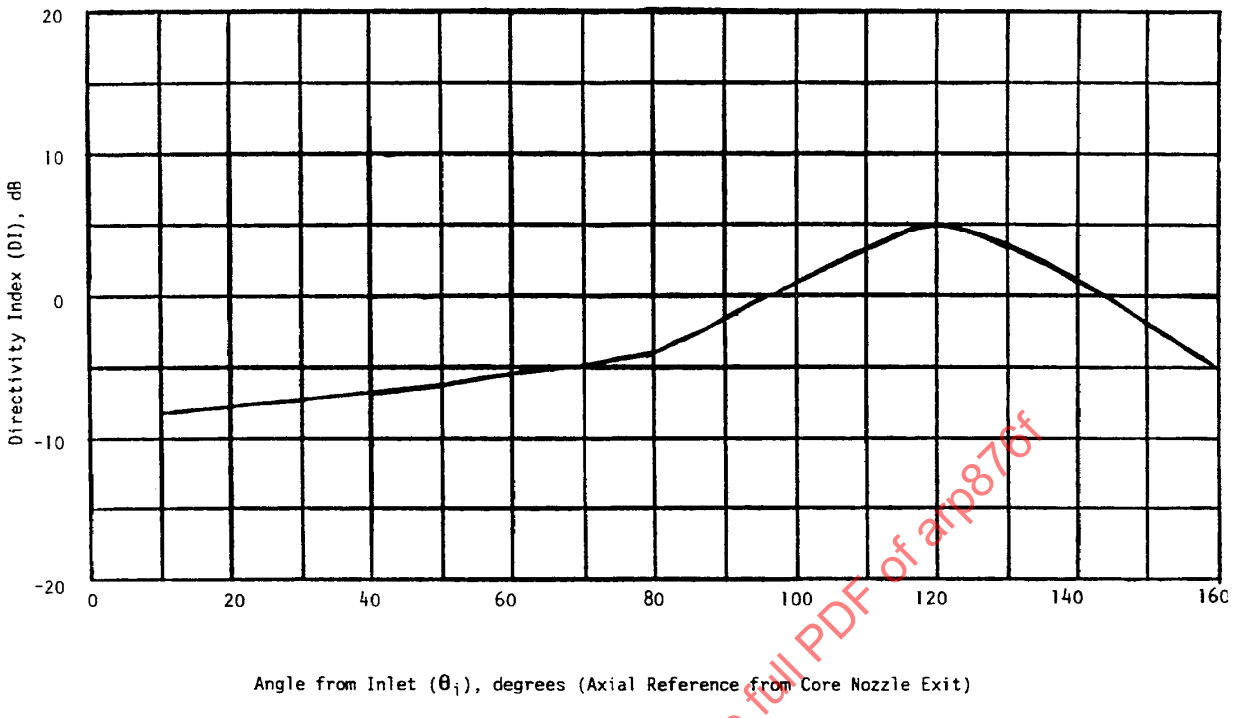

FIGURE 21 - FAIRFIELD DIRECTIVITY FOR COMBUSTOR NOISE

TABLE 17 - SPECTRUM SHAPE FACTOR FOR COMBUSTOR NOISE

1/3 Octave Band Center Frequency (f), Hz	S(f), Relative Power Level (PWL-OAPWL), dB
31.5	-38.7
40	-34.7
50	-31.2
63	-27.2
80	-23.2
100	-19.9
125	-17.0
160	-14.1
200	-11.7
250	-9.7
315	-8.2
400	-7.2
500	-8.2
630	-9.7
800	-11.7
1000	-14.1
1250	-17.0
1600	-19.9
2000	-23.2
2500	-27.2
3150	-31.2
4000	-34.7
5000	-38.7
6300	-43.2
8000	-47.2
10 000	-52.2

TABLE 18 - FARFIELD DIRECTIVITY INDEX FOR COMBUSTOR NOISE

Angle From Inlet$_1$ (θ_i), degrees	Fairfield Directivity Index (DI), dB
10	-8.0
20	-7.5
30	-7.0
40	-6.5
50	-6.0
60	-5.3
70	-4.6
80	-3.9
90	-1.6
100	+0.8
110	+3.1
120	+5.0
130	+3.5
140	+1.2
150	-1.9
160	-5.1
axial reference from core (primary) nozzle exit	

Step 3—The sound pressure level (SPL) at each farfield angle along an arc is found using:

$$SPL\,(f,\theta_i) = PWL\,(f) + DI\,(\theta_i) - 20\log_{10} r + 10\log_{10}\left(\rho a_o W_{ref}/4\pi\, p_{ref}^2\right) \qquad \text{(Eq. 39)}$$

where:

DI = farfield directivity index (Figure 21 and Table 18)

θ_i = angle from inlet, degrees (axial reference from core nozzle exit)

p_{ref} = reference sound pressure (20μPa)

r = arc radius, m

and where the last term is -10.8 dB under standard condition.

The values thus calculated represent an idealized free field case of a nonattenuating atmosphere and absence of effects of a ground surface. In a practical case, these SPLs must be adjusted to account for atmospheric sound absorption and for ground plane effects.

NOTE 1: Accuracy of Prediction

It is estimated that predictions of combustor noise overall power level (OAPWL) will be accurate within +5 to -3 dB, based on correlation of data of turboshaft, turbojet, and turbofan engines of five manufacturers. This accuracy is estimated for the range of 186 to 222 in the Equation 37 correlating parameter.

$$10\log_{10}\left(W_p a_o^2/W_{ref}\right) + 20\log_{10}\left[\left(T_4 - T_3\right)/T_3\right] + 20\log_{10}\left(P_3/P_o\right)$$

NOTE 2: The directivity index is assumed to be the same for all frequencies. Some model tests have indicated a change for very low frequencies, with the peak angles shifting from 120 degrees toward the jet axis. For full-scale engines, such changes should probably be apparent for frequencies below 200 Hz. The perceived noisiness weighting for such frequencies is so small that the error accruing from use of a single directivity for all frequencies is almost negligible for perceived noise level calculations.

8.2 Flight Conditions

It is widely accepted that the effect of forward speed on a source (such as the combustor component) which is effectively moving at the same speed as the aircraft, is affected by a 4th power “Doppler” amplification factor.

To translate the sound pressure levels obtained in 8.1 to flight conditions, a 4th power amplification factor should be applied as follows:

$$SPL_{(flight)} = SPL_{(static)} - 40 \log_{10} (1 - M_a \cos \phi) \quad \text{(Eq. 40)}$$

where:

M_a = aircraft flight Mach number (V_a/a_o)

ϕ = θ_i - ψ

θ_i = angle to engine intake axis

ψ = total incidence angle between aircraft flight direction and engine inlet axis

8.3 References

FAA Report No. FAA-RD-77-4
GE Core Engine Noise Investigation Program - Low Emission Engines
R. K. Matta, G. T. Sandusky, V. L. Doyle (1977)

FAA Report No. FAA-RD-74-125
Core Engine Noise Control Program - Vol. III, Supplement 1 -
Extension of Prediction Methods
S. B. Kazin, R. K. Matta, J. J. Emmerling (1976)

8.4 Parties Contributing to the Formulation of Section 8

AiResearch Mfg. Company of Arizona, USA

Detroit Diesel Allison, USA

General Electric, USA

Nat’l Gas Turbine Establishment, United Kingdom

Pratt & Whitney Aircraft, USA

Rolls Royce Ltd., United Kingdom

SNECMA, France

The Boeing Company, USA

9. NOTES

9.1 A change bar (l) located in the left margin is for the convenience of the user in locating areas where technical revisions, not editorial changes, have been made to the previous issue of this document. An (R) symbol to the left of the document title indicates a complete revision of the document, including technical revisions. Change bars and (R) are not used in original publications, nor in documents that contain editorial changes only.

PREPARED BY SAE SUBCOMMITTEE A-21 S1, GAS TURBINE PROPULSION
OF COMMITTEE A-21, AIRCRAFT NOISE MEASURE AND NOISE AVIATION EMISSION MODELING

INTRODUCTION TO APPENDICES TO ARP876

1. BACKGROUND TO SELECTION OF PREDICTION METHODS IN ARP876

The main body of SAE ARP876, first published in March 1978 to replace the original and outdated SAE AIR876 published in 1965, contains prediction methods agreed by the SAE A-21 Committee on Aircraft Noise to reflect the state of the art at the time of publication. In making its selection of a preferred method the SAE A-21 Committee has to consider:

a. the desirability of publishing a prediction method for any particular noise-producing component of a jet engine;

b. the amount and technical quality of the information on which the component method is based;

c. the simplicity of correlations of available data and the level of input information required to execute a prediction;

d. the accuracy of the final method;

e. any likely foreseeable improvements brought about by new work.

While Item a above is a prerequisite to SAE A-21 Committee activity and item d is considered in each SAE Aerospace Recommended Practice, items b, c, and e are the subject of protracted and exhaustive surveys and discussions in the lead-up to defining a method. In order to understand the background behind the decision to proceed with the publication of each section of SAE ARP876 it was decided to prepare these Appendixes, so as to reflect the deliberations of the Gas Turbine Propulsion Subcommittee of the SAE A-21 Committee, and to reference all available information considered. It is compiled in appendix form to echo the subject matter of the main body of SAE ARP876, and allow for future updating.

2. HISTORY OF THE PREPARATION OF THE APPENDICES TO SAE ARP876

In October 1970 the SAE A-21 Committee on Aircraft Noise deemed it timely to review the validity of SAE AIR876, which was issued in 1965 as a summary correlation of jet engine exhaust noise. The need for a review was largely a function of the emergence of high bypass-ratio turbofan engines with exhaust velocities considerably lower than the range considered in SAE AIR876, and turbojet engines for supersonic transports at the other end of the scale.

An ad hoc group was formed, and reported in 1971 that SAE AIR876 was deficient in several significant areas over and above the question of range of jet velocities covered. Accordingly, a subcommittee was formed in 1971 which then reviewed available information over the subsequent two-year period. In 1973, the subcommittee determined that a new document should be prepared covering known sources of exhaust noise in separate prediction procedures. The topics of single and coaxial jets, shock-associated and internal noise were proposed for study. Turbomachinery noise was specifically excluded because of the proprietary nature of much of the data and because of the complication of the use of acoustically lined engine ducting for installations in high bypass-ratio turbofan engines for civil jet transport aircraft.

The depth and intensity of activity that took place in the preparation of each section of SAE ARP876 was substantial and significant. New data became available as methods were developed, and the methods were adjusted to take account of such developments. In some cases the decision to publish a section at a particular date was a matter of divided opinion, since at any given time there was always a new piece of work about to produce information which might have solved immediate problems. As a result, the material in these Appendixes reflect the fact that, in some instances, alternative procedures were available, and that the method selected for inclusion in SAE ARP876 was, frequently, a matter of consensus rather than unanimous agreement.

APPENDIX A - BACKGROUND TO PREDICTION OF SINGLE STREAM JET MIXING NOISE FROM SHOCK-FREE CIRCULAR NOZZLES (SECTION 5)

A.1 INTRODUCTION

Up to the time when the SAE A-21 Committee on Aircraft Noise decided to take a second look at its published method for predicting jet noise, SAE AIR876 and the work of Coles (A.5.1) were the only published correlations of jet noise that permitted a prediction process to be undertaken. Those works stood the test of time up to the early 1970s when the introduction of the high bypass-ratio turbofan and the development of the supersonic transport revealed a need for the ability to predict jet mixing noise and other associated components of engine noise to a far greater degree of accuracy, both within and outside the jet velocity range thus far considered.

The initial move by the Exhaust Noise Subcommittee[2] was to circulate the then unpublished static engine and model correlations of Ahuja and Bushell (A.5.2) and to seek comparison with other available data. Such data as emerged, from the General Electric Company for models (A.5.3) and full scale engines, Lush, and the Société Nationale d'Etude et de Construction de Moteurs d'Aviation (SNECMA) and the National Gas Turbine Establishment (NGTE) (A.5.4 - A.5.6) revealed a sensible correlation of wideband sound pressure level values from tests of scale model nozzles, when normalized for jet area and density and referenced against fully expanded jet velocity. Discrepancies in the ability of the correlation procedure to collapse the test data were noted, however, at high velocities and temperatures (where it appeared that jet density was a variable rather than unique function) and in the considerable scatter in high frequency sound pressure levels.

A.2 STATIC CORRELATION

By 1973 it had been determined that the high frequency data scatter was probably a function of noise generated internally in some of the model rigs from which data had been acquired. This conclusion was borne out by the even greater variability of data from engines, first indicated by Smith (A.5.7) and later highlighted by Bushell (A.5.8) in the correlation of Figure A1. At that time sources of noise other than those originating in the turbomachine were variously identified and labeled as core, tailpipe, excess or even combustor noise. Additional unpublished data from Pratt & Whitney Aircraft, The Boeing Company, Hamilton Standard, and Pratt & Whitney Aircraft of Canada led to a close inspection of the quality of the rigs and facilities on which the data were acquired, with a view to eliminating those data that were expected to be contaminated by internal noise sources. In view of the multitude of noise sources in data from engines, it was decided to concentrate solely on information from high quality model facilities. In fact, by 1974, the second round of subcommittee activity led to significant new work being undertaken within The Boeing Company, the NGTE (A.5.9) and SNECMA on model jets, and an upsurge in activity on static-to-flight effects throughout industry and government aircraft noise research establishments.

By 1975, the acceptable data base had been reduced to measurements from the high quality facilities at SNECMA, NGTE, Boeing and General Electric. Additional high quality data from the Lockheed-Georgia Company were included at a later stage. The background data and substantiation of the method derived from this work in the period between 1975 and 1977 are contained in major internal reports (A.5.10 - A.5.13) from Lockheed, SNECMA, and Boeing.

The results of all this work were drawn together in the period from 1975 to 1977 in a comprehensive document correlating 1/3rd octave band spectral levels against jet velocity and density for varying temperatures. The document was approved by the SAE A-21 Committee and the SAE Aerospace Council for publication in 1977, and appeared as the initial version of Section 5 of ARP876 in March 1978. The initial version dealt only with jet mixing noise from single stream shock-free circular nozzles under static conditions. The derivation of a transformation function to account for static-to-flight effects, discussed in the following paragraphs, was not finalized until 1980 and published in 1981.

[2] Because of an enlargement of the scope of the subcommittee's responsibilities, the name of the subcommittee was changed in 1980 to the SAE A-21 Gas Turbine Propulsion Noise Subcommittee.

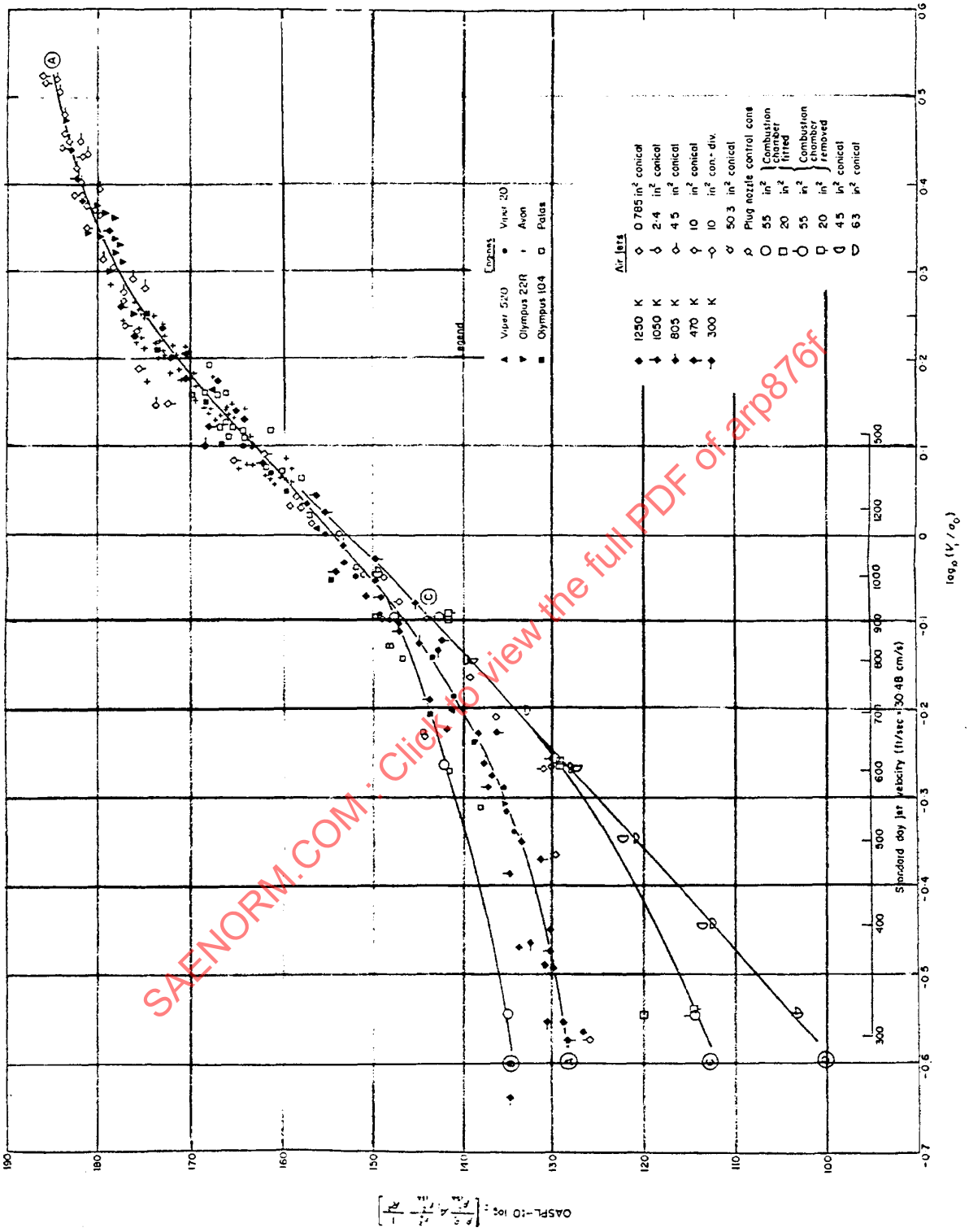

FIGURE A1 - EXTRACT FROM REFERENCE A.8 - EARLY JET MIXING NOISE CORRELATION

A.3 STATIC-TO-FLIGHT EFFECTS

To be useful in predicting operational noise levels, any aircraft noise prediction method requires the ability to predict under inflight conditions. The questions of the changes that occur in the jet mixing structure as a result of forward motion and the resulting noise level and directivity are ones that have been a cause for concern for several years. The original prediction method of SAE AIR876 of 1965 was directed primarily at providing an estimate of maximum “pass-by” noise level for aircraft Mach numbers below 0.35. The recommended curve from which the maximum pass-by noise level was ascertained was essentially an average of ground based and flight test data using relative jet velocity as the correlating parameter. Small differences in spectra were indicated under static and flight conditions, but were not explained.

The first definitive relationship between static engine and aircraft flight levels was published by Bushell (A.5.14) in 1975. Bushell’s relationship was based upon observations of the static and flight levels of a few aircraft powered by turbojet and turbofan engines. It was recognized at the time that the correlation thus produced was at variance both with the classical jet noise theory and with measurements made in wind tunnels, where forward motion was simulated by the tunnel flow (A.5.15 and A.5.16). The main differences were in the prediction of an amplification of engine noise in the forward quadrant under actual flight conditions, but a reduction under simulated flight conditions with models of the same quality as used in defining the basic jet noise correlation of SAE ARP876 (see Figure A2).

The Bushell correlation (Reference A.5.8) used as a basis the transformation function developed by Cocking and Bryce (A.5.16), which utilized an exponent (m) for the ratio of absolute to relative jet velocity and a Doppler amplification factor as shown in Figure A3. That format became the basis for initial studies by the A-21 Subcommittee in 1974. The aircraft static-to-flight effect seemed to be in good agreement with results from a whirling arm facility (A.5.17) and it was not until the appearance of the work of SNECMA (A.5.18 and A.5.19) on the Bertin Aerotrain, work in the NASA Ames 40 ft x 80 ft wind tunnel and other facilities, and new flight test evidence (A.5.20 to A.5.29) that real debate started.

From that time to the date of publication of the static-to-flight section in Section 5 of SAE ARP876, controversy continued over the real effects of forward motion on jet noise. Moreover, there was no ideal solution to the problem, since there was no accepted rationalization or explanation of the differing effects between observations on aircraft, engines under simulated flight conditions, and model jets under various modes of flight simulation.

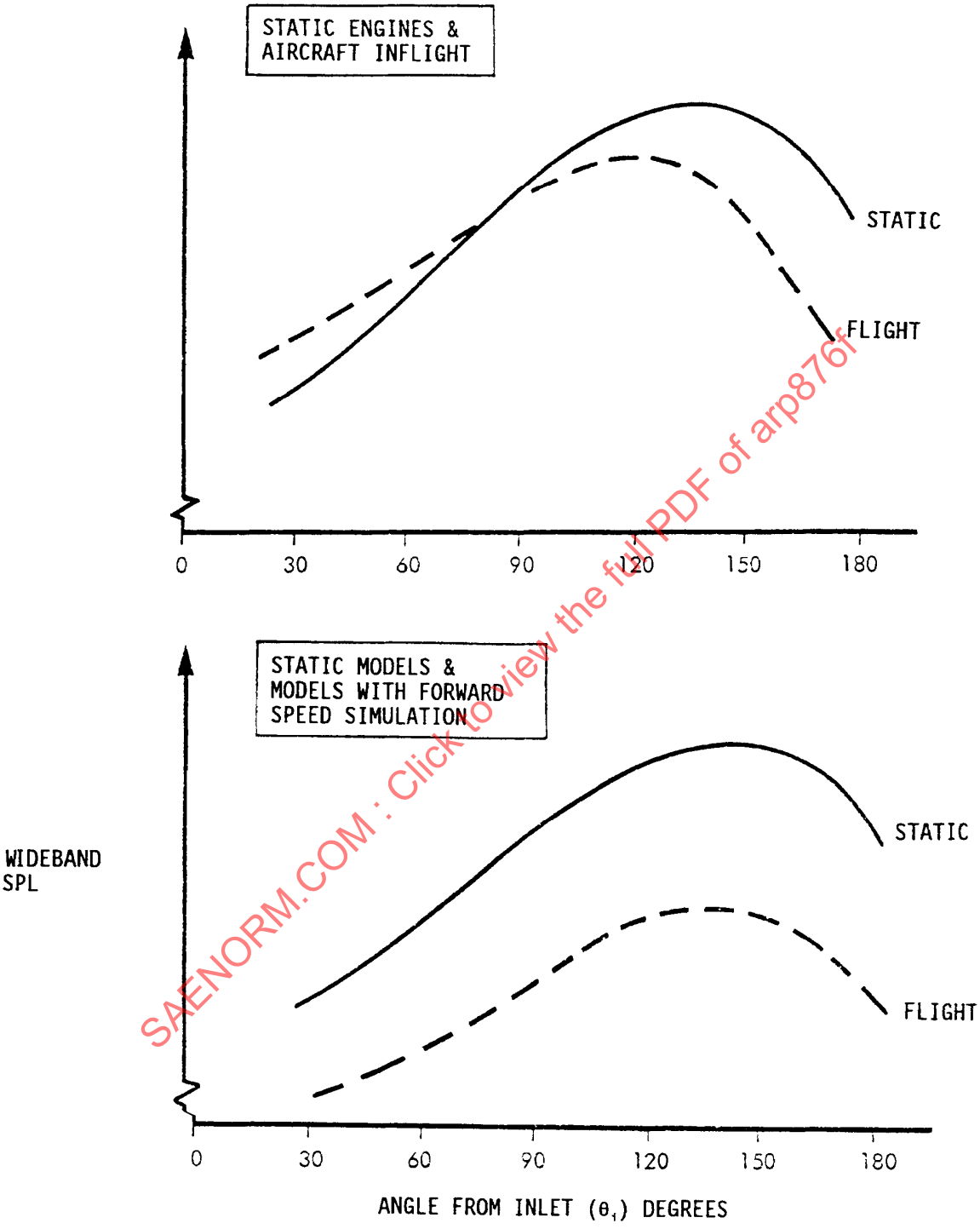

FIGURE A2 - DIFFERING FORWARD SPEED OBSERVATIONS
FROM ENGINE INSTALLATIONS AND MODEL JETS

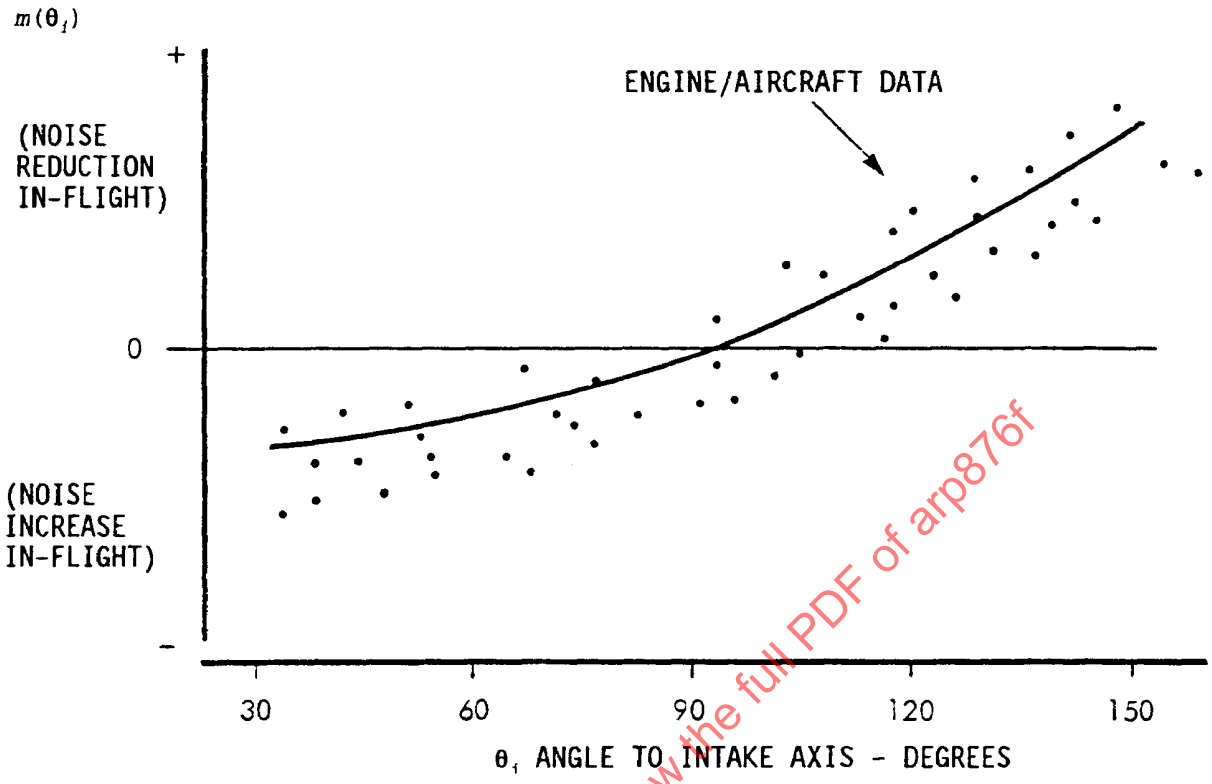

GENERAL RELATIONSHIP

$$SPL_{STATIC} - SPL_{FLIGHT} =$$

$$10 \log_{10} \{(V_j/V_{rel})^{m(\theta_I)}(1 - M_a \cos(\theta_I))\}$$

WHERE:

V_j = ABSOLUTE JET VELOCITY
V_{rel} = RELATIVE JET VELOCITY
M_a = AIRCRAFT MACH NO.

FIGURE A3 - STATIC-TO-FLIGHT EXPONENT - M(θ_I)